A STUDY OF INTERACTIONS BETWEEN LAMINAR FLAMES AND WALLS

by

Paulus Bucher

Thesis submitted to the Faculty of the

Virginia Polytechnic Institute and State University

in partial fulfillment of the requirements for the degree of

MASTER OF SCIENCE

in

Mechanical Engineering

APPROVED:

Dr. Uri Vandsburger, Chairman

Dr. Alan A. Kornhauser, Chairman

Dr. Richard J. Roby

August, 1993

Blacksburg, Virginia

A STUDY OF INTERACTIONS BETWEEN LAMINAR FLAMES AND WALLS

by
Paulus Bucher
Committee Chairmen: Dr. Uri Vandsburger and Dr. Alan A. Kornhauser
Mechanical Engineering

(ABSTRACT)

A basic study on the convective flame-wall heat transfer in diesel engines was performed with a fundamental experiment and simplified theoretical models. Based on the concept of flame tubes, a combustor was designed and optimized to support laminar, stable flame propagation at constant ambient pressure. Measurements of flame position and heat transfer during head-on quenching of premixed methane-air flames with varying mixture equivalence ratios at a metallic surface were made using flame luminosity videography and surface thermometry. Two models were developed to predict the magnitude of single-wall quenching layers and the flame-wall heat transfer at a variable temperature wall. One of the models was a quasi steady-state first law balance which utilizes an Arrhenius reaction equation to represent the temperature sensitivity of the chemical processes according to a single-step reaction mechanism. The second model was based on transient heat conduction theory; a planar, moving heat generating sheet simulated the heat release of a propagating flame front in a one-dimensional slab of gases at rest, bounded at the wall at which quenching occurs. Experimental and model results showed that flame-wall heat transfer is primarily dictated by the reaction rate of combustion and the thermal diffusivity of the gas mixture. The convective heat transfer coefficient was predicted to increase with rising wall temperature. Measured peak heat transfer rates were 25% higher than those reported in the literature. Recommendations are made for the design of an experimental apparatus with which conditions encountered in internal combustion engines can be simulated more closely.

Dedicated to

Michaela

ACKNOWLEDGEMENTS

I would like to thank my advisors Dr. Alan A. Kornhauser and Dr. Uri Vandsburger for their guidance, encouragement, patience and time they have given to me over the past two years. I wish to express my deepest appreciation to Dr. Uri Vandsburger for providing me the opportunity to pursue graduate studies, for his confidence in my abilities and for his continuous support. I would like to thank Dr. Rick Roby for serving on my advisory committee and for helpful conversations regarding my thesis.

I wish to thank my fellow students at Virginia Tech Steve LePera, James Reaney, David Ewens, Chen Ding, Robert Aftel, Ralf Ochel and Douglas Wirth for their help with my experimental system and for their friendship and encouragement. Special thanks are due to James Reaney for his help in preparing this thesis. Thanks also go to the support people in the Mechanical Engineering Department Jerry Lucas and Frank Caldwell for their capable assistance.

Finally I thank Michaela Klotz for her love and moral support.

TABLE OF CONTENTS

LIST OF FIGURES

LIST OF TABLES

Table Page

NOMENCLATURE

Variables

P	Pressure
P_i	Partial Pressure of Species i
T	Temperature in Kelvin
θ	Temperature Difference
ρ	Density
α	Thermal Diffusivity
λ	Temporal Variable of Integration
Φ	Molar Fuel to Air Ratio
δ	Dirac Delta Function
β_m	Eigenvalue
t	Time
Δt	Time Lag
x	Quality
x'	Spatial Variable of Integration
X	Mole Fraction
k	Conductivity
n_i	Number of Moles of Species i
$\dot{q}''$	Heat Transfer Rate Per Unit Area
g_s	Heat Source Strength
c_p	Constant Specific Heat
h_{rp}	Heat of Reaction
S_u	Flame Speed
A	Area
D	Diameter
E_a	Activation Energy
d_{q1}	Single-Wall Quenching Distance
d_{q2}	Parallel Plate Quenching Distance
L	Length

Subscripts

s	Solid Condition
w	Wall Condition
u	Unburned Condition
f	Flame
g	Heat Generation
c	Heat Convection
h	Time of Arrival
j	Numerical Variable
i	Numerical Variable
tube	Flame Tube
th	Thermocouple
sur	Surrounding

Superscripts

a	Adiabatic Condition
e	Experimental Condition
c	Surface Area Corrected
^	Non-Dimensional Quantity

1. Introduction

1.1 Motivation

In recent years, the quest for increasing the efficiency of the diesel engine has focused attention on reducing the heat loss to the coolant during the power stroke of the cycle. In internal combustion engines, the input energy is divided into three approximately equal parts; energy converted into work, energy absorbed by the cooling system, and energy expelled with the exhaust gases. According to the first law of thermodynamics, the division of energy between various categories is unimportant, as long as energy is consistently conserved. The second law of thermodynamics states that it is not possible to obtain 100% conversion from heat to work; some energy has to be rejected, preferably through the exhaust gases where it can be reclaimed. Thus, reducing the energy loss to the coolant does not violate the second law of thermodynamics, and according to the first law of thermodynamics has the potential to increase usable work. Moreover, the cooling system, including pumps, fans, radiator, hoses, etc. could be eliminated (less heat transfer to the cylinder walls means less need to cool the engine) with the benefit of increased brake-power and a more reliable engine design.

The prospect of improving the design and performance of the internal combustion engine has led to research on adiabatic, or low heat rejection (LHR) engines during the past decade. The concept is to reduce in-cylinder heat transfer by insulating the piston and liner with a thin layer of ceramic coatings or ceramic inserts, allowing wall temperatures as high as 1100 K at the interface to the combustion chamber. Based on non-reacting flow heat transfer theory it was hoped that a decreased differential temperature between flame and wall would result in a decreased heat transfer coefficient during the power stroke and

thus reduced overall energy loss to the coolant. However, investigations on LHR engines have produced no clear answer as to whether the efficiency of engines can be increased by means of ceramic insulation. Some investigations on prototype engines indicate that engine insulation causes an increase in in-cylinder heat transfer and a corresponding decrease in efficiency, whereas other research indicates the opposite. Most theoretical analysis and numerical work support the "adiabatic" engine concept, but experimental studies cast serious doubt on the validity of the prediction.

The goal of this study is to investigate flame-wall interaction in a well controlled environment in order to obtain information about the phase and amplitude of heat transfer from reacting flows to walls, which is the key feature to the LHR engine concept. In the long term, this project is expected to address the head-on interaction of both laminar and turbulent flames with walls at variable temperatures under constant pressure conditions.

The work reported here constitutes the first stage of the proposed project, and is focused on the experimental study of a transient laminar flame impinging on a cold wall (room temperature) at constant, atmospheric pressure. The main objectives are the development of techniques to generate test conditions and the gathering of experience with diagnostic techniques. An experimental apparatus was set up and the time resolved heat transfer to an end wall was measured with respect to the position of the approaching laminar flame front. In order to gain insight into the flame quenching process, two simple analytic models were developed, and the results are compared to the experimental findings.

1.2 Previous Work

LHR engine research has been conducted by industry and universities during the past decade; some research involves experimentation, and some involves numerical simulations. Almost all of the numerical studies predict improved thermal efficiency and increased exhaust availability as a result of reduced heat rejection in LHR engines over the conventionally cooled ones. The results of LHR in-engine testing are inconclusive, and even contradictory. In most of the experiments, the conventionally water-cooled engines are modified by coating piston faces, liner and cylinder head with plasma sprayed ceramic layer or by replacing some metal engine components with ceramic inserts. A set of engine performance data is taken under insulated conditions and compared to data from conventional operation. Some research shows a slight increase in engine efficiency and reduced overall heat transfer to the wall, others show lower efficiency and increased heat transfer rates during early expansion as compared to the baseline engines.

Various explanations have been given to explain the poor performance of some LHR engines. One theory which has received much attention says that high cylinder surface temperatures cause a drastic increase in the convective heat transfer coefficient which overcomes the effect of decreased temperature difference between gas and surface. This increase in heat transfer coefficient has been related to a thinning quenching layer between flame and wall. For a cold wall, a flame fails to maintain chemical reactions due to heat loss (is quenched) at some distance from the wall. For hot walls, the temperature difference between flame and wall is smaller, and the flame is quenched shorter from the wall. Thus it is possible that the effect of a thin quenching layer outweighs the effect of a reduced mean bulk temperature and the heat transfer is actually increased.

There are theories which explain the reduced efficiency of LHR engines by reasons that are not related to heat transfer. Some researchers have noted that high wall temperatures led to a significant reduction in ignition delay, caused by the increased gas temperature at the end of the compression stroke. Consequently, the fraction of the injected fuel which burned in the premixed mode was lower. The initial rate of heat release, as well as the favorable rapid initial pressure rise, were reduced and so was the engine performance. Others have argued that the volumetric efficiency suffers if a naturally aspirated engine is operated under insulated conditions, and therefore the efficiency of LHR engines should not be judged on the basis of the frequently employed method of direct comparison between cooled and insulated engine performance data. As a whole, LHR engine performance data has proved to be inconclusive because heat insulation effects various operational parameters and it is not possible to separate the effects in such a complex environment.

There are some numerical and experimental studies that provide information concerning heat transfer from reacting boundary layers to walls. Those studies do not always directly address the phenomena of interest: heat transfer from hydrocarbon flames to hot walls; but provide insight into the physical principles of flame-wall interaction. Numerical modeling of flame-wall interaction with detailed chemical reaction mechanisms has shown that flame quenching at cold walls is a slow process (relative to the time needed for heat diffusion) which allows the hydrocarbons in the quenching layer to diffuse into a temporarily stationary flame front at some distance from the wall. By the time the flame is extinct, the hydrocarbons in the quenching layer are almost entirely consumed. The oxidation of the quenching layer fuel content liberates heat close to the wall and therefore contributes greatly to the wall heat transfer.

Experimental studies have been made to investigate quenching distance, hydrocarbon emissions, and flame-wall heat transfer. The flame quenching distance has been studied using burners and combustion bombs. However, in most experiments, the quenching process involved the propagation of a flame front through small tubes or closely spaced plates. Because of this arrangement, most studies have obtained information about the side quenching process. The flame quenching process in (LHR) engines is largely head-on, which can be described as a truly one-dimensional, transient phenomenon. Very few studies directly address head-on flame quenching. Transient experiments with cold walls have shown that the head-on quenching layer is on the order of 5 times smaller than the two-wall quenching layer. From transient experiments with hot walls it is known that the quenching layer thins with increasing wall temperature.

The results from steady-state experiments, where the heat transfer from a burner stabilized flame to a variable temperature wall is measured, are contradictory. One study claims that the heat transfer to a hot wall increases as compared to heat transfer to cold walls, whereas another study claims the opposite. Heat transfer from transient head-on flame impingement has been studied only for the cold wall case. Although correlations have been successfully established to predict transient flame-wall heat transfer to cold walls, no data is available on the effect of elevated wall temperatures on heat transfer. Clearly, there is a need to study transient flame-hot wall interaction and its effect on heat transfer. Only on the basis of heat transfer data that is measured during the transient flame impingement on a variable temperature wall can the feasibility of the LHR engine concept be judged.

Some of the most important work on LHR engines and related topics is reviewed and divided accordingly in the following outline:

1.2.1 Experimental Studies of Heat Transfer in Prototype Diesel Engines

Experimental studies were carried out on diesel engines, investigating the effect of heat insulation on engine performance. The adiabatic engine concept bears only on diesel engines, because elevated wall temperatures can cause auto-ignition in a gasoline engine. Four investigations are reviewed; each case involves different degrees of insulation, instrumentation and operating conditions and achieves varying results. Two investigations indicate an increase in engine efficiency and a reduction in in-cylinder heat transfer whereas the other studies indicate to the opposite.

An increased engine efficiency is reported by Havstad, et al. [1] and Morel, et al. [2]. Havstad, et al. [1] modified a turbocharged single cylinder engine with zirconia inserts for head, liner and piston top. The in-cylinder heat transfer was reduced 30% in cases of the insulated engine over the baseline engine, and the indicated specific fuel consumption (ISFC) was up to 9% lower. Morel, et al. [2], found that the peak heat flux, as well as the mean heat flux, was reduced with increasing wall temperature in their single-cylinder turbocharged engine where piston and cylinder head were coated with a thin layer of zirconia.

In contrast, Woschni, et al. [3] and Cheng and Wong [4] reported a poor performance of their diesel engines. Woschni, et al. [3] have found a drastic increase in the heat transfer

coefficient during the first part of combustion with increasing wall temperatures, and poor results in terms of ISFC. For their measurements, they used a naturally aspirated single cylinder engine with the piston crown partially insulated by a nimonic coating. Cheng and Wong [4] measured lower unsteady heat flux amplitudes at higher wall temperatures, but attributed this finding to a degradation in the combustion process rather than to a decreased heat transfer coefficient. Compared to the baseline metal engine, their zirconia coated single cylinder engine also showed higher ISFC.

In the experiments that are listed above, the measurements were made with instruments placed at different locations in different engines, with different levels of insulation and different operating conditions. The measurements can be very sensitive to these locations and conditions. Therefore, it is difficult to make direct comparisons between the experiments and to extract the information on how heat transfer is affected by the variation of wall temperature.

1.2.2 Experimental Studies on Flame-Wall Interaction

The objective within this section is to present some of the work that provides insight into the physical principles of flame-wall interaction.

When propagating in an engine cylinder, a flame front encounters a variety of quenching surfaces such as cylinder walls, piston and cylinder head. The orientation of a flame front is approximately parallel to a particular quenching surface during the quenching process, and all other surfaces are too far away to disturb the temperature field at this particular location within the quenching time scale. Such conditions are referred to as the head-on quenching process, and the quenching layer that forms between flame front and wall is

named the single-wall quenching distance. From the perspective of heat transfer, the quenching distance between flame and wall is an insulating layer of cold gases that acts as a thermal barrier. Therefore, the quenching layer thickness is an important characteristic of the flame quenching process.

There is a long history of flame quenching experiments in gaps between two walls or in narrow tubes. Although not directly applicable to the head-on quenching process in IC engines, the side-wall quenching layer thickness is related to the single-wall quenching thickness. Among others, Friedman and Johnston [5] have measured two-wall flame quenching in a combustion bomb between plates at various wall temperatures and pressures. They reported that the quenching distance thins with the -0.5 power of the absolute wall temperature and with the -0.91 power of the chamber pressure.

Very little experimental data is available on single-wall quenching layer distances. In an attempt to understand hydrocarbon emissions of reciprocating engines, a comparison of one-wall and two-wall quenching distances was first done by Daniel [6], based on an in-cylinder measurement. He suggests that single-wall quenching layers are of the same size as two-wall quenching layers. Goolsby and Haskel [7] found that two-surface quenching distances are 2.5 to 12 times greater then those of single-walls, and that two-surface quenching distances are roughly inversely proportional to the wall temperature. The single-wall quenching thickness in a combustion bomb at variable pressures was measured by Girard and Leyer [8] by means of CH^* emissions from the flame front. They found that the single-wall quenching distance decreases with increasing pressure. Fairchild, et al. [9] have conducted experiments where a steady-state flame impinges on two largely spaced variable temperature plates. They concluded that the quenching distance between flame

and the (approximately) single wall narrows with increasing wall temperature. Lavoie [10] has developed a scaling law to relate the two-wall quenching distances to single-wall distances on the basis of a non-dimensional Peclet number. Experimental data, obtained from single- and two-wall quenching processes, consistently show that the quenching layer thins with increasing wall temperature and pressure.

Research that was done to investigate the effect of wall temperature and pressure on flame-wall heat transfer has produced controversial results. The heat loss from the flame to a (approximately) single wall in Fairchild's, et. al. [9] steady-state experiment was reduced for hot walls as compared to cold walls. In a similar experiment, however, Monnot [11] and Germerdonk and Nguyen [12] found that heat transfer from a steady flame increased with rising wall temperature.

Vosen, Greif and Westbrook [13], have measured transient heat transfer from a premixed methane-air flame front to a cold wall for various pressures in a constant volume combustor. They found that when non-dimensionalized by the heat of reaction and the flame speed, the peak heat flux to a cold wall was independent of the mixture equivalence ratio, but dependent on the combustion chamber pressure. So far there is not a single experiment that shows the effect of hot walls on heat transfer in a transient environment. Such data is needed to answer the fundamental question that arises from LHR-engine testing: whether or not a reduced temperature difference from a reacting boundary layer to a wall causes a decrease in heat transfer as is expected from non-reacting heat transfer models.

1.2.3 Analytical and Numerical Models of Flame Quenching

Numerous numerical simulations have been conducted on flame wall interaction. Formulations run from simple, thermal flame propagation to complex descriptions of fluid mechanics and chemical kinetics. Only one numerical study that has enormously contributed to the knowledge of the kinetic aspects of flame quenching and several simple, closed form solutions that are directly related to the development of models in this study are reviewed here.

Westbrook, Adamczyk and Lavoie [14] have constructed a model of the transient flame quenching process that combines an unsteady treatment of fluid mechanics with a detailed chemical kinetic reaction mechanism. Model calculations demonstrate the effects of variations in pressure, fuel-air equivalence ratio, and wall temperature on single-wall quenching distance and remaining fuel in the combustion chamber. It is claimed that the detailed kinetics treatment universally represents the dependency of laminar flame properties such as flame speed and flame thickness on pressure, temperature and equivalence ratio without calibration against experimental flame data. Westbrook, et al. [14] explain that from a kinetics perspective, flame quenching in the cold temperature region close to cold walls is caused by the termination of reaction steps with high activation energies such as pyrolysis and chain branching reactions. Only the radical recombination reactions with their low activation energies can proceed. Since reactions of stable intermediate species and fuel molecules with radicals are the primary sources of chain branching reactions, there remains no effective reaction channel in cold temperature regions close to the wall where fuel can be consumed effectively. Therefore, the rate of fuel consumption towards the end of the quenching process is controlled by the rate at which fuel and stable intermediate species diffuse out of the quenching layer into a higher

temperature region where the radical concentration is still high. Any fuel that reaches this region is rapidly consumed by fuel-radical reactions. The controlling parameter which determines how much unburned fuel remains in the quenching layer was determined to be the time required for the diffusion process.

Quenching distances predicted by the Westbrook, et. al. [14] model are in agreement with single-wall quenching data reported in the literature. However, the unburned hydrocarbon concentrations in the quenching layer were predicted to be much lower than those found in experimental studies. According to model calculations, the fuel content of the quenching layer is almost completely consumed. Westbrook, et al. [14] have therefore suspected that hydrocarbon emissions in IC engines are related to in-cylinder crevices which are too small to support flame propagation, rather than the single-wall quenching process.

Calculations were carried out to study the effects of temperature variation in the unburned gas and wall on the quenching layer thickness. When the wall temperature was raised from 300 K to 400 K, the flame was thinner and traveled closer to the wall. Diffusion and oxidation in this case are said to occur more rapidly than in the lower temperature case, and the laminar transport coefficients increase with local gas temperature.

Although the Westbrook, et. al. [14] study provides great insight in the reaction process during flame-wall quenching, the effect of increased transport coefficients on instantaneous or time integrated heat transfer remains unclear. It should also be noted that turbulence and catalytic reactions with wall surfaces were not included in the model formulation.

Much simpler models of flame quenching were developed by Ishikawa and Branch [15] and Isshiki and Nishiwaki [16]. These models are based on transient heat conduction theory and exclude the detailed treatment of chemical reactions and fluid dynamics. Despite various simplifying assumptions, it seems that these simple models are sufficient to represent the key events of the transient flame quenching process.

Ishikawa and Branch [15] describe a model where chemical reactions are replaced by a heat generation zone, which moves with uniform velocity through a one-dimensional layer of gases until it arrives at the cold quench wall, ignoring the fact that real flames stall at the quenching distance from the wall. Upon arrival at the wall, the heat source is turned off and the period of thermal relaxation begins. According to findings by Westbrook, et. al. [14] it is reasonable to assume a complete consumption of the quenching layer fuel content. Thus the correct amount of heat is liberated by the model, although the location and time of heat release is not represented properly. The authors claim that predicted peak heat fluxes and heat transfer variations with time compare well to their experimental data.

Isshiki and Nishiwaki [16] have calculated single-wall quenching distances, assuming a one-dimensional, oblique thermal flame propagation. Based on an energy balance in a control volume, the transient temperature profiles between flame and wall and the heat transfer to the wall were calculated. All reactions were assumed to be quenched when the wall heat transfer exceeded a certain limit. The distance between flame and wall at the moment of flame quenching was taken to be the single-wall quenching distance. The authors have expressed the quenching distance in terms of a non-dimensional Peclet number which is defined by the quenching distance, the laminar flame speed and thermal

diffusivity. They found that the single-wall Peclet number takes the value of about four-tenths of two-wall Peclet numbers, which is in good agreement with experimental single-wall quenching results.

In both the above models the complex process of flame quenching was reduced to a relatively simple transient heat conduction problem. Results demonstrate that the essence of the flame quenching process was captured. However, those models are designed to satisfy very specific boundary conditions and need to be calibrated against experimental data. Therefore it is not clear, that models based on heat conduction theory are able to represent wall quenching phenomena for the specific conditions of interest, including pressure and temperature variations.

1.3 Present Work

1.3.1 Objective

The results of in-LHR engine testing show considerable disagreement as to the effect of hot walls on heat transfer. Some investigations reported a decrease in heat transfer in the hot wall case as compared to cold walls, while others have found the opposite. LHR engine research has provided experimental evidence that it is impossible to separate the various superimposed effects which are caused by a change in wall temperature. Knowledge of how the heat transfer coefficient is affected by the presence of a hot wall is necessary to judge the LHR engine concept.

There are several investigations where flame-wall interaction is studied in a controlled environment. Some experiments have addressed heat transfer from steady burner flames impinging on variable temperature surfaces. The results are contradictory. Some have

measured an increase, others have measured a decrease in heat transfer with rising wall temperature. Moreover, flame-wall interaction in diesel engines is a transient phenomenon that is not accurately represented by a steady flame quenching process. Experimental data from transient flame quenching in combustion bombs is available for the cold wall case only. To date there is not a single transient flame quenching experiment where in-cylinder heat transfer is simulated as a function of pressure, wall and gas temperature and level of turbulence in a precisely controlled environment.

A systematic experimental study of flame wall interaction in which engine parameters can be simulated, was proposed. The long-term objectives are to measure the effect of varying wall temperature on heat transfer from head-on impinging laminar and turbulent flames.

The present work represents the first stage of a more comprehensive study yet to come. The objectives of the present work are to:

- Gain experience in the design of experimental apparatus that is capable of simulating IC engine conditions
- Set up ambient temperature and pressure version of laminar flame apparatus and create reproducible conditions for flame-wall, head-on interaction
- Test various diagnostic techniques
- Measure magnitude and phase of heat transfer from head-on impinging laminar flames under atmospheric conditions
- Develop simple models that provide insight into the head-on flame quenching mechanisms

- Compare experimental and model results with those reported in the literature
- Develop the conceptual design for a hot-wall and high pressure combustion chamber

1.3.2 Approach and Project Plan

In the final stage of this project, there will be an apparatus that provides a variable pressure environment, where a laminar and turbulent flame impinging on a variable temperature wall can be studied. However, techniques involving the simple cases of flame quenching must first be mastered in order to provide the technology and insight into the quenching process before proceeding with more complicated cases. In an attempt to reduce the complexity of experiment and analysis, an apparatus was designed that allows the study of interactions between premixed laminar methane-air flames and a cold, head-on wall under atmospheric pressure.

Head-on quenching of premixed laminar flames on cold walls relates to the phenomenon of interest, namely flame-wall interaction in adiabatic diesel engines, as follows:

Combustion Characteristics:

The apparatus is filled with a homogeneous combustible gas mixture prior to ignition so that combustion takes place in premixed manner. In diesel engines, combustion occurs in a sequential manner, consisting of a premixed combustion phase and a mixing controlled combustion phase. During the ignition delay period (the time in between the beginning of fuel injection and autoignition) fuel and air form a readily flammable gas mixture. After autoignition, combustion therefore occurs in a premixed mode with characteristicly high heat release rates. A premixed, turbulent flame front propagates from the location of ignition until most of the premixed gases are consumed and the combustion wave arrives

at the relatively cold walls. Thereafter, combustion is controlled by the rate at which fuel vapor mixes with air. Several processes are involved in the mixing controlled combustion phase: liquid fuel atomization, vaporization of fuel, vapor-air mixing and preflame chemical reactions. This study is restricted to the simulation of premixed flame quenching in order to reduce the complexity of the experimental apparatus and analysis by eliminating the diffusion limited combustion phase and its complex physical processes. Results of this study are expected to qualitatively describe the flame-wall interaction in the first phase of the combustion in diesel engines only.

Orientation of the Combustion Wave During Quench:

The apparatus is designed for the study of laminar head-on impinging flames. As the flame propagates between piston and cylinder head in diesel engines, its orientation remains approximately parallel to the cold surfaces and flame quenching is likely to occur head-on. However, flame quenching in diesel engines typically is a turbulent phenomenon due to in-cylinder swirl. The effect of turbulence on the convective heat transfer coefficient is not accounted for in this first study.

Fuel Choice:

The fuel used is methane. There are several reasons for choosing methane as the fuel. Premixed methane-air mixtures provide a relatively soot-free environment for the study of convective flame-wall heat transfer. Radiative heat transfer due to diffusion burning is eliminated. The detailed reaction mechanism for methane also represents a well validated chemical reaction model. Thus a detailed model of the quenching process can be developed and the experimental results can be predicted accurately over a wide range of conditions.

Pressure and Temperature at Quench:

During flame propagation the unburned gases and flame tube walls remain at ambient temperature and pressure. Devices that are needed to maintain temperature and pressure above atmospheric are eliminated. Flame quenching occurs during the work cycle of diesel engines under fluctuating high pressure and temperature conditions. Various thermodynamic properties and kinetic processes are strongly dependent on temperature and pressure of the system. Therefore, at present, quantitative results can only be given for flame quenching at ambient conditions although the quenching process remains qualitatively unchanged for conditions encountered in LHR engines.

The apparatus specified above provides an environment in which it is possible to study the basic phenomenon of flame-wall interaction without the interference of additional processes such as turbulence, radiative heat transfer, pressure and temperature variation during quench, etc. Within this first stage of the overall project, the plan is to experimentally measure time resolved heat transfer as a function of flame position from normally impinging flames under atmospheric conditions as a function of variable mixture equivalence ratios. Models of the flame quenching process must then be developed that correlate well with experimental data. The models also serve as an analytical tool to gain insight into the flame quenching process. The experience in flame tube design, use of instrumentation and the insight into the quenching process should provide the fundamental basis to proceed with experiments that more closely simulate flame-wall interaction under LHR engine conditions.

2. Experimental Design and Procedures

2.1 Introduction

To achieve measurements of the phase and magnitude of heat transfer from head-on impinging laminar flames under atmospheric conditions, an apparatus was designed based on the concept of flame tubes. Historically, flame tubes were used to measure laminar flame speeds of premixed combustible mixtures. Flame tubes are made from transparent tubes that have an inner diameter greater then the quench diameter. They are filled with a homogeneous combustible mixture and ignited at one end of the tube. A laminar flame then travels through the tube consuming fresh gases until the flame is quenched by a screen or a head-on wall.

The flame tube apparatus features two main components: the vertical flame tube, which is made from Pyrex glass, including filling ports to renew the gas mixture, a motorized exhaust valve, ignition electrodes at the top end and an impingement section at the bottom end. Second is the instrumentation and data acquisition system, including a coaxial surface thermocouple, a solid state monochrome CCD camera, timing electronics and a computer. Reasons for selecting this particular apparatus configuration and a description of the apparatus components and data acquisition system are given below.

2.2 Apparatus

2.2.1 Introduction

The primary function of the apparatus is to support laminar premixed flame propagation and to provide a cold surface at which flame quenching occurs head-on. The specific requirements the apparatus must meet are to:

- provide a precisely controlled, homogeneous gas mixture
- remain at atmospheric pressure throughout flame propagation
- provide a source of ignition
- have a test section long enough for the flame to develop a stable, reproducible structure
- allow optical access to detect flame front positions
- provide a quenching surface with thermocouple insert

A detailed description of the apparatus that satisfies these requirements is given below.

2.2.2 Apparatus Design

An atmospheric combustion chamber was developed specifically for this experiment. The design is based on the concept of flame tubes and consists of a vertical glass tube with a vent to the atmosphere at the upper end and an impingement wall at the lower end. Similar to many traditional flame tube experiments, the apparatus is oriented vertically and the flame propagates downwards in order to prevent buoyancy currents in the unburned gas mixture. The main apparatus components, as shown in Figure 2.1 are:

- flame tube
- motorized exhaust valve at the upper flame tube end.
- orifice and quenching screen
- filling and evacuation ports and spark-ignition electrodes
- impinging element at the lower combustion chamber end with centered surface thermocouple

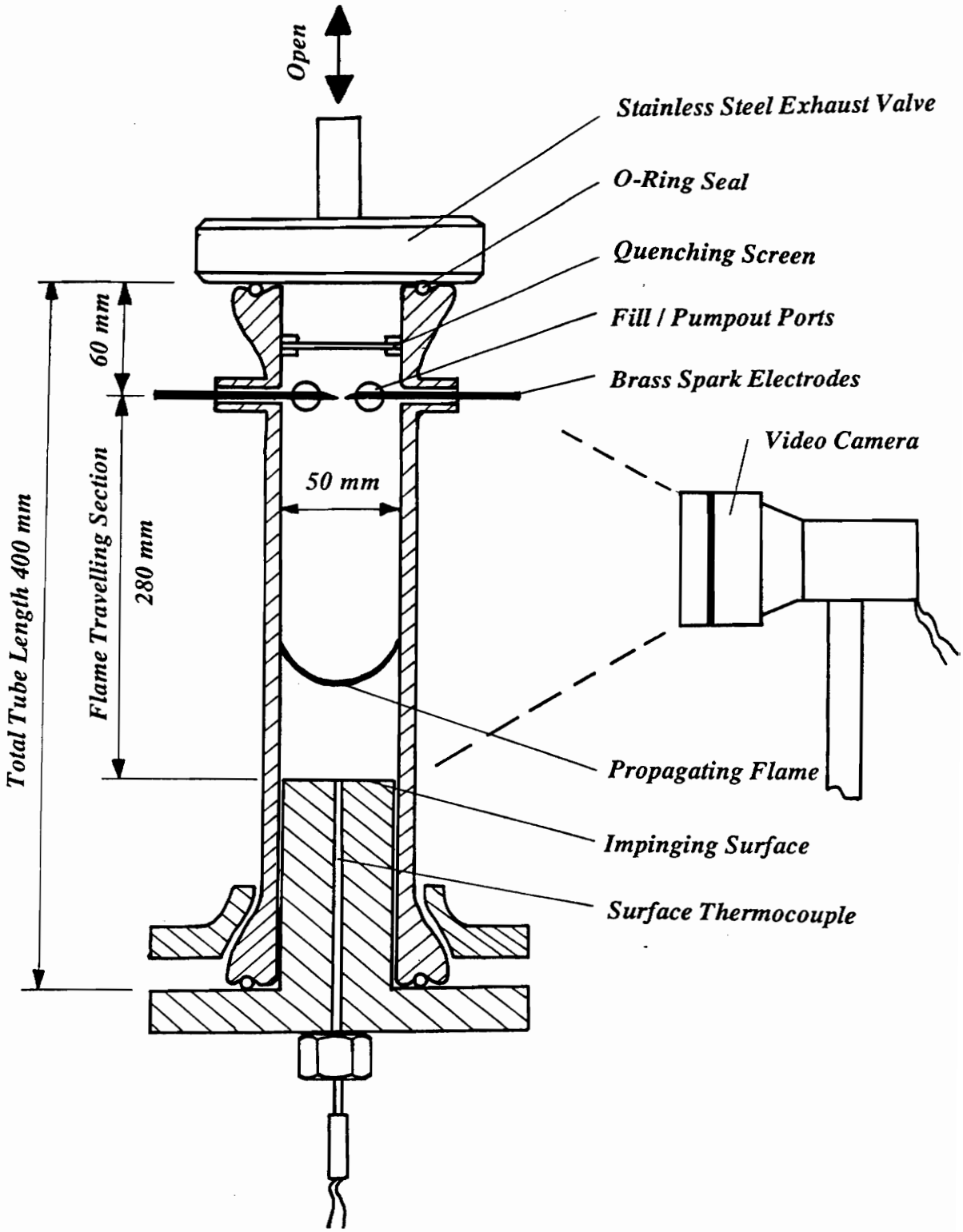

Figure 2.1: Schematic of experimental apparatus

Flame Tube:

The flame tube is the central element of the combustor and supports the development of a laminar structured flame It is made from Pyrex glass, 400 mm long, 50 mm wide and has O-ring seals at both ends. From literature on flame speed measurement, e.g. Coward and Hartwell [17] and Fuller, et al., [18] an inner diameter of 50 mm seemed appropriate to obtain uniform flame movement over some length of the tube.

Motorized Exhaust Valve at the Upper Flame Tube End:

When the stainless steel exhaust valve at the upper tube end is closed, the flame tube is sealed from the environment. The flame tube can be evacuated and filled with the desired mixture of fuel and oxidizer using the method of partial pressures. Shortly before ignition, the exhaust valve is opened by a spindle, which is turned by a small geared DC-motor to allow ambient pressure combustion.

Orifice and Quenching Screen:

A circular quenching screen, made from an aluminum honeycomb structure, is held by retaining rings close to the upper combustor end to prevent open flames external to the combustor. Additional orifices can be installed to affect the pressure drop of the exhaust gases.

Filling and Evacuation Ports and Spark-Ignition Electrodes:

The ports, as shown in Figure 2.2, are located 60 mm below the exhaust valve. Five tubular glass connectors are fused onto the flame tube, serving as gas inlets, evacuation ports and electrode inserts.

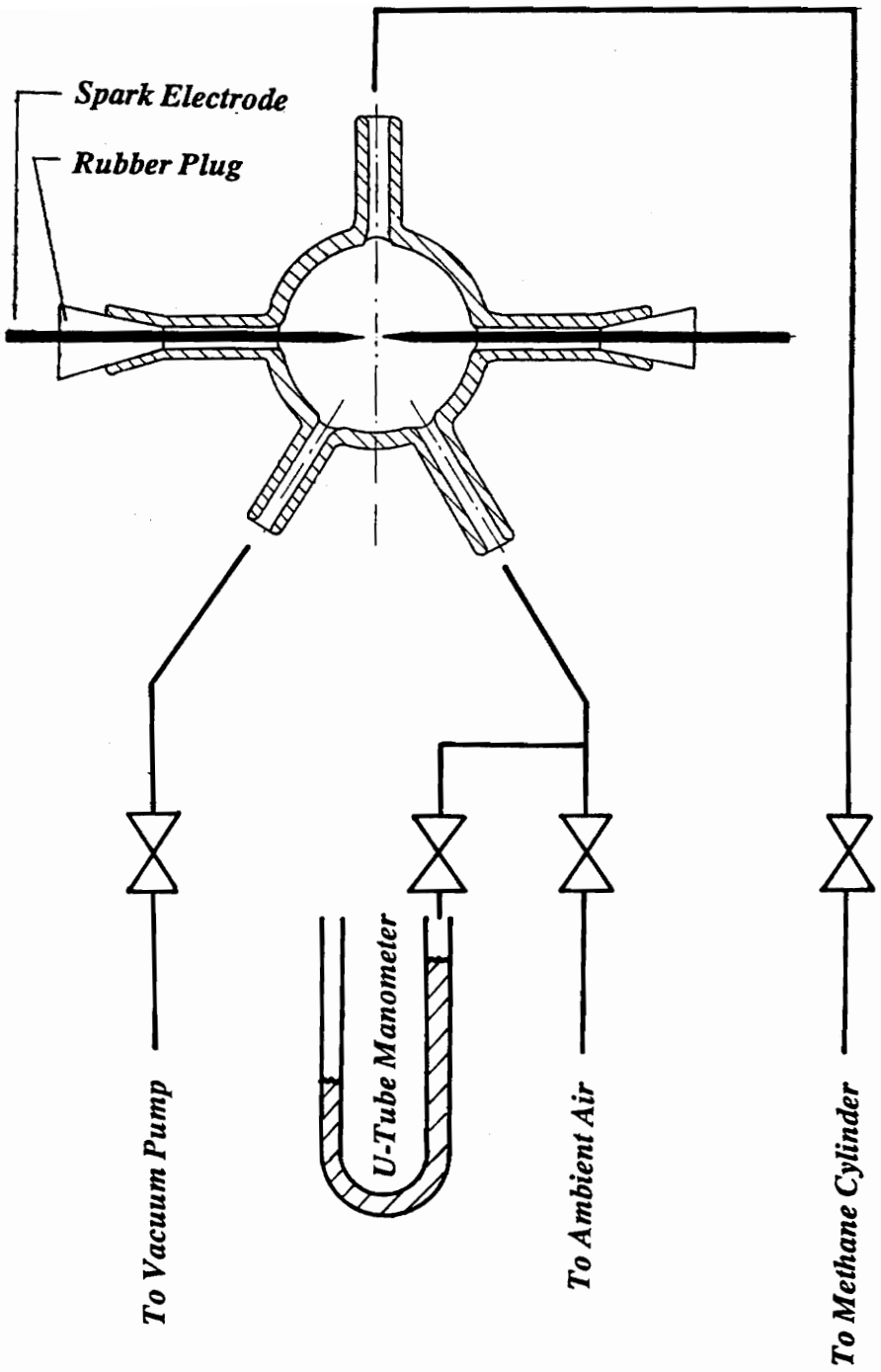

Figure 2.2: Schematic of filling and evacuation ports and gas line connections Impinging Element at the Lower Combustion Chamber End with Centered Surface Thermocouple:

At the bottom end of the flame tube, a coaxial, self renewing chromel-constantan thermocouple is mounted flush into a cylindrical piece of low carbon steel (AISI 4130). Care was taken to match the thermal properties of the thermocouple with those of the surrounding wall. As a result of the momentum and thermal boundary layer in the vicinity of the circular tube wall, the flame front develops a distinct parabolic shape while it is propagating downwards. Since the thermocouple is in line with the flame tube axis, and is small compared to the flame curvature, it is exposed to an approximately one-dimensional temperature field during the arrival of the laminar flame front.

2.2.3 Mixture Control

The flame tube was evacuated before filling the apparatus with a mixture of fuel and oxidizer. A Welch Duo Seal Vacuum Pump, model number 1380 was used for this purpose. The actual in-chamber pressure was monitored by a U-tube type mercury manometer. With silicone vacuum grease applied to all glass-rubber and metal-rubber connections, the chamber is able to hold a pressure of 1 mm mercury over several hours.

The tube was refilled with fuel (commercial grade methane) from high pressure cylinders, and ambient air by partial pressures. According to Dalton's model, the desired stoichiometry is converted into partial pressures of methane and then to mm of mercury, assuming ideal gas conditions. First, the appropriate partial pressure of methane is filled into the chamber by means of a fine needle valve and manometer readings. Second, the ambient air line is opened until manometer readings indicate a balance between atmospheric and in-cylinder pressure. To ensure a homogenous mixture by molecular diffusion it was found necessary to wait at least 30 minutes between the filling process and

ignition. Details about Dalton's model and the determination of appropriate partial fuel and air pressures are given in Appendix A.

2.2.4 Ignition

Ignition of the unburned mixture was provided by two brass electrodes with sharp tips, firing across a 1 mm gap. Once a trigger signal is received, a 13.5 kilovolt, low ampere pulse is released by a DC transformer. The electrodes are mounted into the flame tube by means of rubber plugs and adjusted such that the spark fires across the chamber centerline perpendicular to the flame tube axis.

2.3 Instrumentation and Data Acquisition

2.3.1 Introduction

This section details the diagnostic techniques used to measure the magnitude and phase of flame-wall heat transfer. A fast response surface thermocouple is used to acquire transient surface temperatures of the quench wall. The solution for the temperature field in a one-dimensional, semi-infinite slab with varying wall temperature was used to calculate heat flux. Flame images provide information of the flame structure and flame position during propagation. Temperature measurement and image acquisition are synchronized such that heat flux and flame position form time resolved pairs of information.

2.3.2 Surface Temperature Measurement and Determination of Heat Flux

A Nanmac fast response coaxial chromel-constantan (Type E) surface thermocouple of 1.65 mm diameter is used for the measurement of the time resolved quench wall surface temperature. The thermocouple is mounted flush into the center of the impingement wall

at the bottom of the flame tube. The thermocouple junction of this self-renewing temperature sensor is formed by simply grinding the instrument's surface with sandpaper. The thermocouple signal is amplified with a gain of 500 by a dynamic amplifier, Dynamics serial no. 7526A, and then digitized by a Data Translation 2801A A/D board, driven by the software package PCLAB and operated in the DMA continuous sampling mode to acquire data at its maximum rate of 27,500 samples per second. Thermocouple voltage is converted to temperature data by a FORTRAN program utilizing commonly available conversion charts. The FORTRAN code is provided in Appendix H.

Information about flame-wall heat flux during flame quench is obtained from the temperature history of the quench surface as measured by the surface thermocouple. The fundamental basis for calculating heat flux from transient surface temperatures is considerations of the transient thermal conduction in a semi-infinite, homogenous medium. For a one-dimensional semi-infinite slab with constant properties and specified surface temperature, the heat flux is given by Carslaw and Jaeger [19]

$$q_w''(t) = \left[\frac{k_s \rho_s c_{ps}}{\pi}\right]^{(1/2)} \int_0^t \frac{dT_w(\lambda)}{d\lambda} \frac{d\lambda}{\sqrt{t-\lambda}} \tag{2.1}$$

where λ is the temporal variable of integration. Equation 2.1 shows that the heat flux is a function of the entire surface temperature history and thermal properties of the homogeneous medium. The use of Equation 2.1 requires a semi-infinite, homogeneous medium. From a conduction perspective, the thermocouple insert in the quench wall constitutes a disturbance of the homogeneity. Therefore the quench wall must be treated like a composite medium unless the metal and insert have common thermal properties.

Considering Equation 2.1, the criteria for common materials is

$$\frac{k_{th}}{\sqrt{\alpha_{th}}} = \frac{k_{sur}}{\sqrt{\alpha_{sur}}} \tag{2.2}$$

where index *th* refers to the thermocouple and *sur* to the wall material. For any kind of thermocouple, the requirement of homogeneity can never be fully satisfied, since the thermocouple junction is formed by two different metals. However, the requirement of homogeneity is approximated by matching the outer layer of the coaxial thermocouple (constantan) to its surrounding material. A low carbon steel, AISI 4130, was found to correspond well to the outer thermocouple material made of constantan.

Equation 2.1 is solved for the wall heat flux by the use of a FORTRAN program. The FORTRAN code is provided in Appendix H. Details about the numerical treatment of Equation 2.1 and the properties of the outer thermocouple material (constantan) and solid (AISI 4130) are given in Appendix B.

2.3.3 Transient Flame Images

Images of the traveling flame front are acquired in order to be able to relate heat transfer to the position of the flame front. Initially, it was planned to use either Schlieren or shadowgraph photography to trace the flame movement by means of temperature gradients. An optical system was set up, consisting of a pulsed light source, two mirrors to generate a collimated beam of light, and a camera to obtain multiple exposure flame images. However, the circular flame tube did not support a collimated light beam within the test section, therefore this diagnosis technique was abandoned.

Alternatively, a Cohu Solid State Monochrome CCD Camera model 6400, equipped with a Tokina 28 mm focal length lens is used to trace flame movement. The camera is

mounted perpendicular to the direction of flame movement 1.3 m from the flame tube apparatus (see Figure 1). Luminous images of the propagating flame from ignition to extinction are acquired and recorded onto VHS tape by a Canon four-head video recorder, serial number VR-40A at a rate of 60 fields and 30 frames per second. Once on video tape, the progressing flame was displayed frame by frame on a television screen. Physical distances of the progressing flame front to the wall are read from a luminous scale, which also appeared in the images. The illuminated scale is made from a fluorescent light housing that is painted black and marked with 2 mm divisions. The best images of the luminous flame front are obtained with a shutter speed of 1/2000 second.

With the above technique, a total of 20 to 40 data points of the flame movement are acquired, spaced 1/30 of a second apart in time. Unfortunately it was not possible to obtain higher resolutions of the flame at quench. A high temporal and spatial resolution of the flame at quench would yield more information about the quenching distance.

2.3.4 Synchronization of Heat Flux and Image Acquisition

It is necessary to specify the amplitude and phase of heat transfer in order to describe the interaction of reacting boundary layers with walls. In other words, the flame position with respect to the quench surface and the transient heat flux signal must be synchronized in time. This is accomplished by means of position switches, TTL timing electronics and visual devices that are displayed in the camera field. Details of the electronic timing procedure are discussed in Appendix C.

2.4 Data Processing

2.4.1 Introduction

So far, the experimental techniques to measure flame position and surface temperature have been discussed. In order to obtain information about flame speed and the magnitude and phase of heat transfer the raw experimental data must be processed. Therefore, several procedures are developed.

In the following section a distinction is made between several flame speeds. The fundamental adiabatic flame speed, S_u^a is defined as the velocity of the unburned gases through the combustion wave in the direction normal to the wave surface under adiabatic conditions. The flame burns with adiabatic flame temperature T_f^a and the heat of reaction entirely contributes to the enthalpy of the exhaust gases. Obviously, while propagating in the flame tube, the flame experiences heat loss to the glass tube and only part of the reaction energy is transferred to the gas stream. Therefore, experimental flame temperature T_f^e is lower than the adiabatic flame temperature T_f^a. In the flame tube apparatus, the flame surface assumes a parabolic shape leading to a flame area greater than the tube cross section. Since the reaction surface of a flame front in the flame tube is enlarged compared to a flat flame surface, the experimental flame speed S_u^e is greater than the adiabatic flame speed S_u^a. However, with a procedure that accounts for the difference in flame surface compared to the flame tube cross section it is possible to determine the (corrected) flame speed S_u^c, at which the flame in the experiment would travel if it had a flat surface. On the basis of the corrected flame speed S_u^c, a comparison to adiabatic flame speeds from the literature is possible, although the corrected flame speed is slightly lower then the adiabatic flame speed S_u^a due to heat transfer to the side wall during flame propagation.

The procedures used to determine experimental flame speeds S_u^e , corrected flame speeds S_u^c , and the phase of heat transfer are discussed in the following section.

2.4.2 Determination of Flame Speed

This section details the procedure used to calculate the experimental flame speed from flame position data. Flame images are acquired by means of a video camera and recorded to tape in sequences of 30 frames per second. On a position-time diagram, all data points must fall on a straight line if the flame has traveled at uniform speed. The slope of this line constitutes the flame speed.

It was observed that flame movement is not uniform from ignition to quench. The flame requires up to half the total tube length to reach a steady-state flame speed. At positions very close to the cold wall at the bottom end of the tube the reaction rates are slowed by heat loss to the head-on wall and the flame decelerates. In order to capture the speed of uniform flame movement in an area where the flame front is fully developed but not yet affected by the presence of a wall, the slope of the line, fitted through five points previous to, but omitting the two points closest to quench, is calculated.

2.4.3 Determination of the Corrected Flame Speed

Flame tubes have long been discarded as means to determine the fundamental speed of uniform movement because it is difficult to account for the flame curvature and heat loss to the tube walls. More contemporary ways of making adiabatic flame speed measurements are the flat flame burner method or the soap bubble (constant pressure) method. However, speeds of laminar flames in tubes can still be used as an indication of S_u^a on the basis of following relationship:

$$S_u^{\,c} = \frac{A_{tube}}{A_f} S_u^{\,e} \tag{2.3}$$

where $S_u^{\,e}$ is the flame speed from flame tube measurements, $S_u^{\,c}$ refers to a perfectly flat, and therefore, truly one-dimensional flame front. Equation 2.3 is valid under the assumption that each segment of the curved flame front in a tube consumes an equal amount of the unburned gas mixture. Since the tube cross section A_{tube} is smaller than the flame surface A_f, the corrected flame speed $S_u^{\,c}$ must be smaller than the experimental flame speed $S_u^{\,e}$. The corrected flame speed is expected to be slightly lower than the speed of a flame that propagates in a truly adiabatic environment, $S_u^{\,a}$. On the basis of corrected flame speeds $S_u^{\,c}$, it is possible to validate the experimental results by a comparison to adiabatic flame speeds from the literature.

The surface area of the experimental flame front is determined as follows: the shape of four consecutive flame images close to quench are transferred from the TV screen onto a custom-made transparent scale. Half of the averaged two-dimensional flame curvature, reaching from the tube centerline to the flame tube wall, is approximated by a cubic spline. This spline is then rotated around the tube axis and the surface area of the rotationally-symmetric body is calculated.

The flame area A_f is approximated by averaging several flame images and assuming a rotationally-symmetric flame shape. In reality, flames sometimes are not rotationally symmetric and vary considerably in shape from frame to frame. Copying flame shapes from a TV screen onto a transparent scale is not a very precise procedure. Therefore, the technique is necessarily crude, and the error associated with the measurement of flame surface areas may be as high as ±10%.

2.4.4 Time Reference

In Appendix C, the timing electronics used to synchronize temperature measurements and flame image acquisition are discussed. The time reference is arbitrarily established by a system trigger in the early stage of flame propagation. However, is more meaningful to measure time with regard to a significant event. This event was chosen to be the instance where the maximum heat flux occurs. The times recorded by the instruments are recalculated by a FORTRAN program to relate to this event. Numbers smaller then zero refer to times prior, and numbers greater than zero refer to times subsequent to the occurrence of the peak heat flux.

2.4.5 Phase of Heat Transfer

One would wish to have information about the time resolved heat transfer with respect to the time when the flame is closest to the wall. Information about flame-wall distance is acquired in sequences of 1/30 second only. While one data point shows a freely traveling flame that is not affected by the presence of a wall, the following data point indicates that the flame has already been quenched. Thus, the instance where the flame is located closest to the wall cannot be determined because the image acquisition rate is too low.

However, information about the time dependence of heat transfer on flame position is provided by calculating the time lag between the instance where the flame would impinge at the wall if it had continuously traveled at uniform speed, and the occurrence of the peak heat flux. The idealized time of flame impingement is determined by the intersection of the extrapolated flame position line with x=0 in the time-distance diagram.

2.5 Flame Propagation

2.5.1 Introduction

The manner in which the flame propagates down the flame tube is an important parameter to this experiment for several reasons:

The heat flux is calculated from the temperature history of the transient surface temperature assuming one-dimensional heat conduction (see Section 2.3.2). Such one-dimensional conditions are satisfied by a flame front that approaches the thermocouple with the maximum of its semi-ellipsoid curvature. Suppose a flame front has developed such that the maximum of its curvature is off the flame tube centerline and does not approach the fine surface thermocouple head-on. Temperature gradients in the vicinity of the surface thermometer are no longer one-dimensional and the mathematical model that is employed to calculate heat flux for a one-dimensional, semi-infinite medium fails. In the procedure developed to calculate the flame surface area (see Section 2.4.3), the flame shape is approximated by a rotationally symmetric surface. If a flame surface develops a cellular or uneven structure this approximation is not valid.

Thus, for the validity of the experimental methods and reproducibility of the experimental data, the flame must propagate in a stable, laminar manner. However, various flame instability phenomena were encountered in the first version of the flame tube apparatus and were systematically eliminated in subsequent design changes. This section provides a description of some of the flame instability phenomena and a discussion of the flame tube design changes.

2.5.2 Flame Stability

Ever since Coward and Hartwell [17] introduced the flame tube technique for flame speed measurements in 1932, many researchers have encountered instability phenomena of flame propagation in tubes. A survey of the literature reveals that the disturbances of propagating flame fronts may be caused by the following three mechanisms:

- selective diffusion
- spontaneous acoustic instabilities
- ignition induced pressure waves

Selective Diffusion:

Selective diffusion is an instability phenomenon characterized by the spontaneous break-up of flames in tubes, or by the formation of cells of polyhedral structure in premixed burners. The selective diffusion phenomenon was first encountered by Bubnoff [20]; he sampled exhaust gases of a premixed stoichiometric benzene-air flame above a burner and found that samples taken from the flame tip correspond to a rich mixture whereas samples taken from the sides of the cone correspond to a lean mixture. Coward and Brinsley [21] burned a hydrogen-air mixture near the lean limit in a flame tube. The flame front frequently broke up into a number of small filaments. An explanation for the above phenomena was given by Goldmann [22]: near the lean limit, combustion is maintained by diffusion. Compared to oxygen (in air), hydrogen (in air) has a much higher binary diffusion coefficient, thus causing a converging diffusion stream of hydrogen towards certain spots where the enriched mixture is burned. Concentration gradients towards those spots are created by the inter-diffusion of combustion products into the unburned mixture. Markstein [23] found that spontaneous distortion of premixed flames due to

selective diffusion occurs when fuel and oxidizer have different diffusion coefficients with respect to the diluent.

Spontaneous Acoustic Instabilities:

Instabilities of a complex nature occur in any flow system capable of resonance oscillations. According to Markstein [23], the acoustic vibration is longitudinal (i.e., along the axis of the flame tube), with a frequency close to an eigenmode of the tube and is caused by a feedback coupling between the temperature variation in an acoustic wave and flame structure. These vibrations give rise to abrupt changes in flame shape and oscillatory movement of the flame front as a whole.

Ignition Induced Pressure Waves:

Guenoche [24] has observed a phenomena that is related to the ignition of the unburned gas mixture and describes it as follows: upon ignition, a pressure wave is formed due to the rapid expansion of gases. The pressure wave is reflected at the closed end of the tube and returns towards the propagating flame, which has already moved a small distance downstream. When the compression wave hits the flame front, part of it is reflected into the fresh gases, and part of it is transmitted to the combustion products. For an instant, a stream of unburned gases (usually at rest) is directed towards the flame front, causing an oscillation of the flame and the burned gas column.

The part of the pressure wave which has been reflected into the unburned gases might undergo additional successive reflections between flame and wall, and thus be a continuous, although weakening source of disturbance. The flame front can propagate in a medium at rest only when the initial pressure wave is damped.

Guenoche [24] suggests impeding the downward propagation of pressure waves by means of an orifice installed at the ignition end of the flame tube. He provides a formula to calculate the ratio of orifice opening to tube cross section in order to raise the unburned gas pressure, and thereby damp the pressure waves over a shorter time period.

2.5.3 Flame Tube Design Changes

The current flame tube configuration has emerged from a series of design iterations. The first flame tube apparatus was made from a Pyrex glass tube of 50 mm inner diameter and 660 mm length. Two spark electrodes were inserted about half-way between the exhaust at the upper end and the closed quenching section at the lower end. Sparks were fired continuously during flame propagation due to a manually operated (push button) high voltage power supply. The following flame propagation phenomena were observed by combusting premixed methane-air mixtures ranging from stoichiometric ratios between $\Phi = 0.7$ (lean) and $\Phi = 1.4$ (rich):

A spherical flame surface propagated outwards from the point of ignition until it arrived at the cylindrical flame tube walls. Upon arrival at the wall, the flame front was divided into two parts; one part propagated downwards through the unburned mixture towards the closed tube end at a low speed, and the other part was rapidly pushed out of the exhaust end by the low density combustion products of the flame below.

The descending flame was shaped differently for lean, near stoichiometric and rich mixtures. Lean flame fronts developed a distinctly cellular structure; about a dozen polyhedral shaped, equally sized and spaced flame cells formed a flame sheet that

propagated at uniform speed throughout the mixture. Flame propagation was accompanied by an audible tone with slightly decreasing pitch as the flame approached the bottom end of the flame tube. At near stoichiometric mixtures, the fresh gases were consumed by an undifferentiated, highly turbulent flame almost instantaneously over the whole tube length. The combustion process was accompanied by a loud "pop" as if compressed air was being rapidly released. At rich mixtures, a slow burning, axi-symmetric flame sheet propagated downwards until it was quenched. The flame structure at rich mixtures can be characterized as laminar at all instances during propagation. The sound produced as the rich flame propagated was similar to that of the lean flame.

Except for rich mixtures, flame propagation was unsatisfactory with the early version of the flame tube. In order to improve the flame structure, the design of the apparatus was changed. Spark ignition was suspected of introducing pressure waves due to the rapid expansion of the hot gases between the spark electrodes. Therefore the ignition source was changed to a gradually heated platinum wire. A DC power pulse was controlled by means of a TTL circuit such that the energy released was sufficient to ignite the gas mixture without melting the platinum wire. However, flame propagation appeared to be unaffected by this modification. A slight improvement of the flame structure was achieved using spark electrodes with a power pulse of short duration. The manual push button that was formerly employed to initiate and terminate the power pulse was replaced by a TTL timing circuit. By means of this circuit, the power pulse duration was adjusted to allow only one spark to break the resistance of the gas mixture between the electrodes.

In order to improve the flame structure further, Guenoche's [24] suggestion to install a flow restriction and thereby damp pressure waves was followed. An orifice was installed

at the exhaust end of the combustor reducing the exhaust outlet diameter from 50 mm to 15 mm. Although the noise that was previously associated with flame propagation was eliminated, the installed orifice did not visibly improve the flame structure.

It was felt that the location of ignition along the vertical flame tube axis may be associated with acoustic instabilities. In order to eliminate the upwardly propagating flame, the spark electrodes were moved closer to the exhaust end. The total tube length was reduced to 400 mm, and the electrodes were inserted 60 mm below the upper flame tube end. This modification significantly changed the flame structure of the propagating flame front. Except for lean mixtures with equivalence ratios below $\Phi \leq 0.8$, the flame developed into an even and axi-symmetric structure during propagation. The distance needed to damp out ignition-induced disturbances was dependent on the equivalence ratio of the gas mixture. Rich flames developed a stable flame front immediately after ignition, whereas lean flames very slowly approached a uniform speed of movement. In all mixtures of equivalence ratios between $0.8 \leq \Phi \leq 1.4$, flame propagation was always stable within the last 50 mm prior to flame extinction. Lean flames below Φ=0.8 propagated with a distinct cellular flame surface through the entire tube. According to Markstein [23] the cellular structure of methane-air flames near the lean flammability limit is caused by the selective diffusion phenomenon. Since selective diffusion is a physical process that is not dependent on the flame tube geometry, lean mixtures below Φ=0.8 were excluded from all further investigations.

Thus, by means of systematic design alterations, a flame tube apparatus was developed that supports laminar, stable flame propagation for mixture equivalence ratios between

$0.8 \leq \Phi \leq 1.4$. Flames in mixtures with $\Phi \leq 0.8$ show a lack of stability and had to be excluded from experimental conditions.

2.6 Experiments

2.6.1 Introduction

The objective within the experimental part of this study is to measure heat transfer from laminar flames impinging on cold walls. The apparatus, experimental techniques and the data processing procedures are described previously. This section details the experimental conditions and the experimental procedure.

2.6.2 Experimental Conditions

The flame tube apparatus is designed to support ambient pressure and temperature combustion. The independent variable in this experiment is the fuel-air ratio of the combustible methane-air mixture. In general, the flammability limits for methane are 5-15 percent fuel in air. The flammability limits in this specific combustor as experimentally determined are $0.65 \leq \Phi \leq 1.4$, which corresponds to 7.3 - 12.8 volume percent methane in air. A set of flame speed and heat transfer data was collected for mixtures $0.8 \leq \Phi \leq 1.4$ in increments of 0.1.

2.6.3 Experimental Procedure

The procedure to run experiments consists of the following steps:

1. The atmospheric pressure is read from a barometer next to the experiment.
2. The partial pressures of the methane and air (in terms of mm mercury) of the desired mixture are calculated.

3. The flame tube is evacuated.
4. Methane is throttled into the flame tube until a certain partial pressure is reached.
5. A toggle valve to the ambient air is opened until the internal tube pressure is in equilibrium with the ambient pressure.
6. The filled tube is left for forty minutes for diffusional homogenization.
7. The timing unit is reset and the A/D board is prepared to start DMA sampling on the trigger.
8. The VCR is switched to the recording mode.
9. Normal operation of all circuits is checked by a digital oscilloscope.
10. The exhaust DC motor is activated to lift the exhaust valve.
11. The trigger is released by a position switch, then the spark is fired and the delay circuits are activated.
12 At the end of the experiment, data processing programs are run and the recorded images are viewed frame by frame to measure flame-wall distances.

2.7 Sources of Error

Several sources of experimental error are identified and their effects on heat flux, equivalence ratio and flame speed is discussed within this section. Possible sources of errors are associated with:

- impurities in the fuel
- flame position measurements using flame luminosity
- the determination of flame surface areas from two-dimensional flame images
- the non-homogeneity of impingement wall material

Impurities in the Fuel:

The fuel used is commercial grade methane. According to the manufacturer's specification (Air Products Inc., Allentown, PA) commercial grade methane contains a minimum of 93% methane, a maximum of 7% ethane (C_2H_6), a maximum of 50 ppm water and a maximum of 30 ppm oxygen. The filling process of the flame tube with a fresh combustible gas mixture involves the determination of partial pressures for fuel and air as described in Appendix A. Since ethane consumes 1.75 times more oxygen than methane (assuming all reactants are converted to CO_2 and H_2O), the mixture equivalence ratio my be shifted towards fuel-rich. Calculations have shown that the offset in equivalence ratio may be up to a maximum of 5.05% if the fuel consists of 93% methane and 7% ethane.

Flame Position Measurements using Flame Luminosity:

The instantaneous flame position with respect to the quench wall is determined by comparing the location of the bright flame front with a luminous scale as described in Section 2.3.3. Due to image acquisition with a commercial VHS recorder, the flame on the TV screen appears blurred, exaggerating the flame thickness. The uncertainty associated with the flame position measurements is estimated to be ±0.5 mm. This uncertainty is expected to produce less than a 1% error in flame speed and time lag since the data processing process involves the least square fitting of several flame position data points.

Determination of Flame Surface Areas from Two-Dimensional Flame Images

Corrected flame speeds are determined by the ratio of flame surface area to tube cross section. The shape of four consecutive flame images are transferred onto a custom-made

scale and approximated by a cubic spline. Half of the spline is then rotated around the tube centerline and the area of the rotational surface is calculated (see Section 2.4.3). However, flames are not always perfectly rotationally symmetric as assumed in the above procedure, and blurred flame images make it difficult to identify the exact flame shape. Thus, real flame surface area may deviate from the calculated quantity by an estimated ±10%.

The Non-Homogeneity of Impingement Wall Material

Information about flame-wall heat flux during flame quenching is obtained from the temperature history of the quench surface as measured by the surface thermocouple. In order to validate this procedure, the quenching surface should be a semi-infinite homogeneous medium. It follows from the discussion in Section 2.3.2 that the requirement of homogeneity cannot be satisfied if a thermocouple is to monitor surface temperatures. Assanis and Badillo [25] have developed a numerical model to estimate the effect of small differences in thermal properties between thermocouple elements and wall material on transient heat flux measurements in IC engines. It follows from Assanis and Badillo's [25] numerical study that for the thermocouple design used in this experiment (1.65 mm outer diameter type E thermocouple mounted in AISI 4130 low carbon steel) the error introduced by the impingement wall non-homogeneity is negligible small. The results of Assanis and Badillo [25] from which this conclusion is drawn are presented in Appendix B.

3. Experimental Results

3.1 Introduction

The experimental results from this study are the wall heat flux and flame speed of a planar, premixed, laminar methane-air flame. Using the apparatus described in Chapter 2, heat flux and flame speed data are obtained over a range of mixtures, ranging from $\Phi = 0.8$ to $\Phi = 1.4$ in increments of 0.1. The experimental runs are identified by their equivalence ratio. Because the run to run variation is quite considerable, experiments at each mixture composition are repeated at least three times. The table in Appendix F illustrates how the experimental data is organized.

A description of the events is given in Section 3.2, followed by the experimental results of flame speed in Section 3.3 and heat flux in Section 3.4 . Following the suggestion of Vosen [26], the experimentally measured heat flux is non-dimensionlized in order to account for the change in heat release and flame speed with equivalence ratio. The non-dimensional representation of experimental data is given in Section 3.4.2. A table containing the numerical values of the experimental results is provided in Appendix E.

3.2 Description of Events

In Figures 3.1a, 3.1b and 3.1c, flame position, wall temperature and heat flux are shown over the course of an experiment for a lean, a stoichiometric and a rich mixture respectively. The flame is ignited at a position 30 cm above the tube end. The flame front develops its distinct curved shape and reaches a uniform speed of movement after it has propagated through the top part of the flame tube. The traveling distance needed to reach a steady flame velocity generally is on the order of 5-10 cm; except rich flames, which

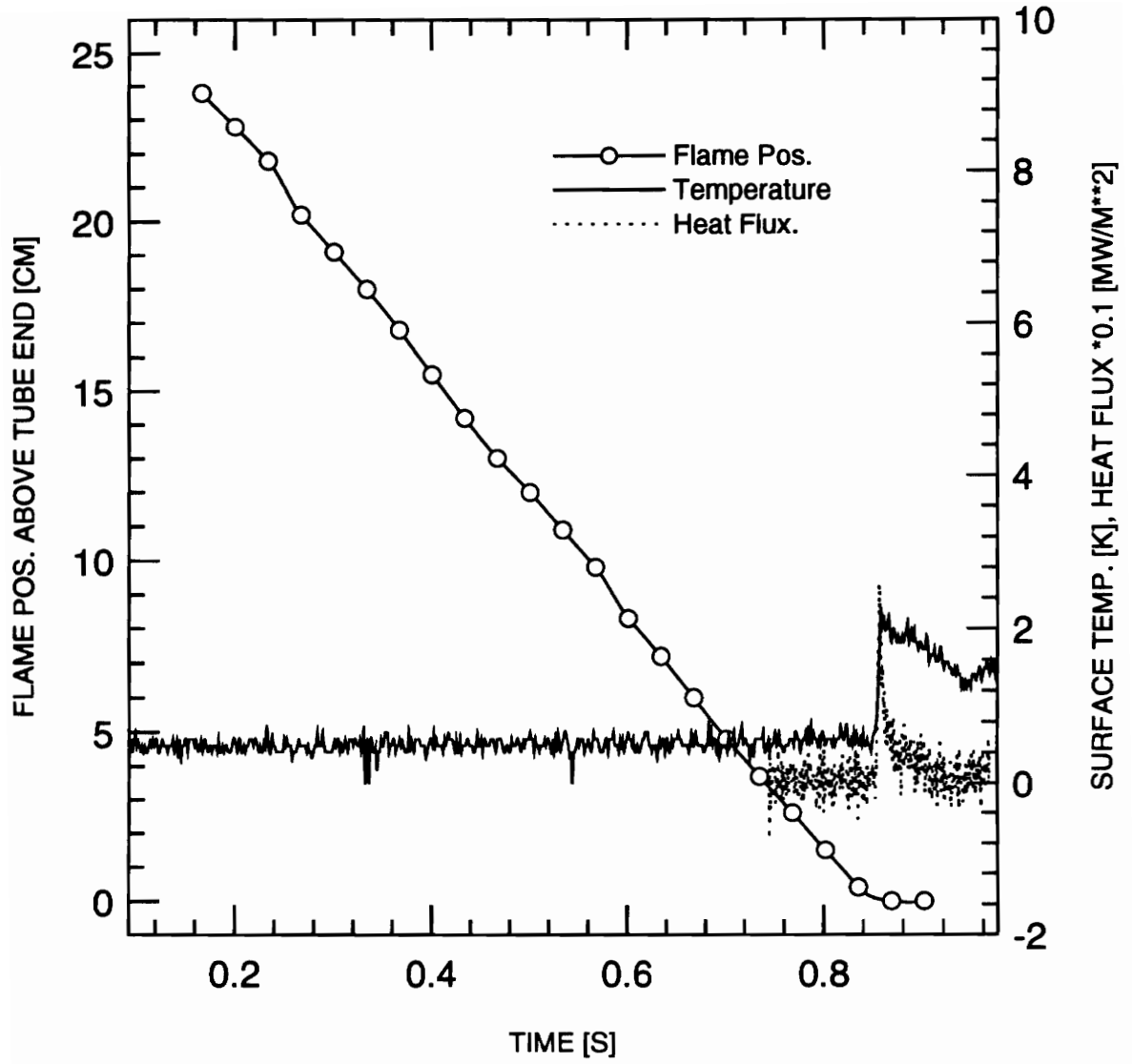

Figure 3.1a: Flame position, wall temperature and heat flux for $\Phi = 0.8$ measured from arbitrary time reference.

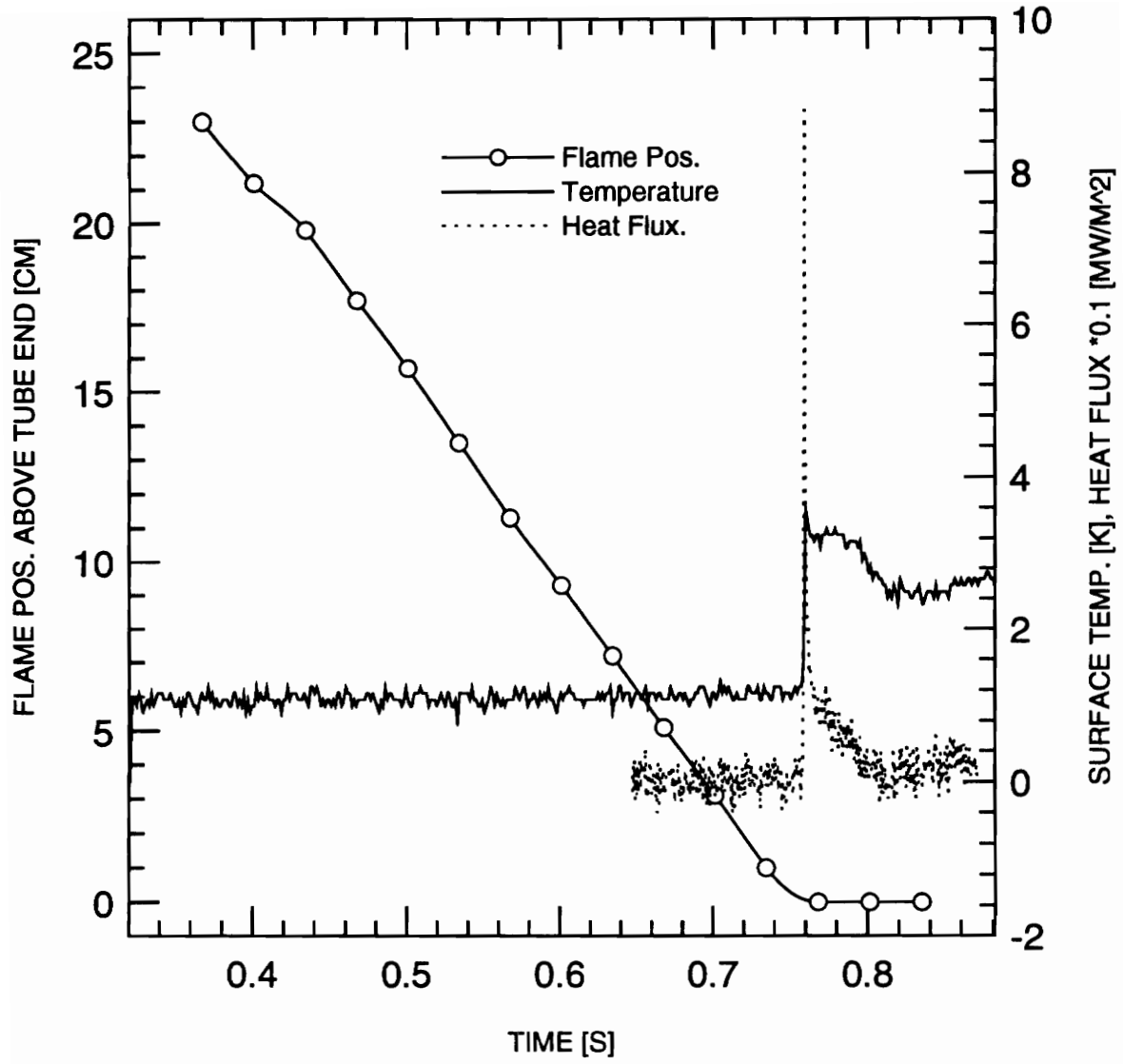

Figure 3.1b: Flame position, wall temperature and heat flux for $\Phi = 1.0$ measured from arbitrary time reference.

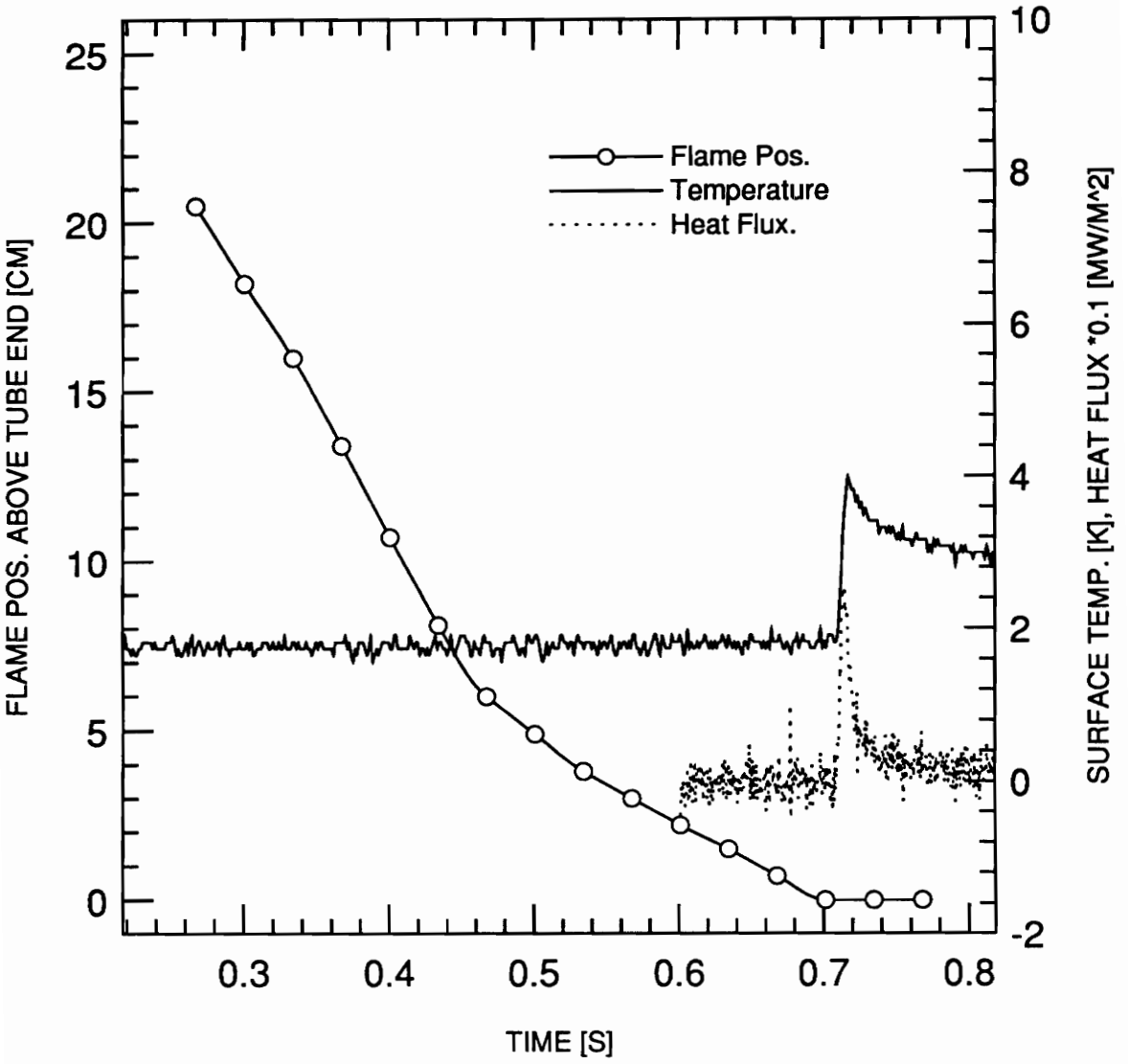

Figure 3.1c: Flame position, wall temperature and heat flux for $\Phi = 1.4$ measured from arbitrary time reference.

tend to more slowly approach uniform speed as they propagate towards the bottom of the flame tube (see Figure 3.1c). Experimental runs, in which the flame has not reached uniform speed at least 5 cm above the wall, were rejected.

Far away from the cold wall, the flame speed and heat release in the flame are not affected by the wall. Closer to the wall, the wall heat flux increases and eventually a position is reached where the heat loss is so great and the flame can no longer progress. The deceleration period of flame movement cannot be acquired because the framing rate of the camera is not sufficiently high to capture the flame during quench. It follows from theoretical calculations (e.g. Westbrook, et. al. [14]) that the flame front remains stationary at the quenching distance for a short period of time, during which combustion is maintained by diffusion of the quenching layer fuel towards the reaction zone. The wall temperature rises rapidly and the heat flux reaches a maximum. As the quenching layer fuel content is consumed, the heat flux decreases.

Figures 3.2a, 3.2b and 3.2c are enlarged sections of a lean, a stoichiometric and a rich flame, respectively, at quench, where the time (abcissa) is given relative to the occurrence of the maximum heat flux. A straight line (least square) is fitted through the five flame positions prior to, but omitting the two positions closest to quench, from which the flame speed is calculated. The difference between the point where this fitted line reaches the wall (x=0) and the occurrence of the maximum heat flux is referred to as the idealized time lag.

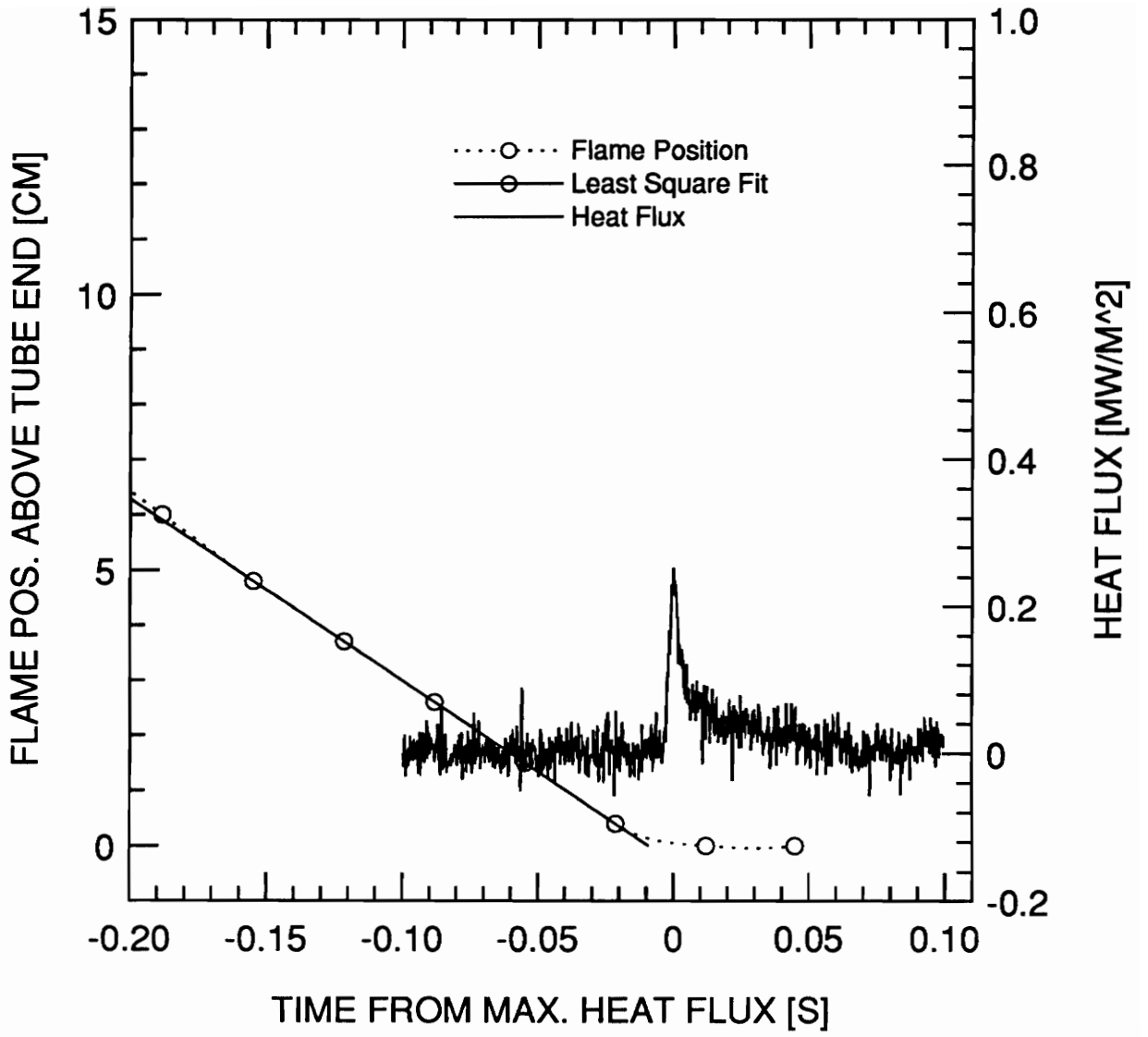

Figure 3.2a: **Flame position and heat flux for $\Phi = 0.8$ during flame quenching, time relative to the occurrence of maximum heat flux.**

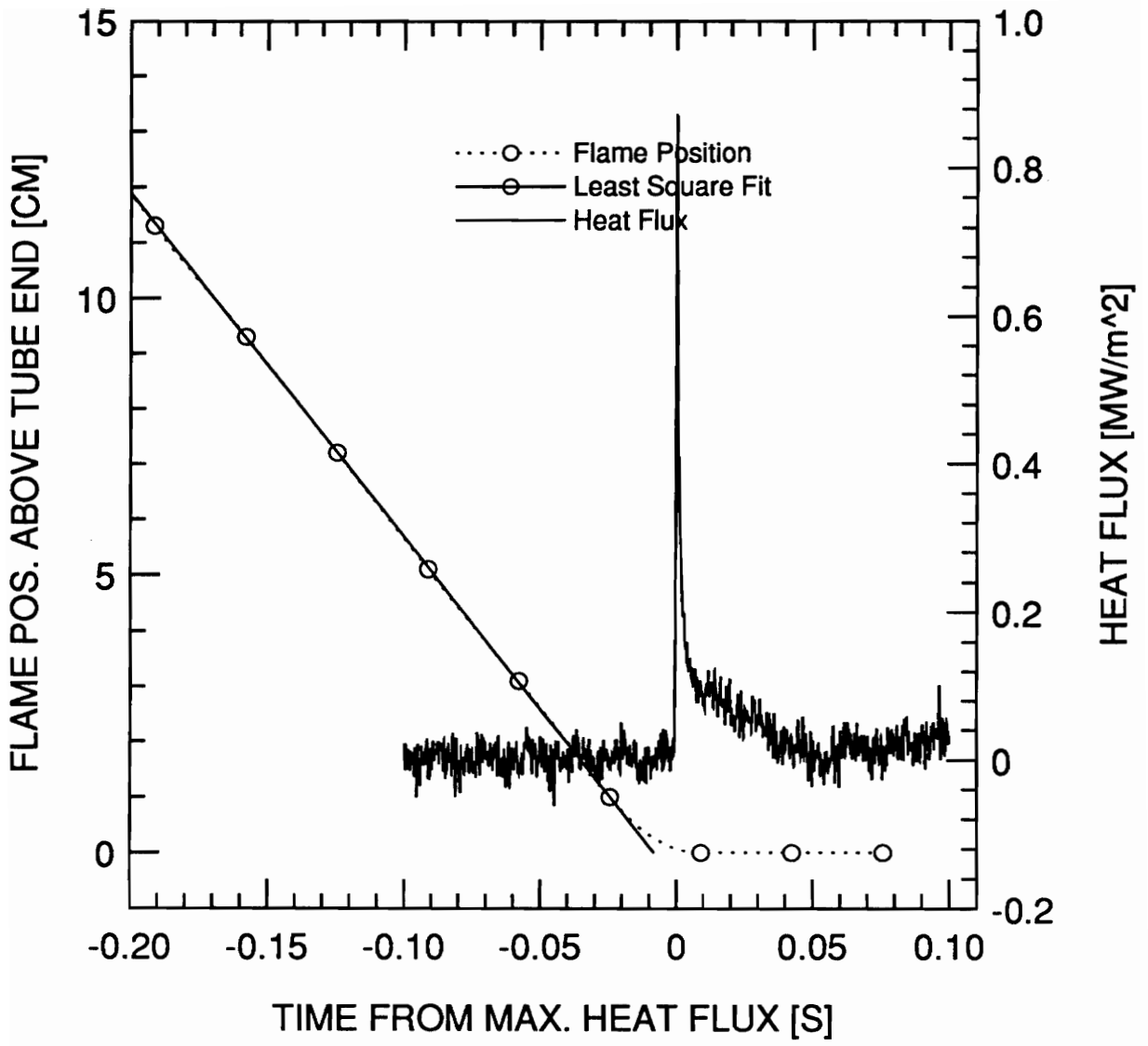

Figure 3.2b: Flame position and heat flux for $\Phi = 1.0$ during flame quenching, time relative to the occurrence of maximum heat flux.

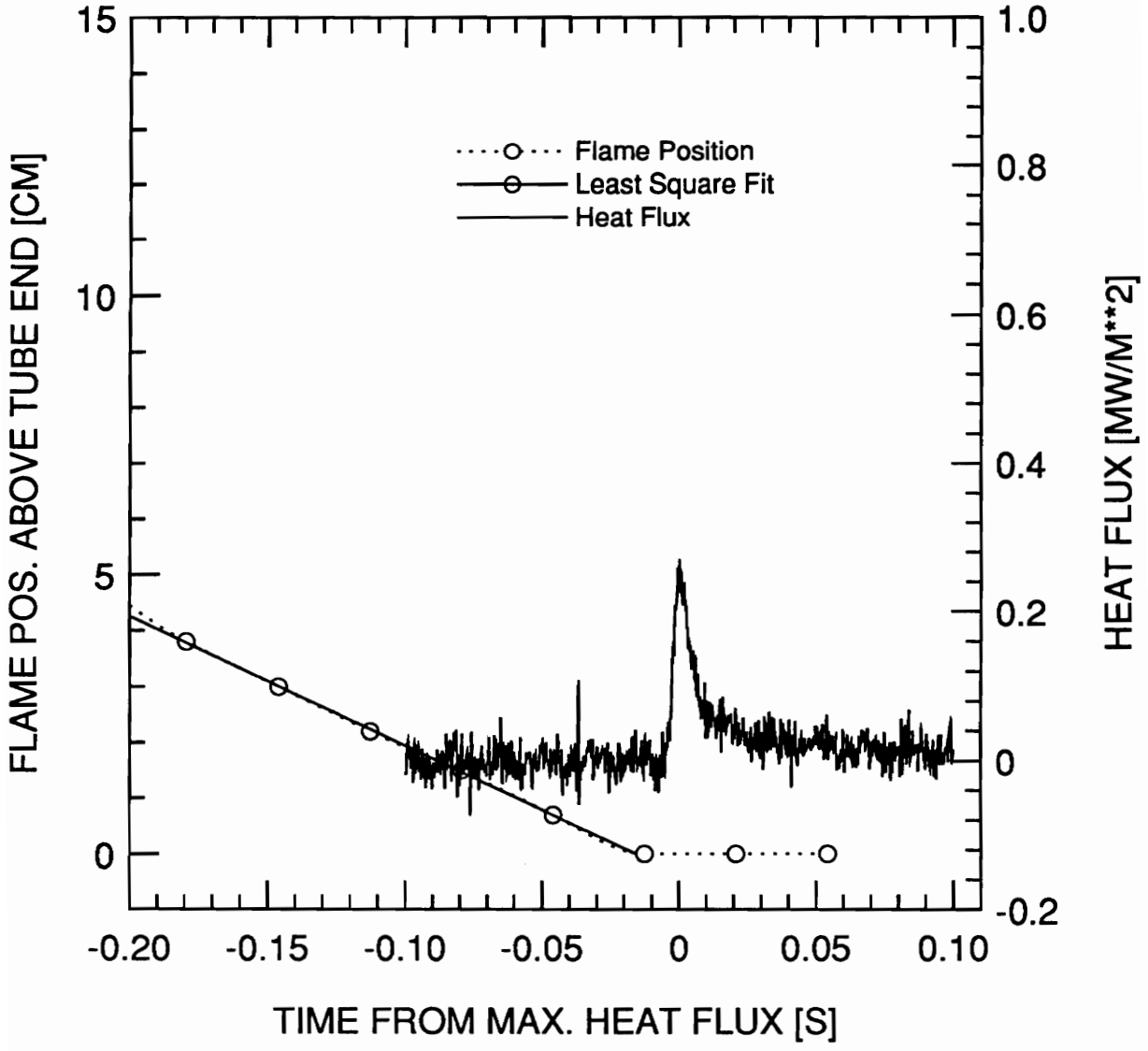

Figure 3.2c: **Flame position and heat flux for $\Phi = 1.4$ during flame quenching, time relative to the occurrence of maximum heat flux.**

3.3 Experimental Flame Speed

3.3.1 Results

Flame speeds as experimentally determined at various equivalence ratios are given in Figure 3.3. Run to run variations of flame speeds for the same mixture equivalence ratio are as high as 20% of the absolute value. The variation of flame speed with equivalence ratio is found to be well represented by a fourth order least square polynomial fit with coefficients as listed in Figure 3.3. The flame speed has a maximum near stoichiometric ($\Phi = 1.05$) and decreases for leaner and richer mixtures.

The (corrected) flame speed at which a flame would travel if it had a flat surface, S_u^c, is calculated from the experimental flame speed by means of a surface area ratio between flame front area and tube cross section (the procedure is discussed in Section 2.4.3). The dependence of S_u^c on the mixture equivalence ratio is also shown in Figure 3.3. The data is represented by a fourth order least square fit. Lower than fourth order curve fits do not represent the data well, and higher order curve fits are unnecessary as the fourth order curve fit is adequate. As expected, the corrected flame speeds are lower and follow the trend of the experimental flame speeds.

3.3.2 Comparison of Flame Speed to Literature

In order to validate the experimental results, a comparison between corrected flame speeds S_u^c and literature results is given in Figure 3.4. Brassin, et al., [27] have measured the speed of methane-air flames in a vertical flame tube. Egerton and Lefebvre [28], have measured the speed of methane-air flames in a horizontal 2.5 cm square tube. Brassin, et. al. [27], and Egerton and Lefebvre [28], have corrected the experimentally measured

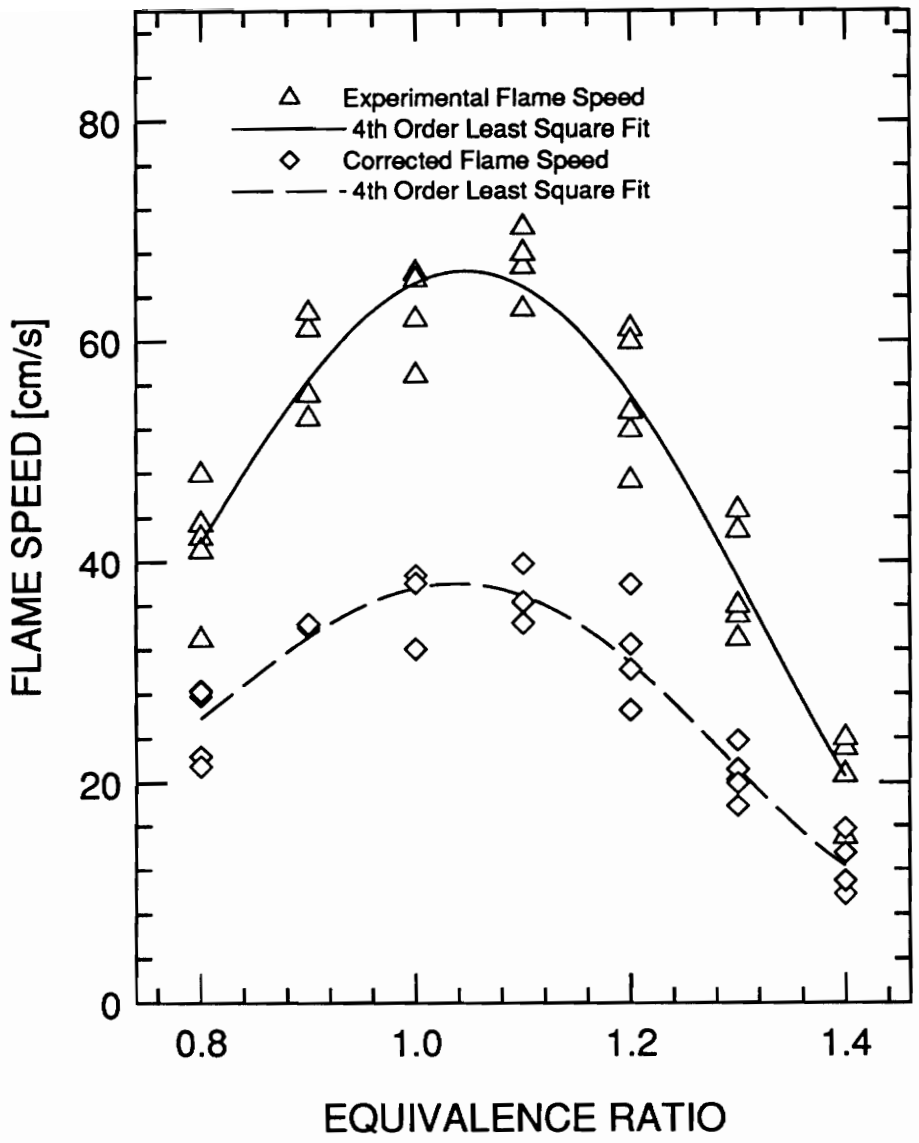

Figure 3.3: **Experimental and corrected flame speed versus equivalence ratio. Coefficients of the fourth order least square fits are: Experimental flame speed, a=1.076E3, b=-4.82E3, c=7.79E3, d=-5.21E3, e=1.23E3, corrected flame speed, a=8.38E2, b=-3.59E3, c=5.64E3, d=-3.73E3, e=8.81E2.**

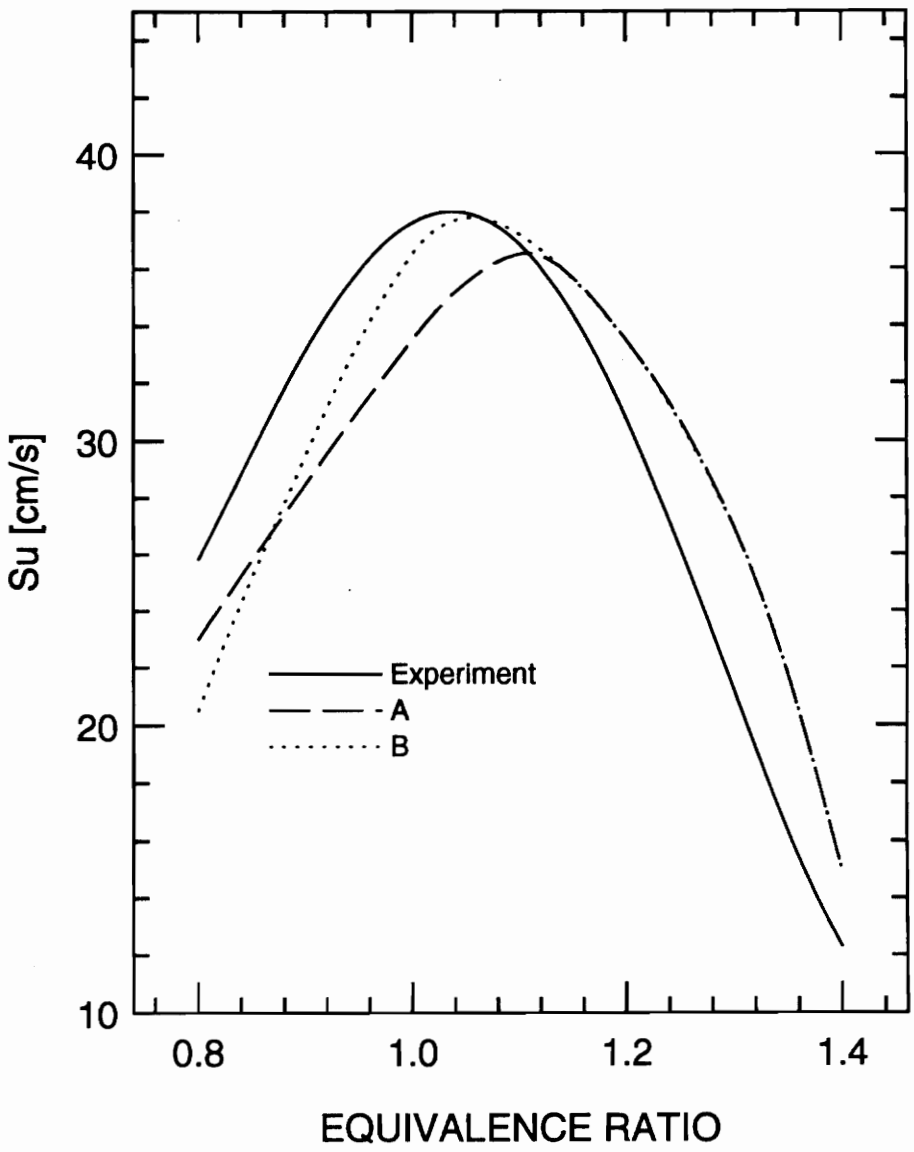

Figure 3.4: **Comparison between corrected flame speed S_u^c and the results of Brassin, et al. [27], source A (methane-air, vertical flame tube, flame speeds corrected for flame surface area) and Egerton and Lefebvre [28], source B (methane-air, horizontal 2.5 cm square tube, flame speeds corrected for flame surface area)**

flame speed for the flame curvature. The experimental results are in good agreement with the published results.

3.3.3 Discussion of Experimental Flame Speed Results

Generally, the scatter of experimental data from run to run is quite substantial. Even though surfaces of propagating flames do not show visible defects (e.g. spontaneous wrinkles or oscillatory movement), the curvature of the flame front and the angle between the flame edges and the wall vary from run to run. Due to the easily disturbed flame-tube system, changes in flame curvature were observed even within a single run. Therefore flame speed is non-reproducible.

The graph of flame speed versus mixture equivalence ratio follows the trend of the theoretical flame temperature, which is in agreement with literature on flame propagation (e.g. Markstein [23]). As the mixture shifts from stoichiometric to fuel-rich, the heat capacity of the products decreases (mainly because the production of CO is favored over CO_2 as the mixture becomes fuel-rich) faster than the heat of reaction; the net result is a peak in flame temperature and flame speed at approximately $\Phi = 1.05$. Apparently, the run to run variations of the experimental flame speeds S_u^e at a given stoichiometry do not collapse to a single corrected flame speed S_u^c by compensating for individual flame surface areas. Therefore the accuracy of flame surface area determination from two-dimensional flame front images in a time averaged manner as described in Section 2.4.3 must be questioned. More accurate methods of determining flame surface areas are needed to properly account for the run-to-run variation of experimental flame speeds.

Considering the difficulties associated with the measurement of flame position and flame surface area in a metastable environment, the corrected flame speed S_u^c is in good agreement with the results of Brassin, et. al. [27], and Egerton and Lefebvre [28].

3.4 Heat Flux

3.4.1 Dimensional Results

Heat flux versus time for three different mixtures is given in Figures 3.2a, 3.2b, 3.2c and the variation of peak heat flux with equivalence ratio is shown in Figure 3.5. Values of the maximum heat transfer rates, obtained at identical mixtures vary as much as 20% about the least square mean value from run to run. However, a fourth order least square fit through the data indicates a roughly parabolic trend with a clear maximum heat flux at $\Phi = 1.05$.

Both the peak value of heat flux and the area underneath the heat flux graph versus time in Figures 3.2a, 3.2b and 3.2c are dependent on the mixture composition. Visible examination shows that this area, and therefore the total heat transferred to the wall, is largest for slightly richer than stoichiometric flames.

The idealized time lag, which is the difference between the instant when the flame would impinge at the wall if it had continuously traveled at uniform speed and the occurrence of the maximum heat flux, is shown in Figure 3.5. Experimental data is so widely scattered that it is difficult to identify a trend. Generally, the time lag is in the order of .015 s. A quadratic least square fit through the time lag indicates a slight increase in time lag as the mixture composition changes from lean to rich.

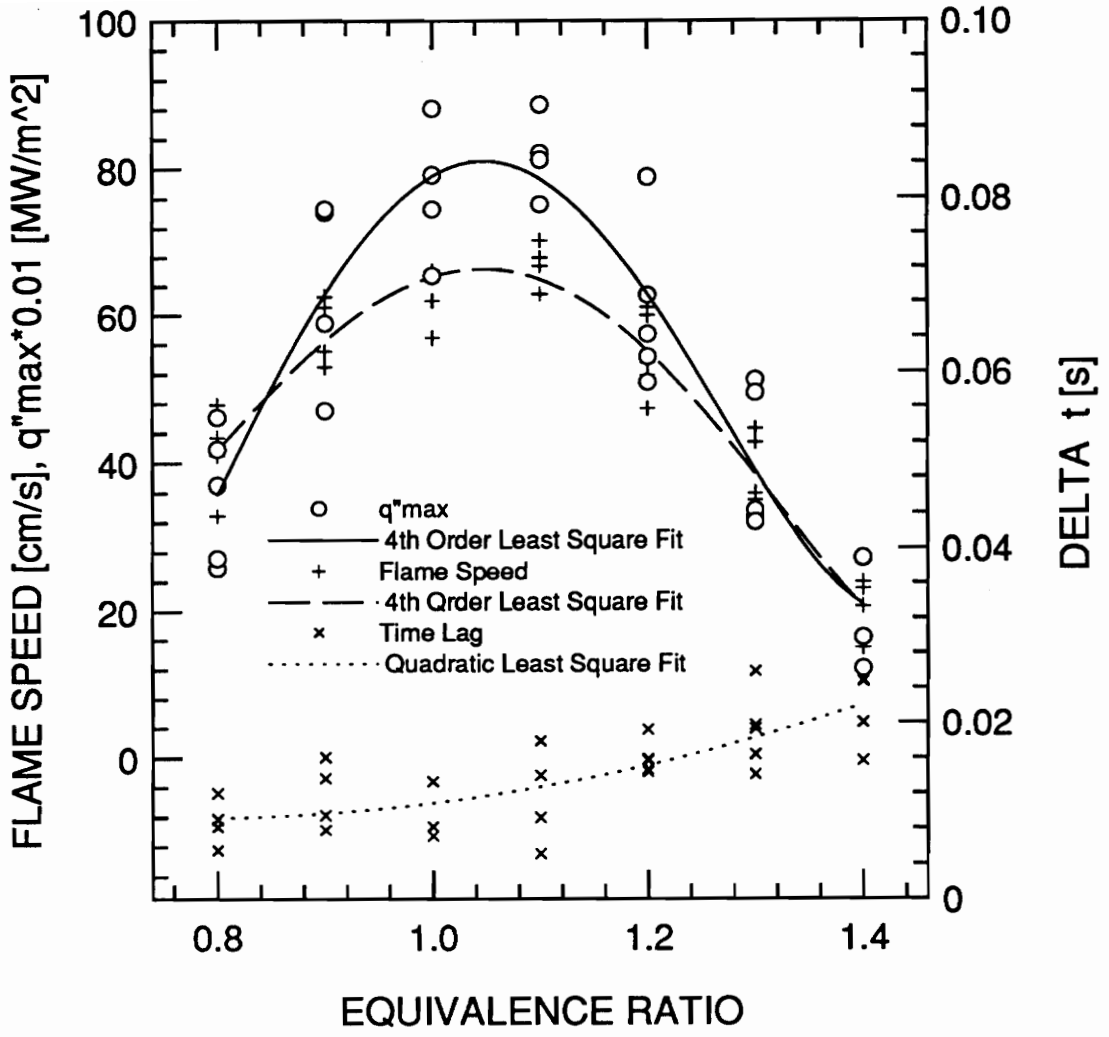

Figure 3.5: **Maximum heat flux, experimental flame speed and time lag versus equivalence ratio. Coefficients of the fourth order least square fit of peak heat flux data are: a=2.22E3, b=-1.01E4, c=1.65E4, d=-1.12E4, e=2.70E3, and coefficients of the quadratic least square fit of the time lag are: a=2.87E-2, b=-5.05E-2, c=3.27E-2**

3.4.2 Non-Dimensional Representation

Following the suggestion of Vosen [26], the heat flux is non-dimensionlized based on the flame speed and unburned gas properties.

$$\hat{t} = \frac{t(S_u^{\,e})^2}{\alpha_u} \tag{3.1}$$

$$\hat{q}'' = \frac{q''}{\rho_u S_u c_{pu} \Delta T_f^{\,a}} \tag{3.2}$$

Subscript u refers to the unburned gas condition and $\Delta T_f^{\,a}$ is the difference between the unburned gas and the adiabatic flame temperature. By non-dimensionalizing the heat flux with the steady-state heat release of the flame (Equation 3.2) and the time with the ratio of the squared flame speed over the thermal diffusivity (Equation 3.1), Vosen [26] claims that most of the effects which influence unsteady flame-wall interaction are taken into account.

Vosen [26] provides very little explanation as to why this particular non-dimensional groups should be used. According to Vosen [26], the Lewis number, which is the ratio of the thermal diffusivity to mass diffusivity, for a methane-air quenching process is unity. Therefore, thermal and mass diffusion are accounted for by the non-dimensionalization of the time. The use of the squared flame speed as a scaling factor is left without explanation. It is not obvious why the time should be scaled by the squared flame speed (other than for the reason of canceling the units).

Kornhauser [29] has developed a flame-wall heat transfer model and derived the non-dimensional variables for time and heat flux that are identical to those used by Vosen [26]

(Equation 3.1 and Equation 3.2). Kornhauser's [29] model and the derivation of the non-dimensional variables are discussed in Appendix D.

Figure 3.6 shows non-dimensional heat flux versus non-dimensional time at various mixture equivalence ratios. The heat flux graph is scaled such that the data almost collapses into a single trend. Heat flux graphs for near stoichiometric mixtures are relatively smooth, whereas heat flux graphs for lean and rich mixtures fluctuate due to a reduced signal-to-noise ratio (i.e. the measured heat flux amplitudes are small for lean and rich mixtures as compared to near stoichiometric mixtures).

In Figure 3.7, the non-dimensional measures of peak heat flux for all experimental runs are given versus mixture equivalence ratio. Due to widely scattered data, it is not clear whether the non-dimensional peak heat flux follows a linear or a non-linear trend. In order to determine the polynomial fit that most adequately represents the relationship between heat flux and equivalence ratio, an analysis of variance was carried out by means of the statistical software package SAS [30].

A multiple regression model (which includes all first and second order polynomials) was employed for the analysis of variance, and various model discriminators (i.e., the press statistic, C_p statistic and the coefficient discriminator R^2) are taken into account.

According to the statistical model discriminators, the variability of non-dimensional peak heat flux data is accounted for roughly 10 times better by a second order model as compared to a first order model.

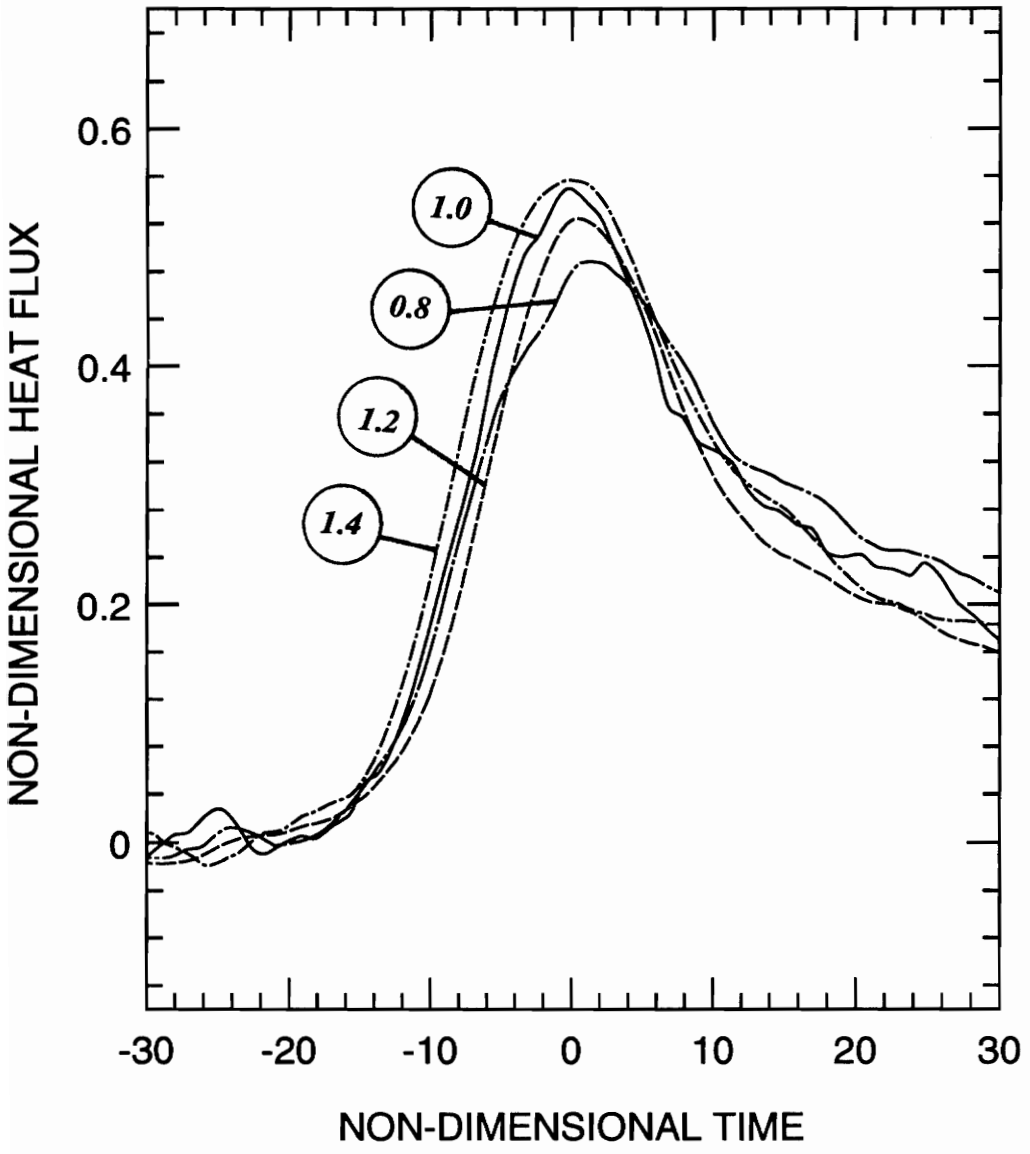

Figure 3.6: **Non-dimensional heat flux versus non-dimensional time at mixture equivalence ratio $\Phi = 0.8,\ 1.0,\ 1.2,\ 1,4$. According to Vosen [19] and Kornhauser [29], the heat flux and time are non-dimensionlized by** $\hat{q}'' = \dfrac{q''}{\rho_u S_u c_{pu} \Delta T_f^a}$ **and** $\hat{t} = \dfrac{t(S_u^e)^2}{\alpha_u}$.

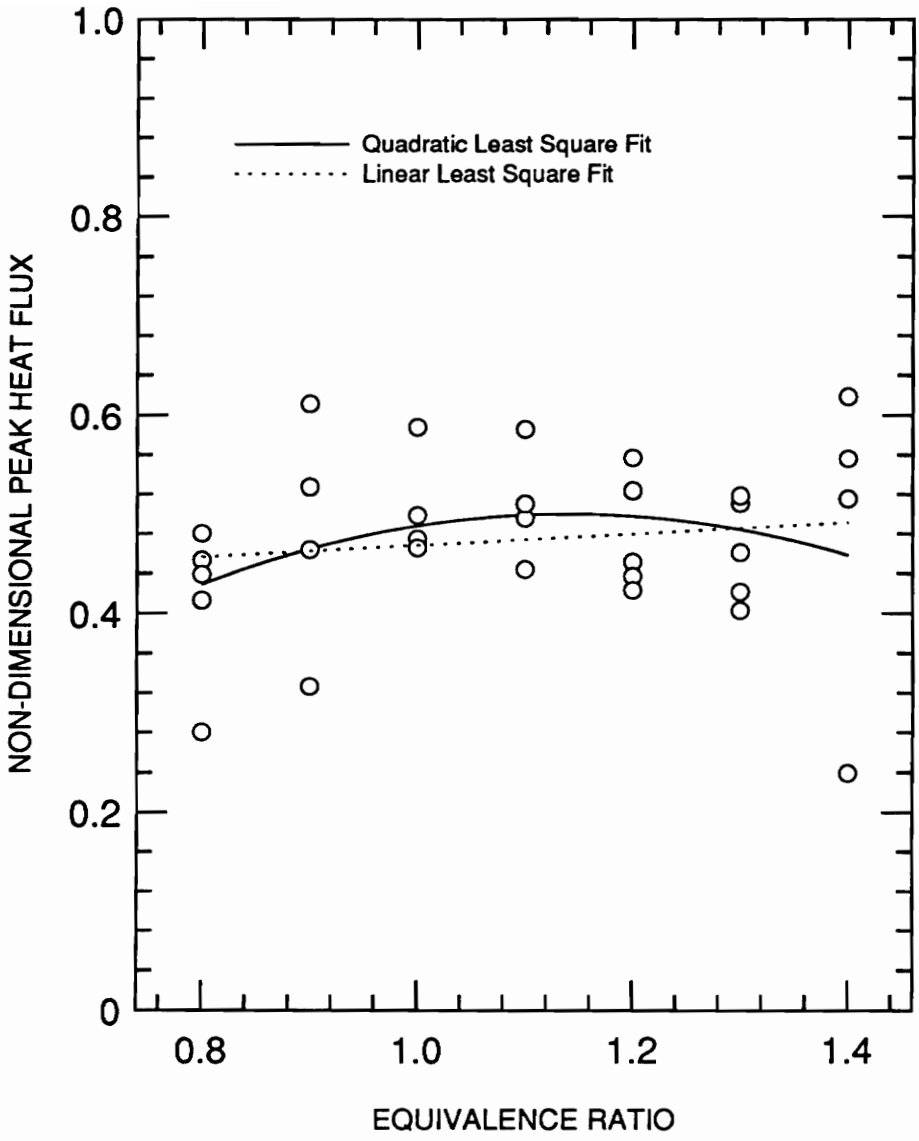

Figure 3.7: **Non-dimensionlized peak heat flux versus equivalence ratio (all data). The coefficients of the quadratic least square fit are: a=-0.302, b=1.407, c=-0.617. According to Vosen [26] and Kornhauser [29], the heat flux and time are non-dimensionlized**

by $\hat{q}'' = \dfrac{q''}{\rho_u S_u c_{pu} \Delta T_f^a}$ **and** $\hat{t} = \dfrac{t(S_u^e)^2}{\alpha_u}$

There is statistical evidence that the variance of non-dimensional peak heat flux with equivalence ratio should be interpreted on the basis of a non-linear model. Thus a second order least square fit with coefficients as listed in Figure 3.7 is chosen to represent the data. The non-dimensional peak heat flux fit shows a maximum for near stoichiometric mixtures and decreases (relatively) symmetrically for lean and rich mixtures.

Non-dimensional time delay versus mixture equivalence ratio is given in Figure 3.8. A second order least square fit reveals that the non-dimensional measure of the time delay strongly depends on the mixture composition; it is largest for near stoichiometric and decreases for both lean and rich mixtures.

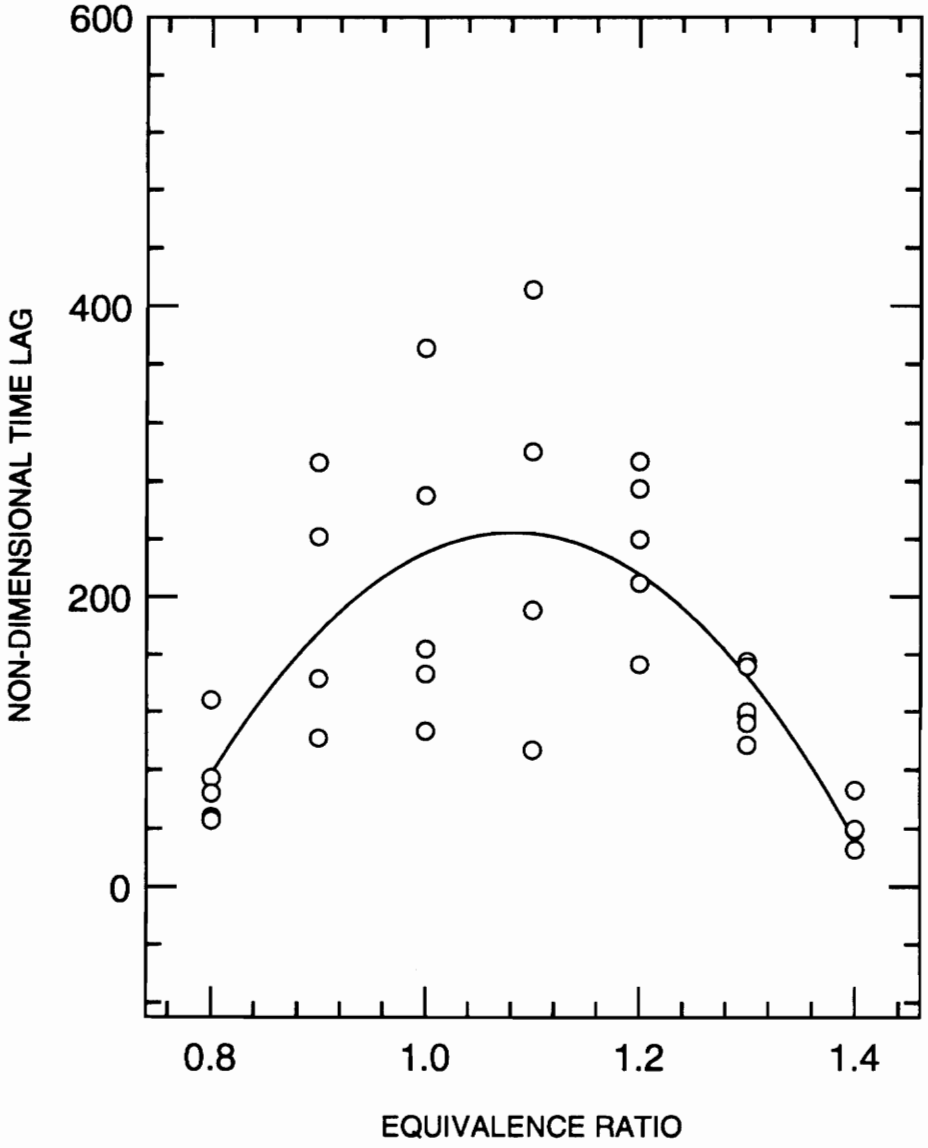

Figure 3.8: **Non-dimensional representation of the time lag between idealized flame impingement and the occurrence of the maximum heat flux. According to Vosen [26] and Kornhauser [29], the time is non-dimensionlized by**

$$\hat{t} = \frac{t(S_u^e)^2}{\alpha_u}.$$

3.4.3 Comparison to Literature

Vosen [26] has measured unsteady heat transfer from premixed methane-air flames to a single cold wall in a constant volume combustion bomb under the assumption of constant pressure at quench. Heat flux data from Vosen [26] (measured at ambient wall temperature, $\Phi = 1.0$ and P=1.19 atm at quench) is compared to heat flux data from this study (measured at ambient wall temperature, $\Phi = 1.0$ and P=1 atm). Both heat flux curves are arranged in Figure 3.9 on common axis such that times t<0 refer to times prior the instance of maximum heat transfer, and the time t=0 corresponds to the instance of maximum heat transfer. Results vary considerably in heat flux amplitude (25%) and duration between both studies.

Vosen [26] found the non-dimensional peak heat flux to be independent of the mixture equivalence ratio. Most of the effects that influence transient flame-wall interaction, Vosen [26] says, have been compensated for by scaling with characteristic values for time and heat flux. However, this study indicates a weak dependence of the non-dimensional peak heat flux on the mixture equivalence ratio.

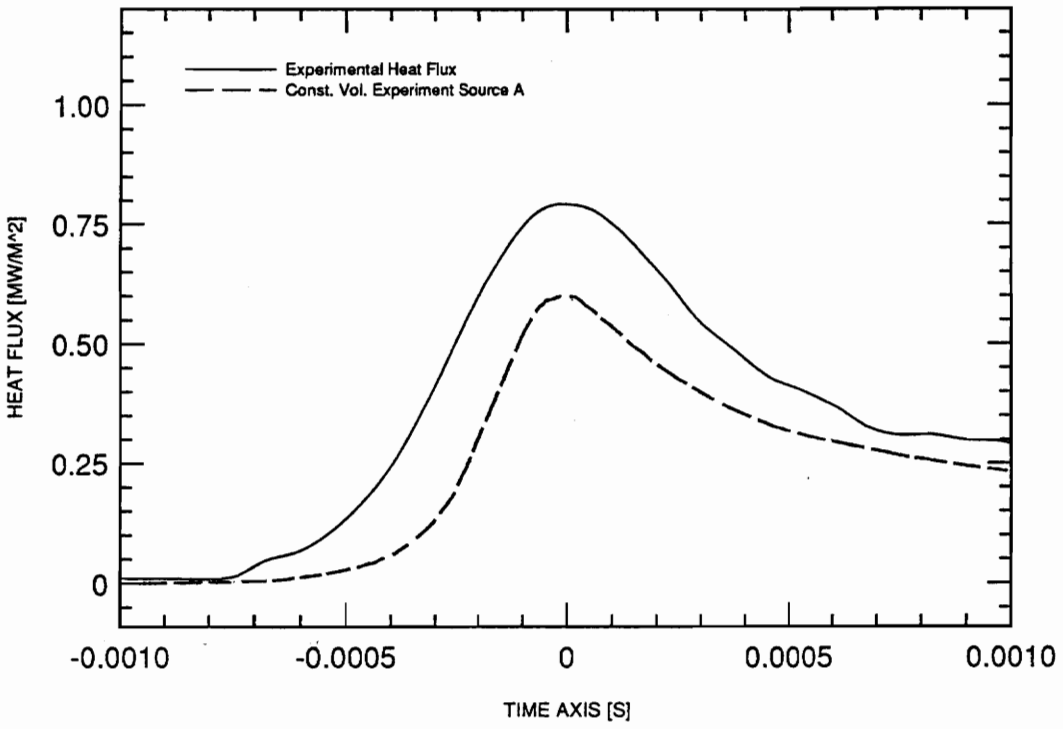

Figure 3.9 **Comparison of experimental heat flux (P=1 atm, T_u=293 K, $\Phi = 1.0$) to heat flux data from Vosen [26] (constant volume combustion chamber, pressure at quench P=1.19 atm, T_u=293 K, $\Phi = 1.0$), time t=0 referes to peak heat flux time, t<0 refers to times prior to quench.**

3.4.4 Discussion of Experimental Heat Flux Results

The variation of peak heat flux with equivalence ratio is a symmetric phenomenon with the symmetry axis at $\Phi = 1.05$. Generally, the peak heat flux follows the trend of flame speed and flame temperature. This is not surprising, for the heat release rate of a flame front, which is a function of flame speed and heats of reaction, is expected to have a dominant effect on flame-wall heat transfer. Consequently the maximum heat flux is obtained for peak values of flame heat release, which occurs slightly on the rich side of stoichiometric.

Flame speed and heat flux vary dissimilarly from run to run under identical mixture conditions; there is no relationship between large heat flux amplitudes and high flame speeds, or vice-versa. The variation of peak heat flux may be affected by the orientation of the flame front with respect to the wall at quench. Ideally, the flame front should impinge at the wall with the maximum of the flame curvature aligned with the surface thermocouple at the center of the tube axis. However, it is observed that the most forward area of the flame sometimes is slightly off axis, and flame quenching at the location of the thermocouple occurs sidewise with already retarded chemical reactions. Flame-wall heat transfer from sidewise impinging flames is found to be significantly reduced as compared to head-on impinging flames. Although the data from experiments where the flame front showed obvious defects was discarded, the flame of "good" experimental runs still vary in flame curvature from run to run under identical conditions. The variation of flame-wall heat flux under identical mixture compositions may be explained on the basis of large scale flame surface defects and the resulting sidewise impingement process. Both an improvement in the flame structure and an advanced flame front diagnosis technique is needed to reduce the experimental error.

There is a 25% difference between Vosen's [26] heat flux amplitude as compared to the results from this study. It appears to be unlikely that compression heating due to constant volume combustion contributes significantly to the wall heat flux considering that the pressure at quench between both experiments differs only by 0.19 atm. It may be likely that flame quenching on Vosen's [26] surface thermometer occurred sidewise. The pressure at quench in Vosen's [26] experiment was controlled by the position of the ignition source relative to the temperature gauge. When the ignition position was close to the gauge, quenching occurred at the onset of flame propagation at a pressure (P=1.19 atm) only slightly above the initial pressure (P=1 atm). Because Vosen's [26] experiment used a constant-volume combustion chamber, pressure within the vessel at quench increased with distance from the ignition source. It is the author's experience that premixed flames immediately after spark ignition are characterized by cellular, oscillating structures. Some time is needed for the flame front to develop into a smooth surface. Therefore it is possible that under some of Vosen's [26] experimental conditions, the flame front was not fully developed at quench on the surface thermometer, and the flame impinged sidewise. However, the case of sidewise versus head-on flame impingement on the cold wall cannot fully explain the difference between Vosen's [26] heat flux data and the heat flux measured in this study.

The time lag is interpreted as the difference in time scale between flame movement and heat diffusion. Among other factors, the time lag may be affected by the flame speed, flame deceleration close to the quench wall, quenching distance, thermal diffusivity of quenching layer gases, and the diffusion process of unburned hydrocarbons into the (temporarily stationary) flame front. The experimental data discussed so consistently indicates symmetric trends with the axis of symmetry being slightly on the rich side of

stoichiometric at $\Phi = 1.05$. It is difficult to explain the asymmetrically increasing time lag between idealized flame impingement and maximum heat flux as the mixture becomes fuel-rich in Figure 3.5. Detailed information about the quenching layer thickness and transient temperature distribution during the quenching process is needed to further study the effect of various parameters on the time delay.

Figure 3.6 demonstrates the effect of scaling the time by the ratio of the squared flame speed and the thermal diffusivity (Equation 3.1). Apparently, the non-dimensional heat flux graphs at various mixture equivalence ratios collapse to a single trend with respect to the non-dimensional time scale. According to Vosen [26], the Lewis number, which is the ratio of thermal to mass diffusivity, for a methane-air quenching process is unity (Le=1). Therefore thermal and mass diffusion are accounted for by non-dimensionalization.

Vosen [26] claims that most of the effects which influence the amplitude of wall heat transfer are taken into account by non-dimensionalizing the heat flux with the heat release of a steady flame (Equation 3.2). However, the non-dimensional heat flux as determined in this study is found to be weakly dependent on the mixture equivalence ratio as shown in Figure 3.7. If the heat flux is properly scaled in order to account for the effect of the mixture composition on flame-wall heat transfer, it should be possible to represent the non-dimensional peak heat flux data by a straight line. According to a statistical analysis, the data is better represented by a parabola than a straight line. Consequently, there must be additional parameters affecting flame-wall heat transfer that are not accounted for in Vosen's [26] non-dimensionalization. The non-linearity of the non-dimensional heat flux may be explained on the basis of changes in quenching layer thickness.

Figure 3.10 shows the variation of the single-wall quenching distance with mixture equivalence ratio for propane-air flames. The quenching layer is largest for lean and rich flames, and is smallest for near stoichiometric mixtures. One would expect the quenching layer to significantly affect heat transfer. At lean and rich mixtures, heat is released at some distance to the wall, and flame-wall heat transfer is hindered by a a layer of relatively cold, insulating quench layer gases. The unburned hydrocarbons in the quenching layer must diffuse over a relatively large distance in order to be oxidized by the flame front, therefore the heat release rate due to the diffusion limited combustion period is low. For near stoichiometric mixtures the quenching layer thickness is substantially reduced, diffusion of fuel from the quenching layer into the flame front is relatively fast and the heat of reaction is released quickly at a position close to the wall. Thus, not only the heat of reaction but also the quenching layer thickness changes significantly with mixture equivalence ratio and both must be accounted for in order to compensate for the effect of equivalence ratio on non-dimensional flame-wall heat flux.

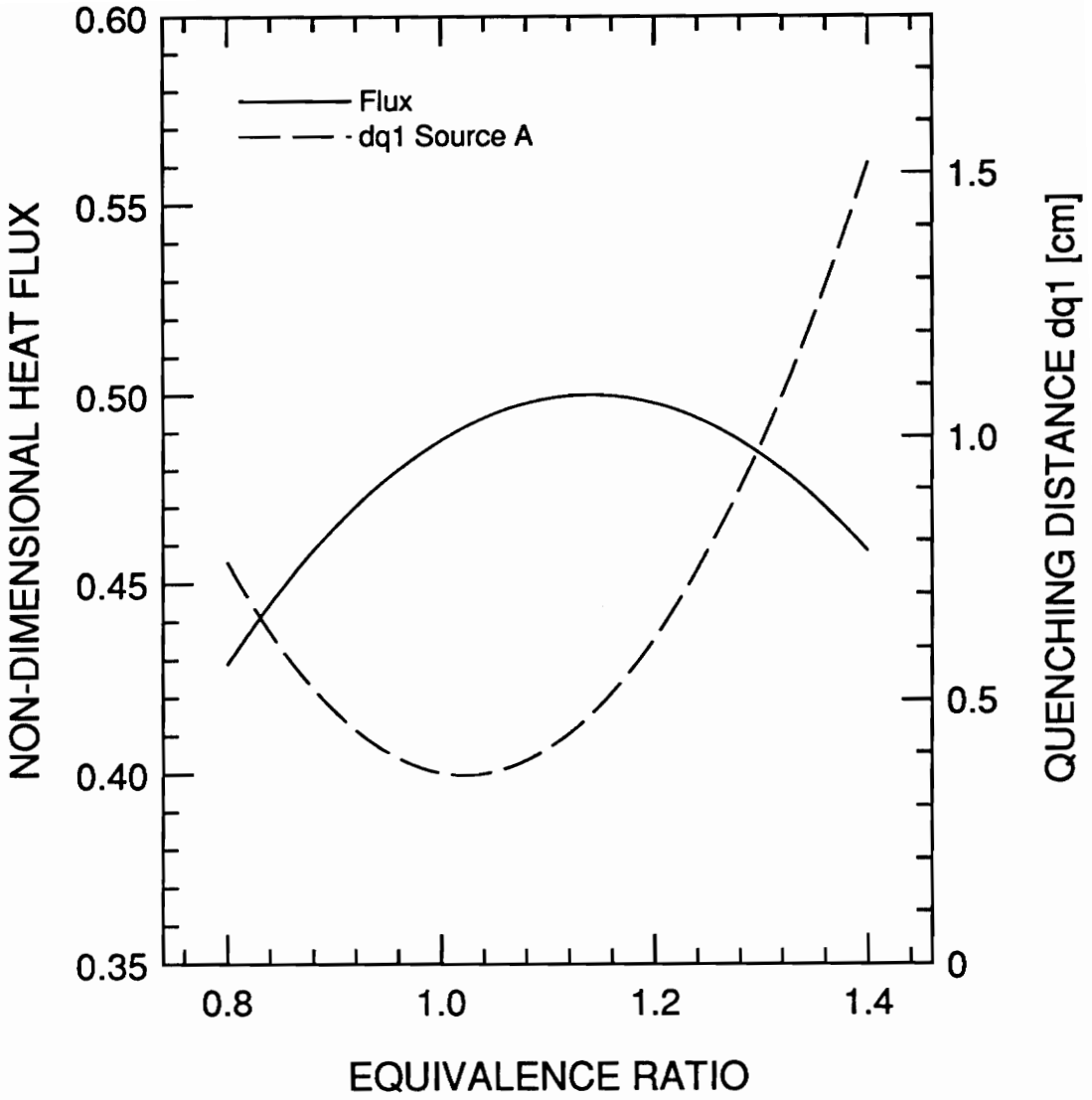

Figure 3.10: Non-dimensional peak heat flux and single-wall quenching distance d_{q1} for methane-air mixtures from Harris, et. al [31] (source A) versus equivalence ratio. According to Vosen [26] and Kornhauser [29], heat flux is non-dimensionlized by

$$\hat{q}'' = \frac{q''}{\rho_u S_u c_{pu} \Delta T_f^{\,a}} .$$

4. Models to Correlate with Experimental Data

4.1 Introduction

4.1.1 Motivation

The goal of the modeling work is to predict single-wall quenching layer thickness (d_{ql}) and flame-wall heat transfer as a function of premixed methane-air equivalence ratios and unburned gas temperatures, ranging from room temperature up to auto-ignition temperature at ambient pressure. The model data is then correlated with experimental and literature results.

Flame-wall interaction was numerically studied in great detail by Westbrook, Adamczyk and Lavoie [14], Hocks, et al. [32], Adamczyk and Lavoie [33], Kurkov and Mirsky [34] and others. Formulations of chemical processes range from one-step, Arrhenius-type global reactions to detailed reaction schemes, consisting of a set of elementary reactions with experimental values for kinetic constants. The purpose of modeling within this study was to reduce the complexity of the problem to its main physical processes and thereby to find a simple formulation that approximates the trends of the experimental findings without losing the phenomenological picture.

Two independent models are developed. The first model is described in Section 4.2 and is based on a quasi steady-state first law balance on a one-dimensional control volume between the moving flame front and the cold wall. This model will be referred to as the "first law balance model". It is constructed originally to predict flame-wall heat flux and quenching layer thickness. For reasons discussed later in this section, flame-wall heat

transfer cannot be represented accurately by this model, therefore it is used to predict single-wall quenching layer thickness only.

The second model is described in Section 4.3. A planar, moving heat generating sheet simulates the heat release of a traveling flame front in a one-dimensional slab of gases at rest, bounded by the wall at which quenching occurs. This transient conduction problem is solved in terms of a Green's Function and is referred to as the "transient heat conduction model". This model is utilized to predict instantaneous flame-wall heat transfer as a function of variable wall temperature and mixture composition.

4.1.2 Basic Assumptions

The following simplifications and assumptions underlie both models:

- The temperature of the wall at which quenching occurs remains constant throughout the quenching process. This assumption is justified by experimental observations; the wall surface temperature rise of about 5 K due to flame-wall heat transfer is small compared to the temperature difference across the flame of more then 1000 K.

- Prior to ignition, the gas temperature is the same as the wall temperature T_u. There is no wall heat flux prior to flame quenching. The gas properties are taken at the unburned gas temperature T_u and are assumed to remain constant throughout flame propagation. Realistically, density, and to a lesser extent conductivity and heat capacity vary with temperature. Mixture properties also

change when reactants convert to products. Neither the correct adiabatic flame temperature, nor the true time dependency of heat transfer can be accurately calculated with invariant mixture properties. A constant mixture density allows the products behind the flame front to be at rest. More realistically, the combustion products should be pushed away in the opposite direction of flame travel, because more and more low density combustion products are generated while the flame propagates. However, meaningful results can be obtained for the phenomena of interest: thermal gradients between flame and wall are located ahead of the flame front in the mostly cold gas region. Within this region, the assumption of constant mixture properties at T_u is justified.

- Combustion is assumed to take place within an infinitely thin reaction layer. In other words, the reactants are consumed and, with heat release, converted to products by a flame front of zero width. This assumption implies a one-step irreversible reaction and the elimination of conservation equations for a multi-component reaction system. In order to permit a simple mathematical formulation, the model cannot represent the interaction of chain branching, chain propagating and chain terminating reaction steps. Real hydrocarbon flames burn in such a sequential manner, and it is known (e.g. Westbrook, et al. [14]) that especially the intermediate reaction products support the consumption of quenching layer hydrocarbons during the quenching process. Flame quenching as predicted by one-step kinetics occurs quickly, and does not account for heat generation due to the consumption of quenching layer hydrocarbons.

- Radiative flame-wall heat transfer is assumed to be negligible compared to conductive heat transfer.

With the above assumptions it is possible to solve the governing equations for flame-wall heat transfer and quenching layer thickness within the scope of this thesis. Despite several severe simplifications it is possible to obtain meaningful trends that correlate well with literature and experimental results.

4.2 First Law Balance to Predict Quenching Layer Thickness

4.2.1 Development of Model

This model is used to approximate the quenching distance d_{q1} as a function of equivalence ratio and unburned gas temperature. The single wall quenching distance d_{q1} is defined as the position of closest approach of the reaction zone to the wall. The quenching layer thickness is a characteristic quantity of the flame quenching process.

An analysis is made for a one-dimensional system in which a flame approaches an end wall. Since the temperature rise of the wall due to flame-wall heat transfer is small, the wall temperature is assumed to be constant. In a region where flame propagation is unaffected by heat loss to the end wall, an energy balance on the flame front may be written as

$$\dot{q}_g'' = \dot{q}_c'' \tag{4.1}$$

where $\dot{q}_g''$ is the rate of heat production by chemical reactions in the infinitely thin flame front,

$$\dot{q}_g'' = S_u \ \rho \ h_{rp} \tag{4.2}$$

and $\dot{q}_c''$ is the rate at which heat is consumed by preheating the reactants from the unburned gas temperature up to the flame temperature

$$\dot{q}_c'' = S_u \rho \ c_p (T_f - T_w) \tag{4.3}$$

Essentially, this is the concept of the adiabatic flame temperature; the liberated heat of combustion is balanced by the heat capacity of the gas mixture.

In the vicinity of a cold wall, a convective heat loss term to the wall has to be included in the above first law balance. For this reason, the control volume is expanded to enclose the entire one-dimensional gas region between flame front and the end wall. Heat loss from the system to the wall is the derivative of the temperature with respect to the distance x at the wall:

$$\dot{q}_w'' = -k \frac{\partial T}{\partial x} \Big|_{x=0} \tag{4.4}$$

and the energy balance reads:

$$\dot{q}_g'' = \dot{q}_c'' + \dot{q}_w'' \tag{4.5}$$

Temperature profiles in the preheat zone between flame and wall must be known in order to determine the heat loss to the wall. Neglecting radiation, there is conductive heat transfer from the flame front into the unburned gas mixture in the preheat zone, and convective heat transfer to the gases that stream through the flame front in the opposite direction:

$$k \frac{d^2T}{dx^2} - \rho \ S_u c_p \frac{dT}{dx} = 0$$

with boundary conditions

$$T = T_f \quad at \quad x = x_f$$

$$T = T_u \quad at \quad x = 0 \tag{4.6}$$

As shown in Figure 4.1 the origin of the coordinate system is at the cold wall. At a given time, the flame position is known by the relationship:

$$x_f = x_{start} - S_u t \ . \tag{4.7}$$

and the flame temperature T_f that corresponds to a given flame position is determined by the energy balance in Equation 4.5. Assuming constant properties, the solution to the above differential equation (Equation 4.6) is obtained by integration with respect to the x coordinate twice and using the boundary conditions:

$$T = T_u + \frac{T_f - T_u}{exp\left(\frac{S_u}{\alpha} x_f\right) - 1}\left[exp\left(\frac{S_u}{\alpha} x\right) - 1\right] \tag{4.8}$$

The resulting exponential temperature profiles in the preheat zone are shown in Figure 4.1. As time progresses, the flame position advances closer to the wall and the slope of the exponential temperature profile becomes steeper, resulting in increased temperature gradients at the wall.

Gas-wall heat flux is obtained by means of the first derivative of Equation 4.8 at the wall (x=0):

$$\dot{q}_w'' = -k\frac{dT}{dx}\bigg|_{x=0} = -k\left[\frac{T_f - T_w}{exp\left(\frac{S_u}{\alpha} x_f\right) - 1}\right]\left[\frac{S_u}{\alpha} exp\left(\frac{S_u}{\alpha} x\right)\right] \tag{4.9}$$

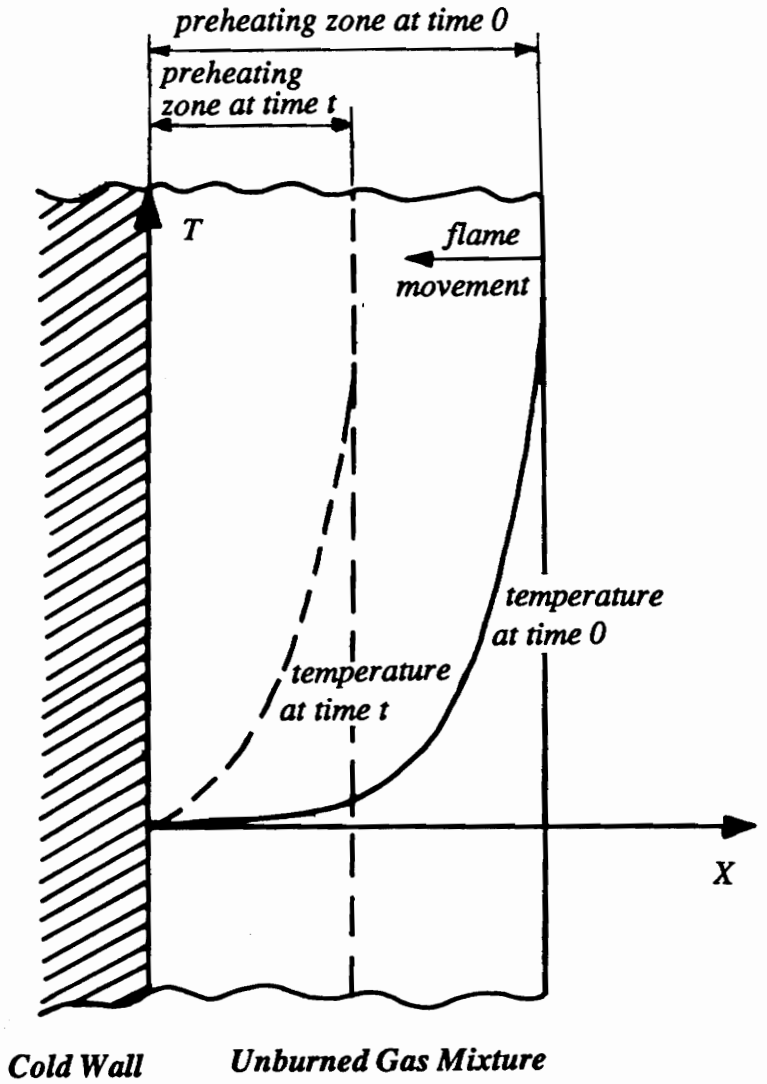

Figure 4.1 One-dimensional control volume of the 1st law balance model.

The flame speed is coupled to the flame temperature; as a result of excessive heat loss to the wall, the flame temperature and, therefore, flame speed decreases at locations close to the wall. The temperature sensitivity of flame speed is represented by an Arrhenius type single-step reaction equation that correlates decreased flame temperatures in the vicinity of the wall to a corresponding lower flame speed. The freely propagating flame speed (i.e. S_u^c) and the freely propagating flame temperature (i.e. T_f^c) and the actual flame temperature as determined from the energy balance are the required input parameters. The actual flame speed according to the Arrhenius type relationship between temperature and flame speed is:

$$S_u^{actual} = exp\left[-\frac{E_a}{2R}\left(\frac{1}{T_f^{actual}} - \frac{1}{T_f^{free}}\right)\right] S_u^{free} \tag{4.10}$$

The activation energy is taken to be 30 kcal/mole as determined for a one-step hydrocarbon reaction mechanism by Westbrook and Dryer [35]. Using Equation 4.10 and an activation energy of 30 kcal/mole, a flame temperature drop on the order of 300 K is sufficient to extinguish all chemical reactions, thus, flame quenching occurs very rapidly. As pointed out earlier, this is not quite true for hydrocarbon flames because the quenching layer fuel content continues to be consumed during flame quenching.

It is important to note that this quasi steady-state model assumes that the instantaneous flame speed and flame temperature have always been the same. Therefore, it does not account for the time history of the quenching process. Thus, the portion of the wall heat transfer resulting from earlier released heat (e.g. when the flame burned with the steady-state temperature shortly before being affected by the presence of a cold wall) that diffuses

through the insulating quenching layer gases subsequent to flame extinction is not represented.

The above equations are used in a quasi steady-state marching scheme as follows: at a given time, the flame position is calculated and the corresponding flame temperature and flame speed are found from the energy balance by means of a FORTRAN program through iterations (the FORTRAN code is provided in Appendix H). This procedure is repeatedly executed for successive finite time steps in intervals Δt apart from one another. As the flame approaches the end wall, heat loss to the wall drastically increases, the flame speed sharply drops to zero and flame propagation stalls. The distance between the location of flame extinction and the wall is the quenching distance d_{q1}.

4.2.2 Results and Discussion

Calculations are performed using the above model to predict the single-wall quenching layer thickness as a function of equivalence ratio and unburned gas temperature. One set of quenching layer data is calculated for the variation of the mixture equivalence ratio between $0.8 \geq \Phi \geq 1.4$ at T_u=293 K and P=1.0 atm. Another set of data is calculated for stoichiometric mixtures at variable unburned gas temperatures and P=1.0 atm (this condition is not experimentally investigated). Flame temperature, flame speed, heat of reaction and thermal mixture properties are the required model input parameters that have to be determined individually for the simulated conditions. The input parameters, the results and a discussion of a simulation of mixture equivalence changes at ambient unburned wall temperature and pressure are given in Section 4.2.2.1. The input

parameters, the results and a discussion of the simulation of unburned gas temperature variations at constant ambient pressure are provided in Section 4.2.2.2

4.2.2.1 Variation of Methane-Air Equivalence Ratio at T_u=293K and P=1 atm

Input Parameters

Quantitative values of quenching distances are predicted for adiabatic and experimental flame conditions. In the adiabatic case, flames travel with adiabatic flame speed until they are thermally affected by the presence of the cold wall. Values of the adiabatic flame speed S_u^a are taken from Andrews and Bradley [36]. As a result of the constant heat capacity assumption, the heat of reaction for the individual mixtures has to be calibrated in order for the flame to burn with an adiabatic flame temperature T_f^a in regions far away from the wall. The chemical equilibrium solver program STANJAN [37] is used to calculate density and heat capacity of the unburned gas mixture at T_u=293 K as well as the adiabatic flame temperature T_f^a at various equivalence ratios. Mason and Saxena's [38] estimation method is utilized to determine thermal conductivities of the individual gas mixtures.

The quenching layer thickness also is predicted for experimental conditions, where both flame temperature and flame speed of the freely propagating flame are decreased due to flame side-wall heat loss to the glass tube. The flame speed S_u^c for individual fuel-air equivalence ratios is experimentally determined, but information about the corresponding flame temperature T_u^c is missing. However, as pointed out earlier, the flame speed is

dependent on the flame temperature, coupled by temperature sensitive rates of reaction. Equation 4.10 constitutes a relationship that correlates the (lower) corrected flame speed from experiments, S_u^c, to a corresponding (lower) flame temperature T_f^c on the basis of a single-step global Arrhenius type reaction. Solved for the flame temperature T_f^c, equation 4.10 reads:

$$T_f^c = \frac{1}{ln\left(\frac{S_u^c}{S_u^a}\right)\frac{2R}{E_a} - \frac{1}{T_f^a}} \tag{4.11}$$

where T_f^a and S_u^a are the adiabatic flame temperature (from STANJAN [37] calculations) and adiabatic flame speed (from Andrews and Bradley [36]), respectively. S_u^c is the experimentally obtained and flame surface area corrected flame speed. Results of the experimental flame temperature T_f^c at various mixture equivalence ratios are given in Figure 4.2. The heat of reaction of the individual mixtures in Equation 4.2 is slightly adjusted (lowered) to compensate for the constant heat capacity assumption so that the flame travels at the experimental flame temperature T_f^c in regions far away from the cold wall.

Results

Typical trends of flame temperature, flame speed and wall heat flux during flame arrival at the end-wall are illustrated in Figure 4.3 for a stoichiometric mixture and adiabatic flame conditions. Corresponding successive temperature profiles during quench between flame and wall are shown in Figure 4.4.

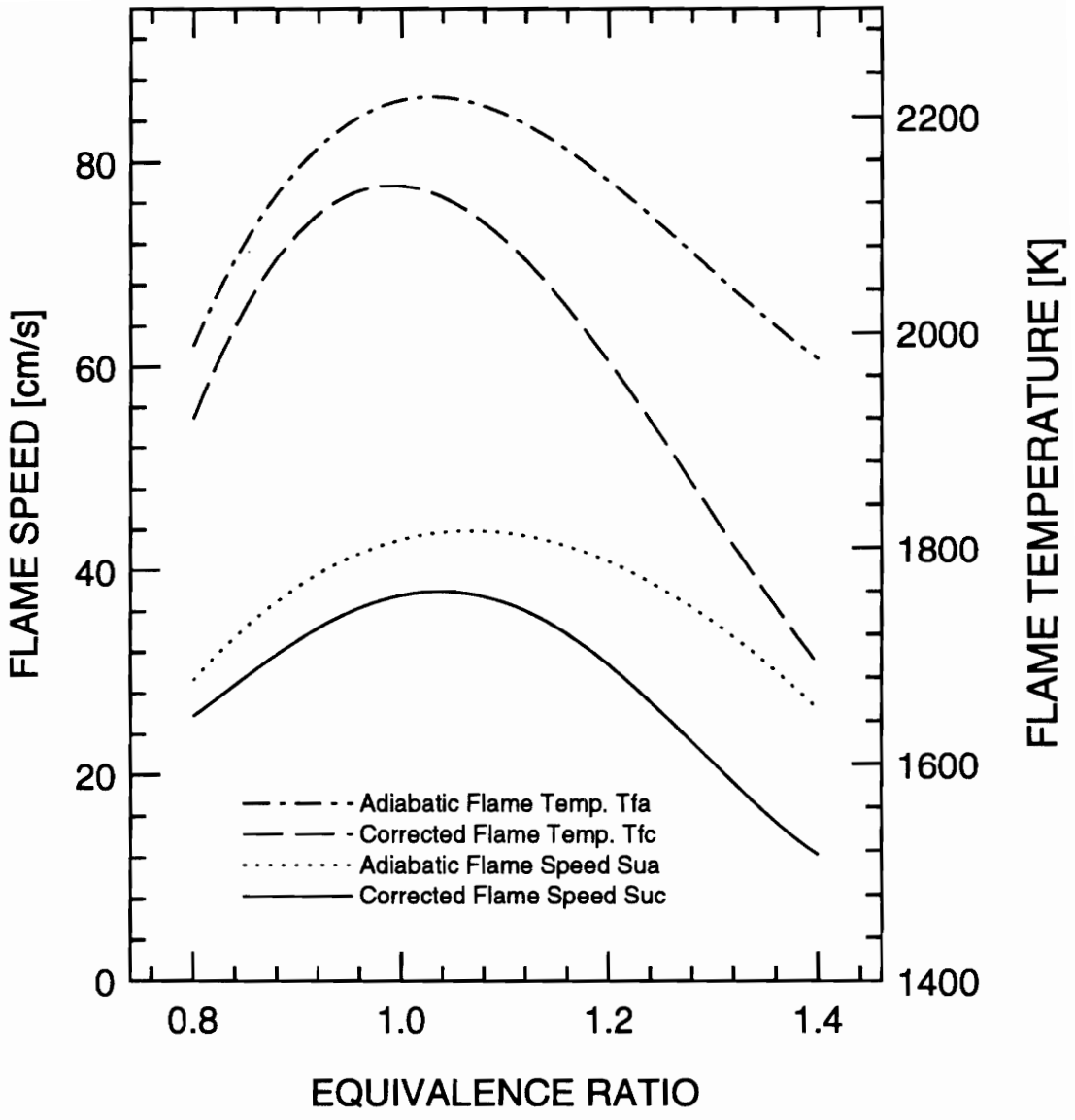

Figure 4.2 **Calculated experimental flame temperature T_f^c as a function of the experimental (corrected) flame speed S_u^c, adiabatic flame temperature T_f^a and adiabatic flame speed S_u^a. Adiabatic flame temperatures from STANJAN [37] calculations, and adiabatic flame speeds from Andrews and Bradley [36].**

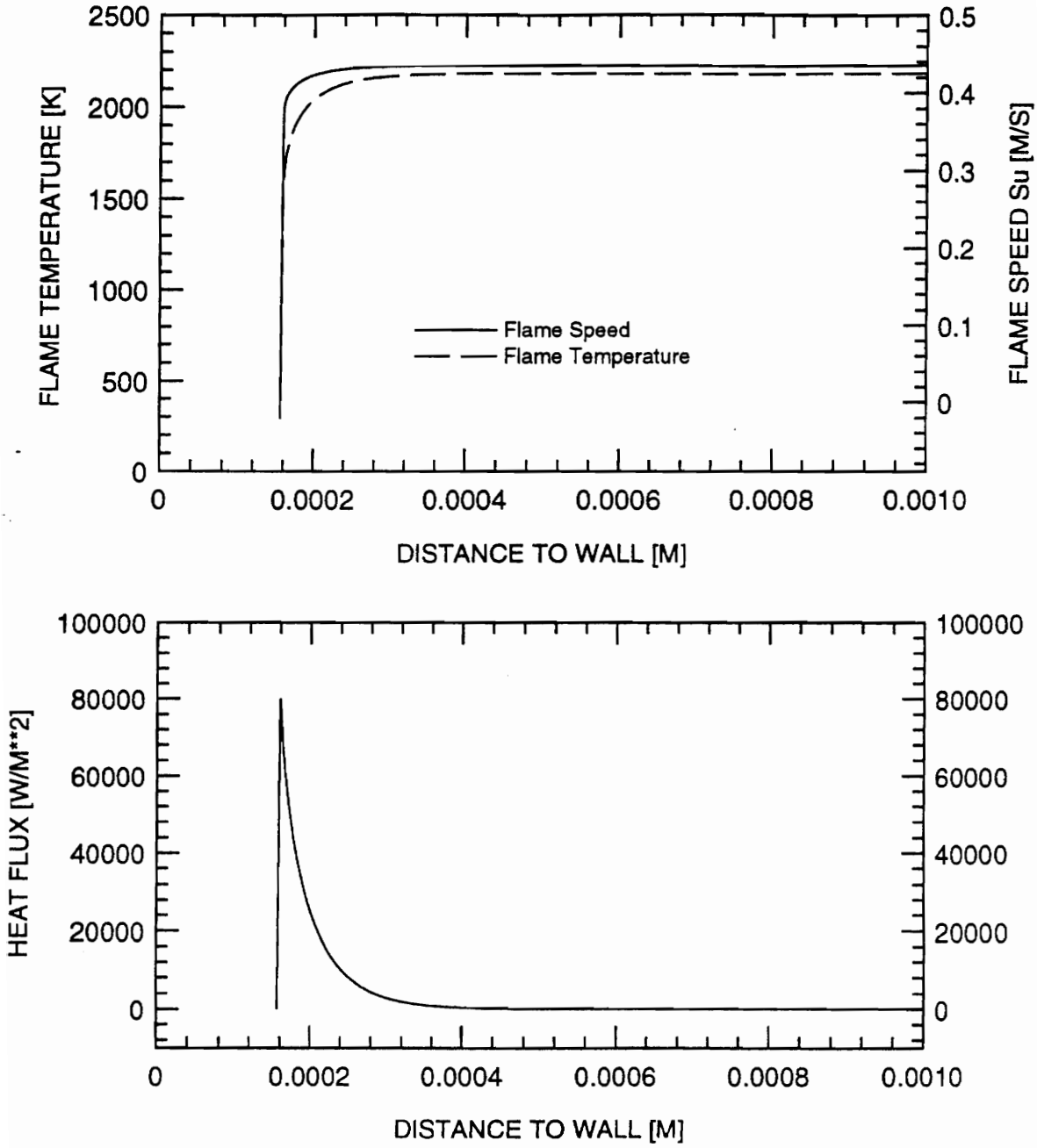

Figure 4.3: Calculated flame speed, flame temperature and wall heat flux for a stoichiometric and adiabatic flame front during quench.

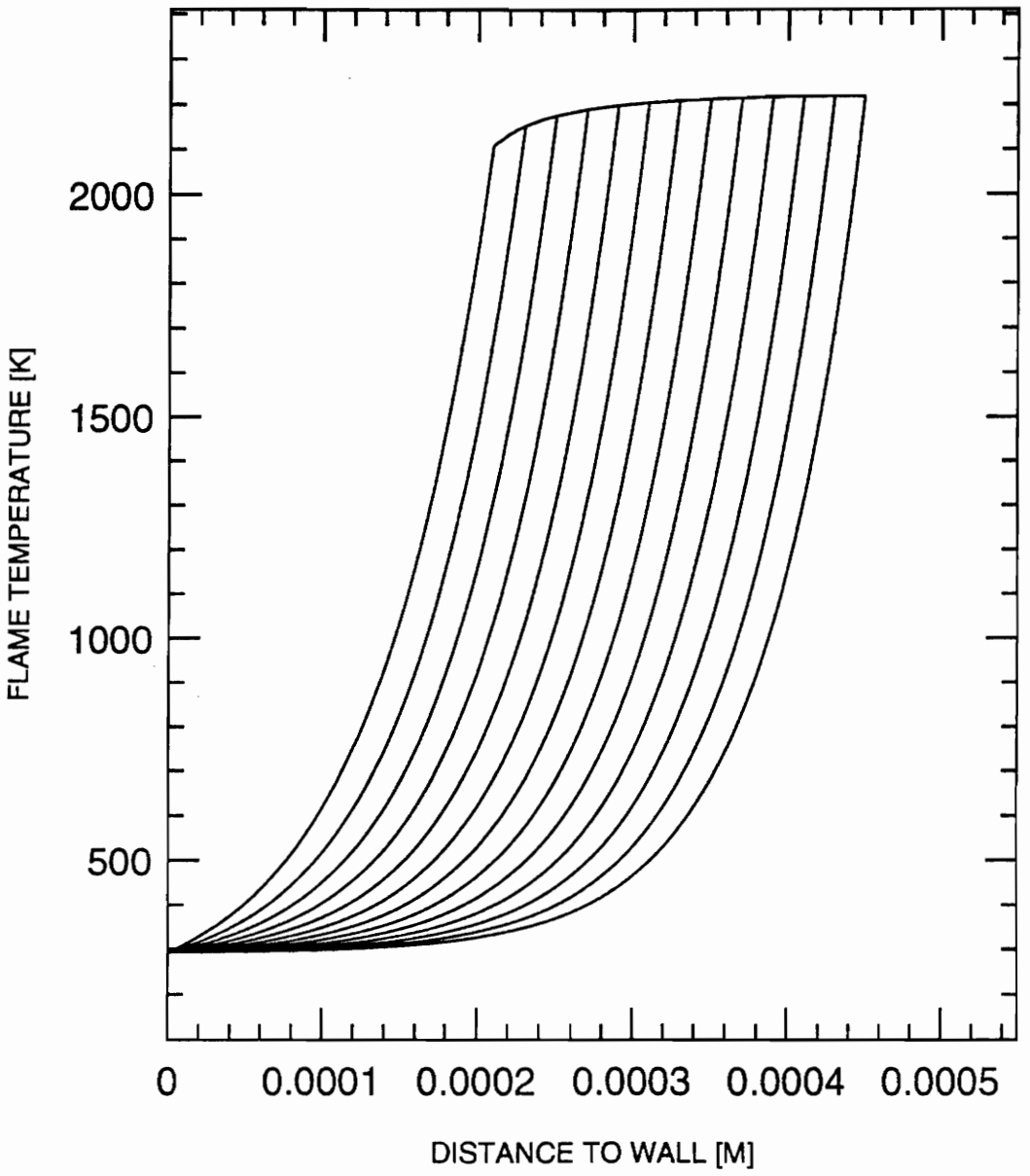

Figure 4.4: Several consecutive temperature profiles between flame and wall for a stoichiometric and adiabatic flame front at quench. The temperature profiles are spaced $\Delta t = 0.045$ ms from one another.

In an area unaffected by heat transfer at some distance from the wall, the flame travels at uniform flame speed and uniform flame temperature without loosing heat to the wall. Gradually, the temperature gradients at the wall become very steep (see Figure 4.4), heat is transferred to the wall and, being sensitive to temperature changes, flame speed decays (see Figure 4.3, upper graph). The fuel consumption rate is immediately affected by a reduced flame speed, less heat is liberated and the heat transferred to the wall becomes a much greater fraction of the overall energy balance. As a result, flame speed and flame temperature drop in an exponential manner, and flame propagation stops at some distance from the wall. Since there is no consumption of fuel after the flame movement is terminated, the heat transfer rate immediately drops to zero (see Figure 4.3, lower graph).

The quasi steady-state model assumes that there are no temperature gradients across the one-dimensional layer of gases after the flame has been quenched, and therefore does not accept for the heat transfer due to heat diffusion (of the previously heated gases) subsequent to flame extinction. During flame quenching of a stoichiometric and adiabatic flame at ambient unburned gas temperature and pressure, the first law balance predicts a maximum heat flux amplitude of about 0.08 MW/m^2.

The calculated quenching layer thickness as a function of equivalence ratio has a minimum for near stoichiometric mixtures and increases for both lean and rich mixtures under adiabatic and (simulated) experimental conditions as shown in Figure 4.5.

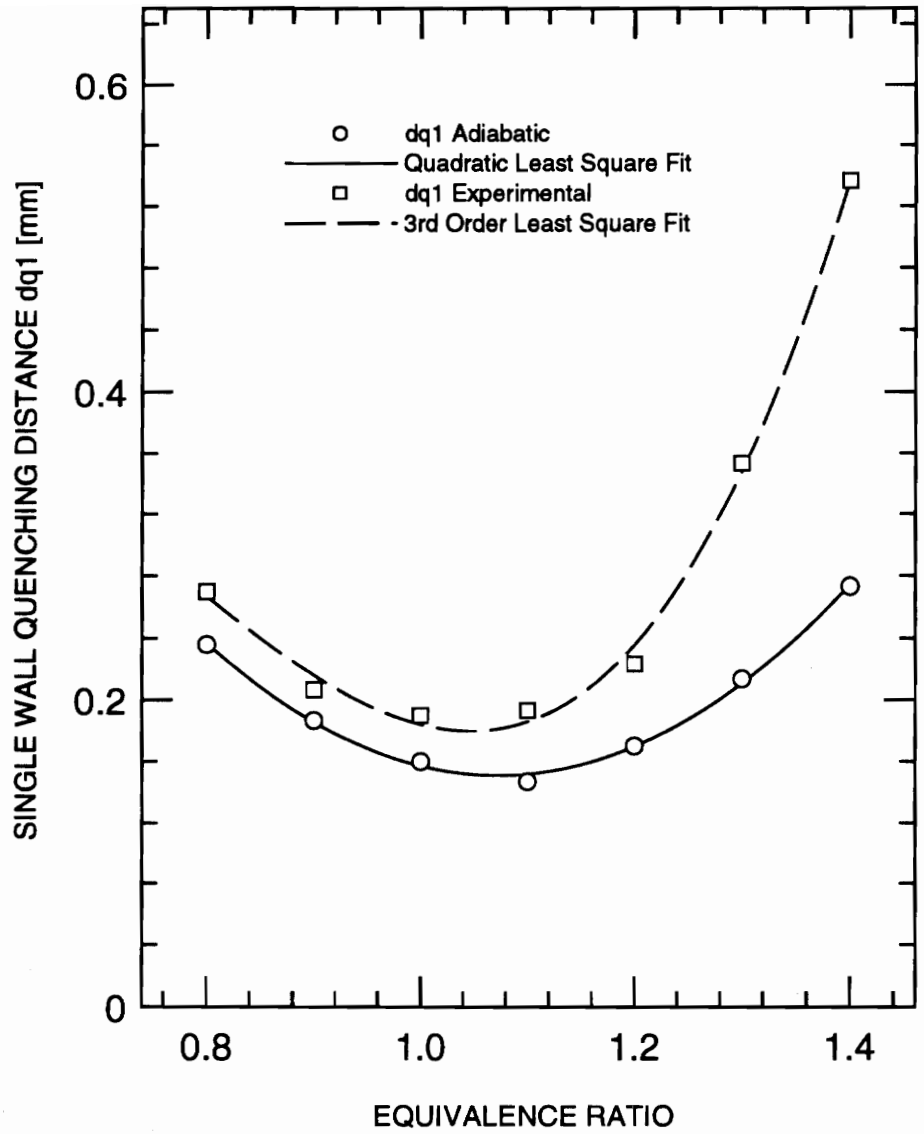

Figure 4.5: **Quenching layer thickness d_{qI} under adiabatic and experimental conditions as a function of mixture equivalence ratio at constant unburned gas temperature (wall temperature) T_u=293 K and P=1 atm. Coefficients of curve fits are: adiabatic quenching thickness a=1.479, b=-2.477, c=1.154, experimental quenching thickness a=-0.368, b=3.690, c=-5.546, d=2.410.**

Comparison to Literature

The calculated single-wall quenching distance at various equivalence ratios (T_u=293 K and P=1 atm) is verified by comparison to literature. Single-wall methane-air quenching distances in the literature are sparse. Harris, Grumer, von Elbe and Lewis [31] have experimentally determined the quenching distance for methane-air mixtures between parallel plates at room temperature and atmospheric pressure. Lavoie [10], has developed a relationship to correlate the parallel-plate quenching distance to a single-wall quenching distance:

$$\frac{d_{q1}}{d_{q2}} = 0.20 \tag{4.14}$$

Equation 4.14 was specifically developed for propane-air mixtures and has not been validated for methane-air mixtures. Since there is a lack of information regarding single-wall quenching distances as a function of methane-air equivalence ratios, the parallel plate quenching distance measurements of Harris, et. al. [31] are converted to single-wall quenching distances by means of Equation 4.14 and plotted in Figure 4.6 together with the results of this simulation. Figure 4.6 also shows single-wall quenching distances as calculated by Westbrook, et. al. [14] (methane-air, $\Phi = 1$, T_u=300 K, p=1atm) and Adamczyk and Lavoie [33] (propane-air, T_u=293 K, P=1 atm) under consideration of elementary reaction kinetics including the conservation equations for a multicomponent reacting system.

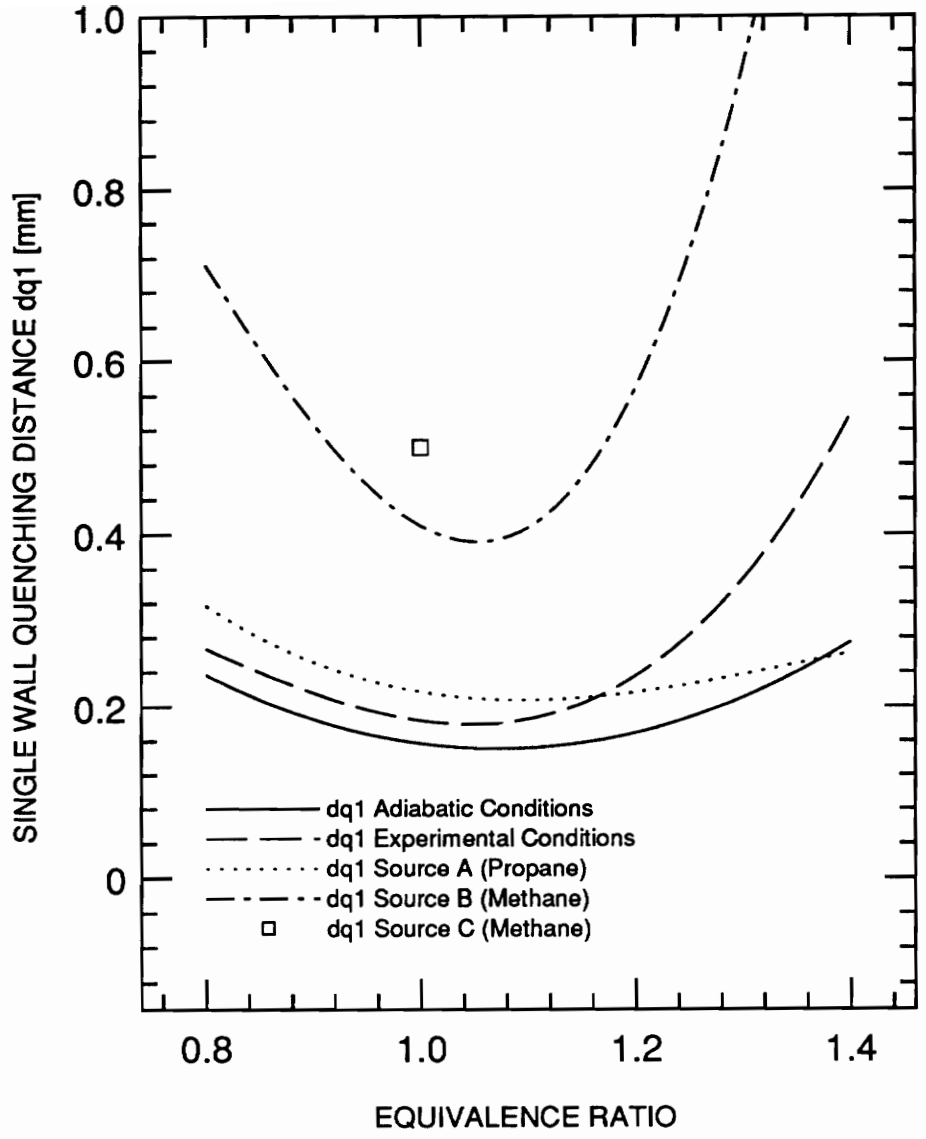

Figure 4.6: **Calculated single-wall quenching distances under adiabatic and experimental conditions compared to numerical results from Adamczyk and Lavoie [33] (A), Westbrook, et. al.[14] (B) and experimental results from Harris, et. al. [31] (C). All quenching layers at P=1 atm and $T_u \approx 293$ K.**

The calculated results agree with literature data, in that the quenching layer has a minimum thickness at near stoichiometric mixtures and thickens as the mixture becomes lean and rich. Compared to the results of Harris, et. al. [31] and Westbrook, et. al. [14] this simulation underpredicts the methane-air quenching layer by a factor of 2.

Discussion

The adiabatic as well as the corrected flame speed is lower for both lean and rich mixtures and peaks at slightly richer than stoichiometric (see Figure 4.2). For fast burning mixtures (near stoichiometric), the temperature profiles in the preheat zone are very steep due to the large fraction of convective heat transfer as compared to the conductive heat transfer. As a result, flame movement is affected by the presence of a heat sink very late and flame quenching occurs close to the wall. For slow burning mixtures (lean and rich) heat penetrates further into the unburned gas mixture due to an increased portion of conductive, and a decreased portion of convective heat transfer. Now the flame is affected earlier by heat loss and flame movement stops further away from the wall. Thus, the competition between conduction in the direction of flame movement and convection in the opposite direction is responsible for the change in quenching distance with equivalence ratio.

As expected from the above discussion, the quenching layer thickness increases for the slower burning experimental flames as compared to adiabatic flames. Large quenching gaps are reported for rich experimental flames because of their extremely low flame speed. A comparison with the literature on quenching layers shows that trends of quenching layers as a function of the equivalence ratio are predicted well.

4.2.2.2 Variation of Unburned Wall Temperature from T_u =293 K to 1100 K at Constant Equivalence Ratio Φ=1 and P=1 atm

Input Parameters

Quenching experiments at various wall temperatures and pressures to simulate the flame-wall interactions in diesel engines are projected, but have not yet been carried out. However, a simulation is made to obtain a trend, describing the effect of variable wall temperatures on quenching layer thickness at ambient pressure. The unburned gas temperature is raised from 300 K up to 1100 K in increments of 100 K. According to Heywood [39], 1100 K is the auto-ignition temperature for premixed methane-air flames at P=1 atm.

Since no experimental data is available at this point, calculations are performed for adiabatic flame conditions only. Adiabatic flame speed as a function of the unburned gas temperature T_u is given by Andrews and Bradley [36] by the following correlation:

$$S_u^a - 10\frac{cm}{s} = 0.000371 T_u^2 \ \frac{cm/s}{K^2} \tag{4.12}$$

This correlation has been developed and validated by the authors for unburned gas temperatures up to 800 K.

The difference in temperature across a flame front is assumed to be independent of the unburned gas temperature T_u. Therefore adiabatic flame temperatures at various unburned gas temperatures are calculated according to:

$$T_f^a = T_u + \Delta\ T_f^{a}{}_{(\Phi=1.0,\ T_u=293\ K)} \tag{4.13}$$

Thermal properties of the stoichiometric methane-air mixture as a function of unburned gas temperature T_u are approximated by those of air. To compensate for the assumed constant heat capacity, the heat of reaction is calibrated to yield adiabatic flame temperature T_f^a in regions where flame propagation is unaffected by the cold wall.

Results

Figure 4.7 shows calculated quenching distances together with flame speed from Andrews and Bradley [36] and thermal diffusivity of air versus unburned gas temperature T_u. As the unburned gas temperature rises from T_u=293 K to T_u=1100 K the quenching layer shrinks from 0.2 mm to 0.1 mm.

Comparison to Literature

For comparison, the experimental two-wall quenching layer thickness found by Friedman and Johnston [5] for wall temperatures between 300 K and 550 K and propane-air mixtures is correlated with a single-wall quenching distance by means of Lavoie's [10] relationship, (Equation 4.14) and shown in Figure 4.8. Single-wall or parallel-plate quenching distances for methane-air at elevated wall temperatures are not available in the literature.

This study and the experimental results from Friedman and Johnston [5] agree that the quenching layer shrinks as the wall (unburned gas) temperature increases. However, there is considerable disagreement over the magnitude of quenching layer shrinkage. This study suggests a gradually decreasing quenching gap with increasing unburned gas temperature, whereas the experimental results from Friedman and Johnston [5] show a drastic drop in quenching layer thickness. Following the trend of Friedman and Johnston's [5]

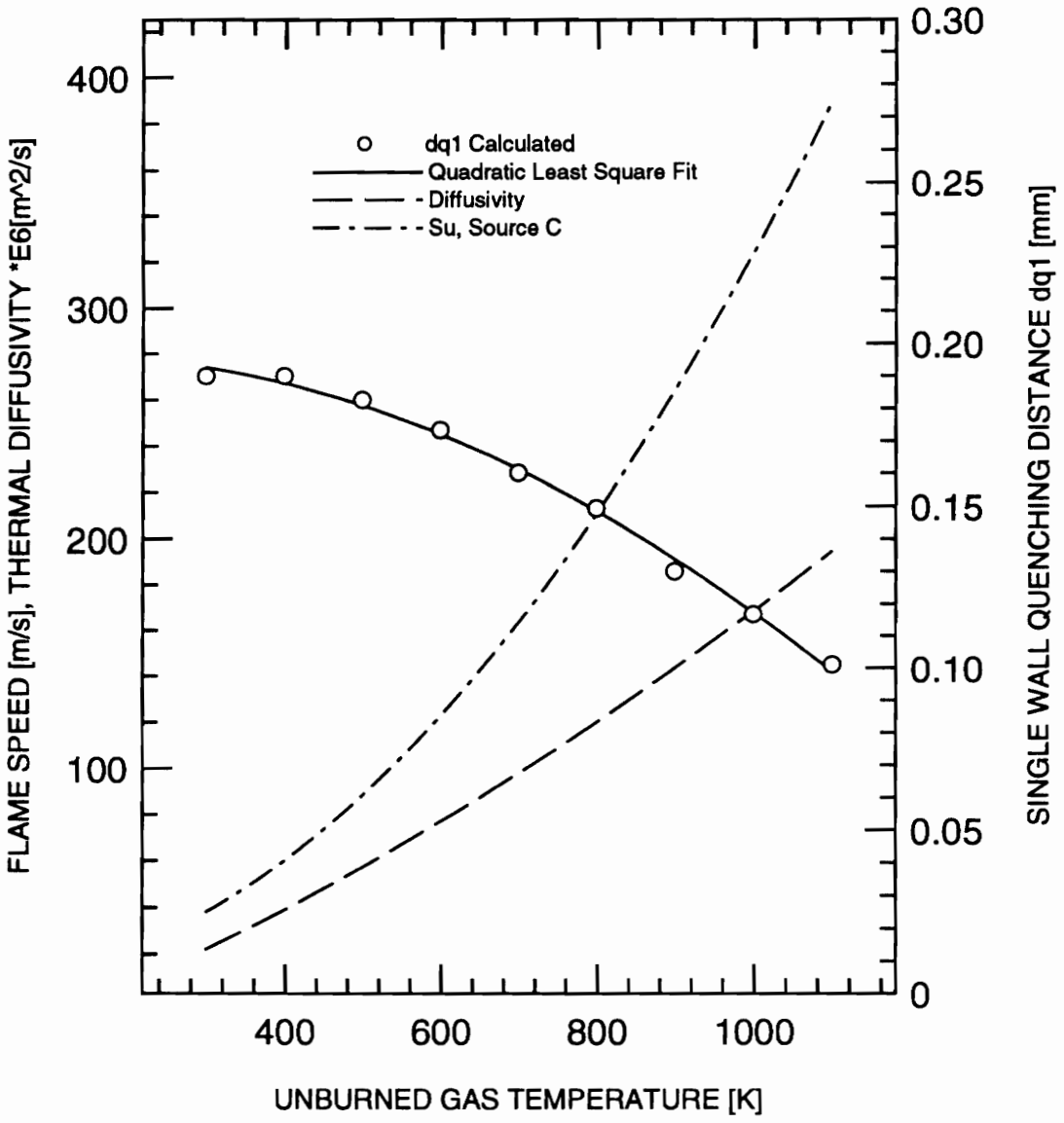

Figure 4.7: Calculated single-wall quenching distance d_{q1}, thermal diffusivity of air and adiabatic flame speed $S_u^a - 10\frac{cm}{s} = 0.000371T_u^2\frac{cm/s}{K^2}$ from Andrews and Bradley [36] for methane-air mixtures versus unburned wall temperature T_u at P=1 atm. Coefficients of curve fit are: a=0.1963, b=1.699E-5, c=-9.644E-8.

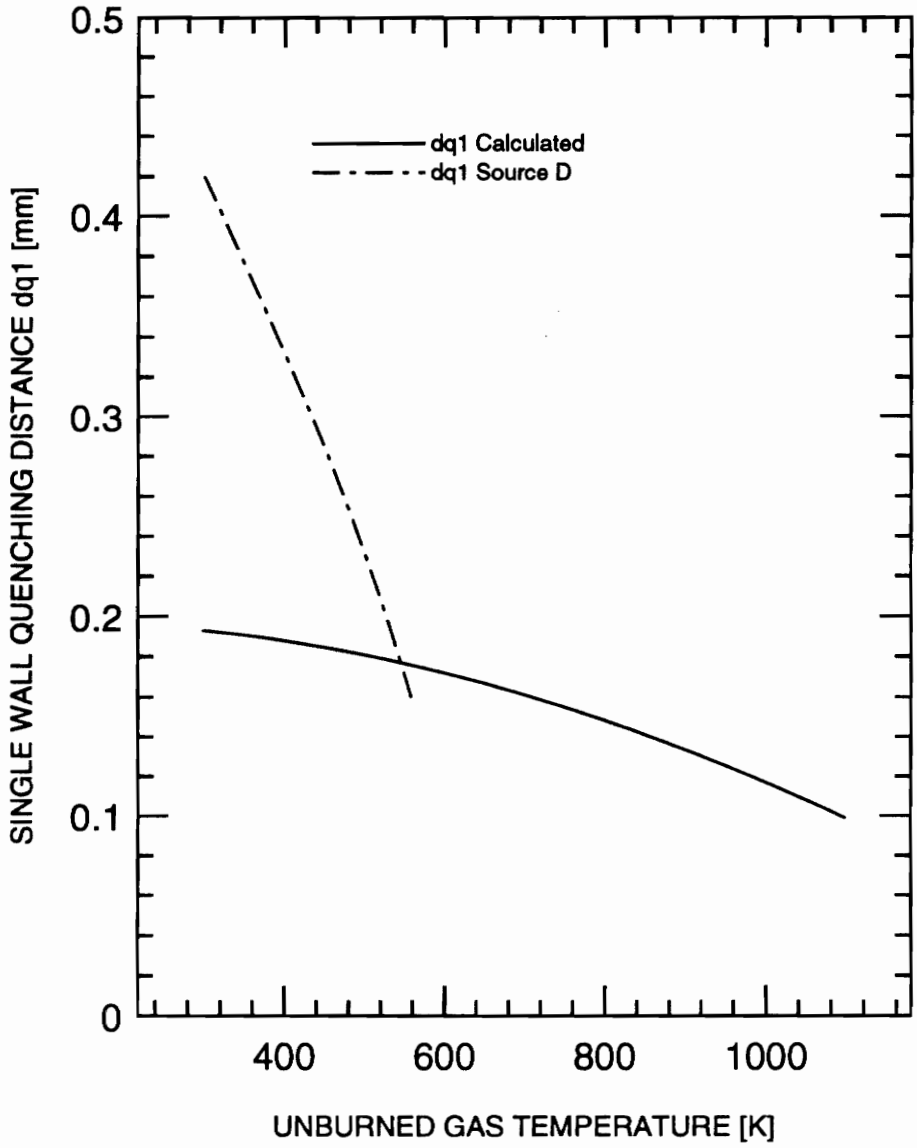

Figure 4.8: **Calculated quenching layer thickness d_{q1} at elevated unburned gas temperature compared to Friedman and Johnston's [5] experimental two-wall quenching thickness which is correlated with a single-wall quenching distance by Lavoie's [10] relationship $\frac{d_{q1}}{d_{q2}} = 0.20$.**

experimental data, there would not be a quenching layer at 700 K, which is difficult to explain. It must be pointed out here that a Lavoie's [10] correlation is used to calculate single-wall quenching distances from Friedman and Johnston's [5] two-wall quenching distances, which is verified for mixture variation at ambient temperatures only.

Discussion

Flame speed and thermal diffusivity have opposing effects on the quenching layer thickness: as the flame speed increases, the temperature profile in the preheat zone steepens due to increased convective heat transfer and the quenching layer tends to become thinner. At the same time, conductive heat transfer into the preheat zone is enhanced by the increased thermal diffusivity, and the quenching layer tends to become thicker. The net product is a decrease of quenching layer thickness from 0.2 mm to 0.1 mm, because the flame speed increases with the second power of the unburned gas temperature, whereas the thermal diffusivity is increased approximately linearly with temperature.

4.2.3 Evaluation of 1st Law Balance Model and Summary

Calculated quenching layer thickness for variation of equivalence ratio and variation of unburned gas temperature are in good agreement with the trend of quenching layer data from the literature. The calculated heat transfer rates to the wall during flame quenching differ considerably from those measured in the experiment. Experiments show heat flux amplitudes of 0.9 MW/m^2 during flame quenching at T_u=293 K for stoichiometric methane-air mixtures, whereas for identical conditions this simulation indicates a peak heat flux of 0.08 MW/m^2 only. The reason for this discrepancy is that the kinetic aspects of

the flame quenching process are represented by a single Arrhenius type reaction equation only (Equation 4.10). This equation represents the temperature sensitivity of a one-step global reaction, which is an enormous simplification of the complex quenching process, and flame extinction occurs quickly. As shown by Westbrook, et. al. [14], flame quenching is a relatively slow process that is characterized by the diffusion of hydrocarbons and oxygen from the quenching gap towards the flame front, which remains stationary at the quenching distance with an active pool of radicals until the quenching layer fuel content is consumed. A proper representation of chemical reactions (including intermediate species) and diffusivity of matter during flame-wall interaction would result in a large increase of heat flux amplitude and duration. It is also necessary to formulate governing equations that capture the entire time history of the quenching process in order to account for heat transfer due to heat diffusion subsequent to flame extinction.

In summary, the results of an analytical investigation by means of the first law balance model are:

- It is not possible to adequately describe the flame-wall heat transfer by representing chemical kinetics during flame quenching by an Arrhenius type equation that accounts for the temperature sensitivity of the reaction rates according to a single-step reaction mechanism. The diffusion and the consumption of the quenching layer hydrocarbons by a temporarily stationary flame front are essential features of the flame quenching process.
- Transient effects must be accounted for by the governing equations in order to represent the time history of the quenching process and the wall heat transfer due to diffusion of heat subsequent to flame extinction.

- Calculated single-wall quenching layers are in agreement with the trend of single-wall quenching layers in the literature. Minimum single-wall quenching distances at T_u=293 K and P=1 atm are predicted for mixtures near stoichiometric ($\Phi = 1.05$). The quenching layer thickens for both leaner and richer mixtures. Generally, the predicted single-wall quenching layer thickness is in the order of 0.2 mm.
- The quenching layer thickness shrinks with increasing unburned gas temperature.

4.3 Transient Heat Conduction Model to Predict Flame-Wall Heat Transfer

4.3.1 Development of Model

This analytical model is developed to approximate heat transfer during flame quenching at cold and heated walls up to 1100 K. The analysis is based on a one-dimensional, fully transient heat conduction system, in which a moving heat generation sheet is used to simulate the heat impact of a traveling flame.

It is concluded in Section 4.2.4 that flame-wall heat transfer cannot be calculated by a one-step reaction mechanism, where the flame is rapidly extinguished due to heat loss at some distance to the wall without consuming the fuel content of the quenching layer. The numerical work of Westbrook, Adamczyk and Lavoie [14] shows that fuel oxidation during flame quenching is maintained until all quenching layer hydrocarbons are consumed. Combustion of the quenching layer fuel by a temporarily stationary flame front seems to largely contribute to wall heat transfer.

In order to account for complete combustion of the unburned gas mixture during the quenching process, the flame front is represented by a heat generation sheet that travels at uniform speed (the flame speed) along a one-dimensional slab all the way to an end wall. Figure 4.9 shows the slab of cold gases, bounded by a wall at $x=L$, from where the heat generation sheet begins to travel at time $t=0$ (ignition) and the quench wall at $x=0$. The distance L in between the walls is selected so that flame quenching at $x=0$ is thermally unaffected by heat transfer to the wall at $x=L$ (i.e. $L \approx \infty$). Initially, the entire gas mixture and walls is at uniform temperature T_u.

The mathematical formulation is given by:

$$\frac{\partial^2 T(x,t)}{\partial x^2} + \frac{1}{k} g(x,t) = \frac{1}{\alpha} \frac{\partial T(x,t)}{\partial t}$$

$$in \qquad 0 < x < L, \qquad t > o$$

with boundary conditions

$$T = T_u \quad at \quad x = 0, \qquad t > 0$$

$$T = T_u \quad at \quad x = L, \qquad t > 0$$

and initial condition

$$T = T_u \quad for \quad t = 0, \quad in \quad 0 \le x \le L \tag{4.15}$$

It is most convenient to represent the moving heat source in terms of the Dirac delta function:

$$g(x', \tau) = g_s \delta(x' - S_u \tau), \qquad 0 < t \le t_h$$

$$g(x', \tau) = 0 \qquad\qquad t > t_h \tag{4.16}$$

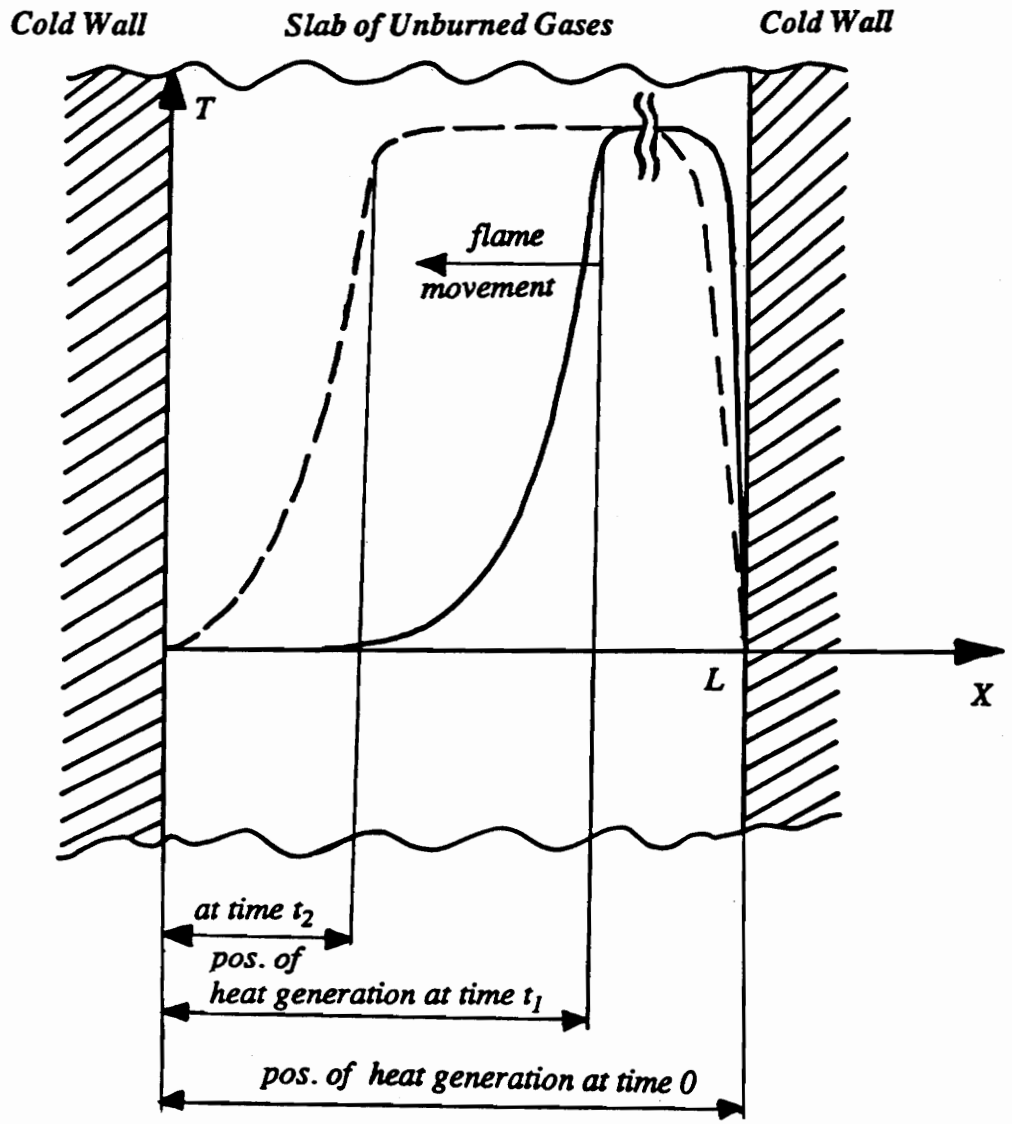

Figure 4.9: The considered transient heat conduction in a finite slab with specified temperature boundary conditions, homogeneous initial condition and moving heat generation sheet.

where the strength of the sheet heat source is $\dot{g}_s'' = h_{pr} S_u$ in W/m^2 and constant. At time $t=0$, the heat generation sheet begins to propagate from $x=L$ in the negative x-direction. After the heat source has moved throughout the entire slab of gases with uniform speed S_u, it arrives at time $t=t_h$ at the left boundary $x=0$. Upon arriving, heat generation is switched off so that for times $t>t_h$ heat is transferred out of the system only.

A set of non-homogeneous boundary conditions are introduced by Equations 4.15, therefore the one-dimensional transient heat conduction problem is solved by the use of Green's function. A discussion of the mathematical details for the solution of Equations 4.15 are given in Appendix E.

The solution for the transient temperature distribution in the one-dimensional slab is:

$$\theta(x,t) = \frac{2\alpha\, g_s}{kL} \sum_{m=1}^{\infty} \sin(\beta_m x) \left[\frac{1}{(\alpha\beta_m^2)^2 + (\beta_m S_u)^2} \right]$$
$$\left[\alpha\beta_m^2 \sin(\beta_m S_u t) - \beta_m S_u \cos(\beta_m S_u t) + \beta_m S_u \exp(-\alpha\beta_m^2 t) \right]$$
$$in \qquad 0 \le x \le L \quad for \quad 0 < t \le t_h$$

$$\theta(x,t) = \frac{2\alpha\, g_s}{kL} \sum_{m=1}^{\infty} \sin(\beta_m x) \left[\frac{1}{(\alpha\beta_m^2)^2 + (\beta_m S_u)^2} \right]$$
$$\left\{ \left[\exp(\alpha\beta_m^2 (t_h - t)) \left(\alpha\beta_m^2 \sin(\beta_m S_u t_h) - \beta_m S_u \cos(\beta_m S_u t_h) \right) \right] \right.$$
$$\left. + \beta_m S_u \exp(-\alpha\beta_m^2 t) \right\}$$
$$in \qquad 0 \le x \le L \quad for \quad t > t_h$$

where β_m are the eigenvalues of the problem:

$$\beta_m = \frac{m\pi}{L}, \qquad m = 1, 2, 3, \ldots$$

and $$\theta = T - T_u \tag{4.17}$$

Wall heat transfer is calculated from the first derivative of the transient temperature distribution at $x=0$. The length of the one-dimensional slab of gases is selected so that heat transfer during arrival of the heat generation sheet at $x=0$ is not affected by heat dissipation to the wall at $x=L$.

A FORTRAN program was written to carry out the indicated summations in order to obtain the temperature distribution as a function of position and time, and the transient heat flux to the wall at $x=0$. The FORTRAN code is presented in Appendix H.

Calculations are performed using the transient heat conduction model to predict flame-wall heat transfer as a function of methane-air equivalence ratio and unburned gas (wall) temperature. One set of heat flux data is obtained for the variation of methane-air equivalence ratio between $0.8 \leq \Phi \leq 1.4$ at constant unburned gas temperature T_u=293 K. The second set of data is calculated for variable unburned gas (wall) temperatures between 300 K $\leq T_u \leq$ 1100 K, the latter being the auto-ignition temperature of methane in air at $\Phi = 1$ and P=1 atm.

4.3.2 Results and Discussion

Flame-wall heat transfer is calculated by means of a transient heat conduction model with variations of the methane-air mixture ratio at constant ambient wall temperature and with elevated wall temperatures up to 1100 K at stoichiometric mixtures. The fact that real hydrocarbon flames are quenched at some distance to a cold wall is ignored, and the heat

generation sheet, which is used to simulate flame propagation, moves at uniform speed through the entire one-dimensional slab of gases until it reaches the cold boundary, to which the instantaneous heat flux is calculated.

4.3.2.1 Heat Flux at Variable Equivalence Ratio, Wall at Ambient Temperature and P=1atm

Input Parameters

In order to predict heat transfer as measured under experimental conditions, the experimental (corrected) flame speed S_u^c is selected to be the speed at which the heat generation sheet moves through the one-dimensional slab of gases. Heats of reaction for the individual mixtures, from which the heat sheet strength is determined by $\dot{q}_s'' = h_{pr} S_u^c$, are calibrated so that the temperature behind the heat source (flame front) in regions far away from the wall is T_f^c from Equation 4.11. Thermal properties of the gas mixture are taken from STANJAN [37] calculations and are assumed to be constant at the unburned gas (wall) temperature.

Results

Several consecutive temperature profiles in the early stages of heat source (flame) propagation are plotted in Figure 4.10 at times Δt apart from one another. The heat source is located at the peak of the individual temperature profiles and advances from its onset (ignition) in intervals $\Delta x = S_u \Delta t$ towards the positive x-direction (the situation shown in Figure 4.10, where a moving heat source gradually increases the local gas

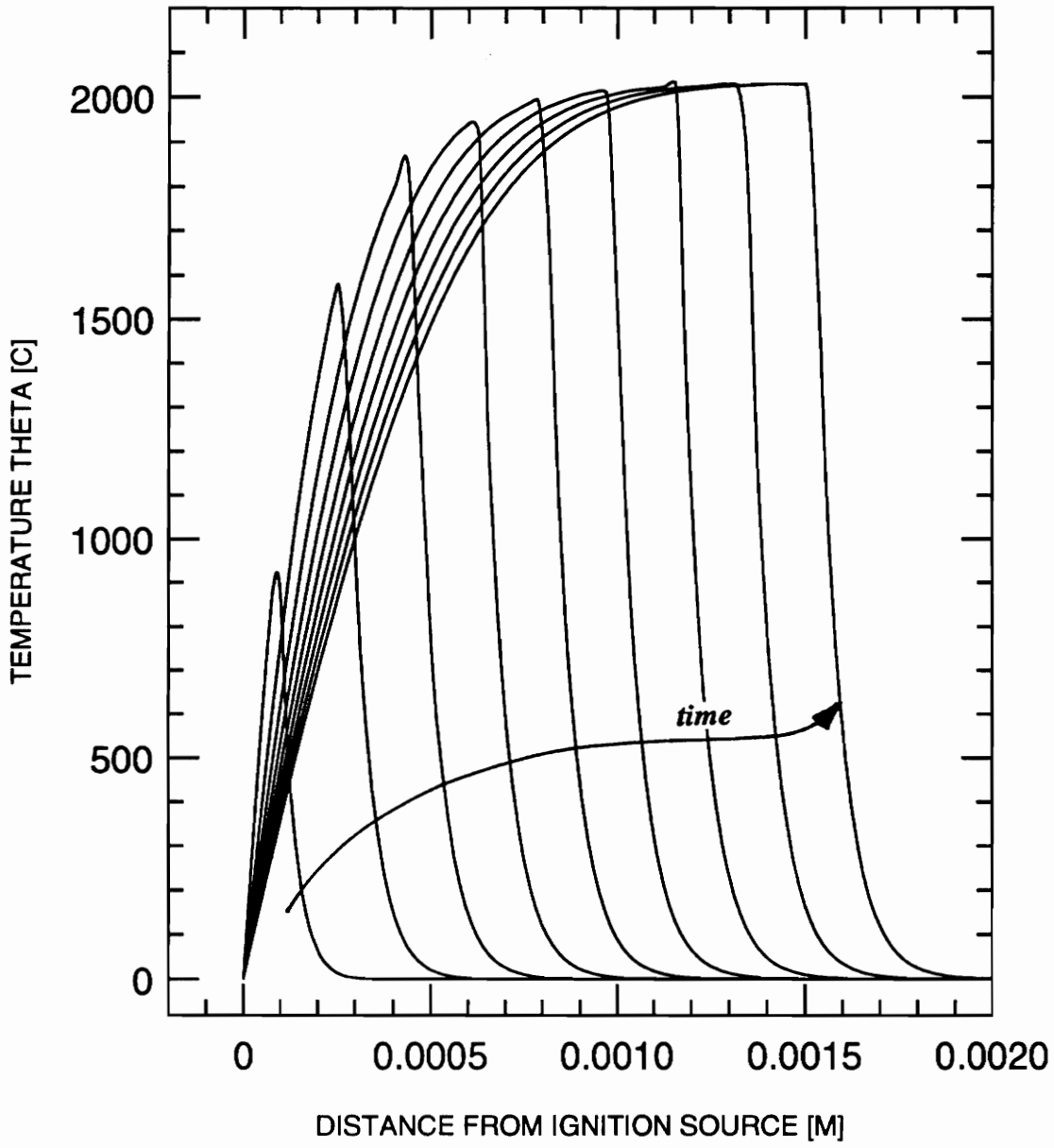

Figure 4.10: **Development of temperature profiles from ignition for a stoichiometric mixture at T_u =293 K and P=1 atm. The temperature profiles are spaced Δt=0.44E-3 apart from one another.**

temperature, is physically unrealistic since an ignition source must locally heat gases above the autoignition temperature in order to initiate flame propagation). Soon, a steady temperature (flame temperature) is reached because the heat source propagates out of the growing heat transfer boundary layer at the wall ($x=0$). As a result of conduction in the positive x-direction, and convection in the opposite direction, the temperature ahead the heat source decays exponentially.

Upon arrival at the end wall, the heat generation source is switched off and the thermal gradients relax. Temperature profiles during quench are shown in Figure 4.11. The dashed lines correspond to temperature profiles at times $t > t_h$, where the heat generation source is inactive. Figure 4.12 shows temperature profiles under the same conditions as Figure 4.11 at higher time resolution.

Heat transfer is calculated from the temperature gradients at the wall. In Figure 4.13, wall heat transfer together with positions of the approaching heat generation source are displayed for a stoichiometric mixture at T_u=293 K. The origin of the time coordinate refers to the instant where the heat flux reaches the maximum value. As indicated in Figure 4.13 by the dotted line, the peak heat flux occurs shortly before the heat generation sheet arrives at the wall.

Figure 4.14 shows the calculated peak heat transfer rates and velocity of the moving heat source as a function of methane-air equivalence ratios at T_u=293 K. Peak heat transfer rates are large for near stoichiometric mixtures, and level off for increasingly lean and rich mixtures.

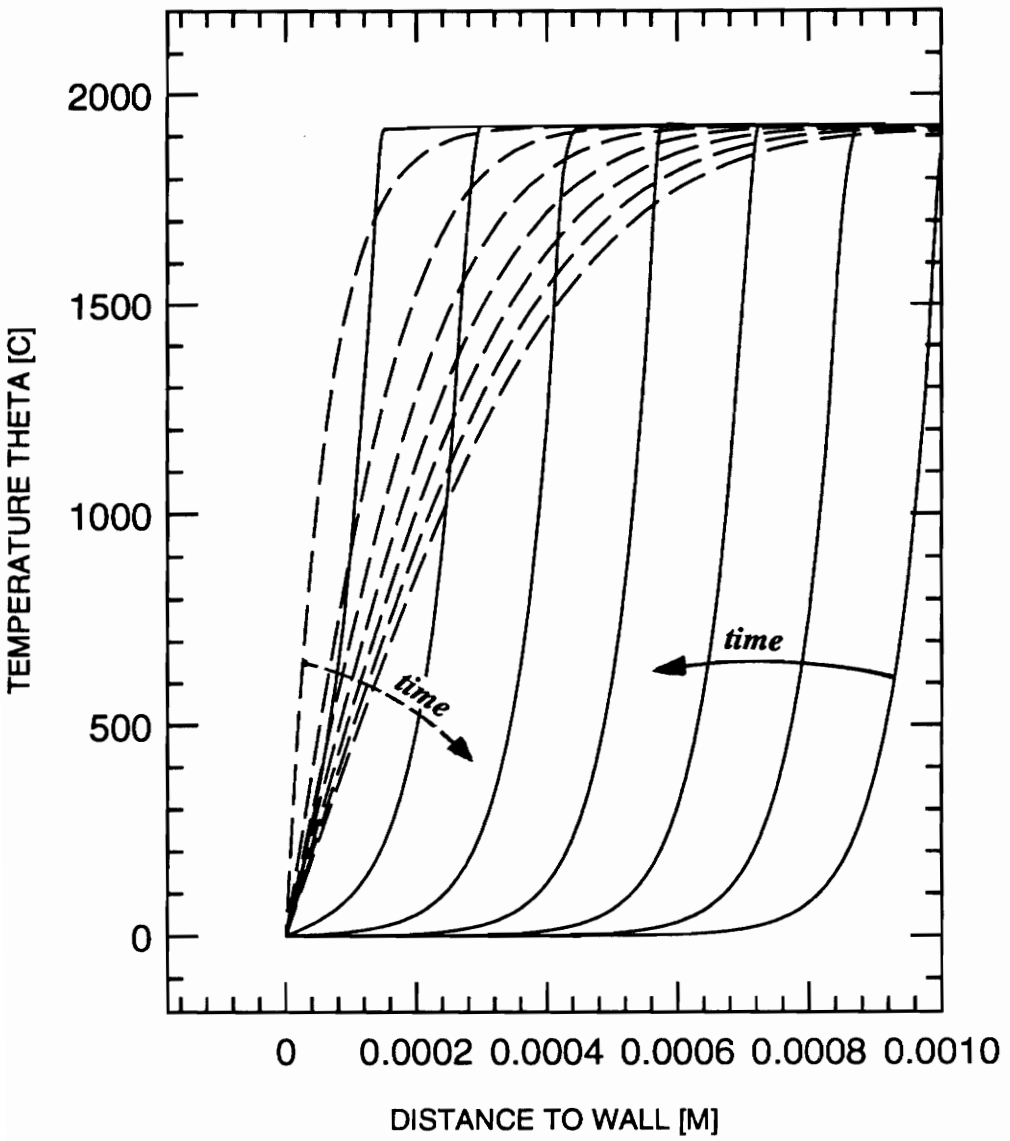

Figure 4.11: **Temperature profiles during heat source arrival at the cold wall for a stoichiometric mixture, Δt=0.37E-3 s apart from one another, solid lines for times $t \leq t_h$ and dashed lines for times $t > t_h$, T_u=293 K and P=1 atm.**

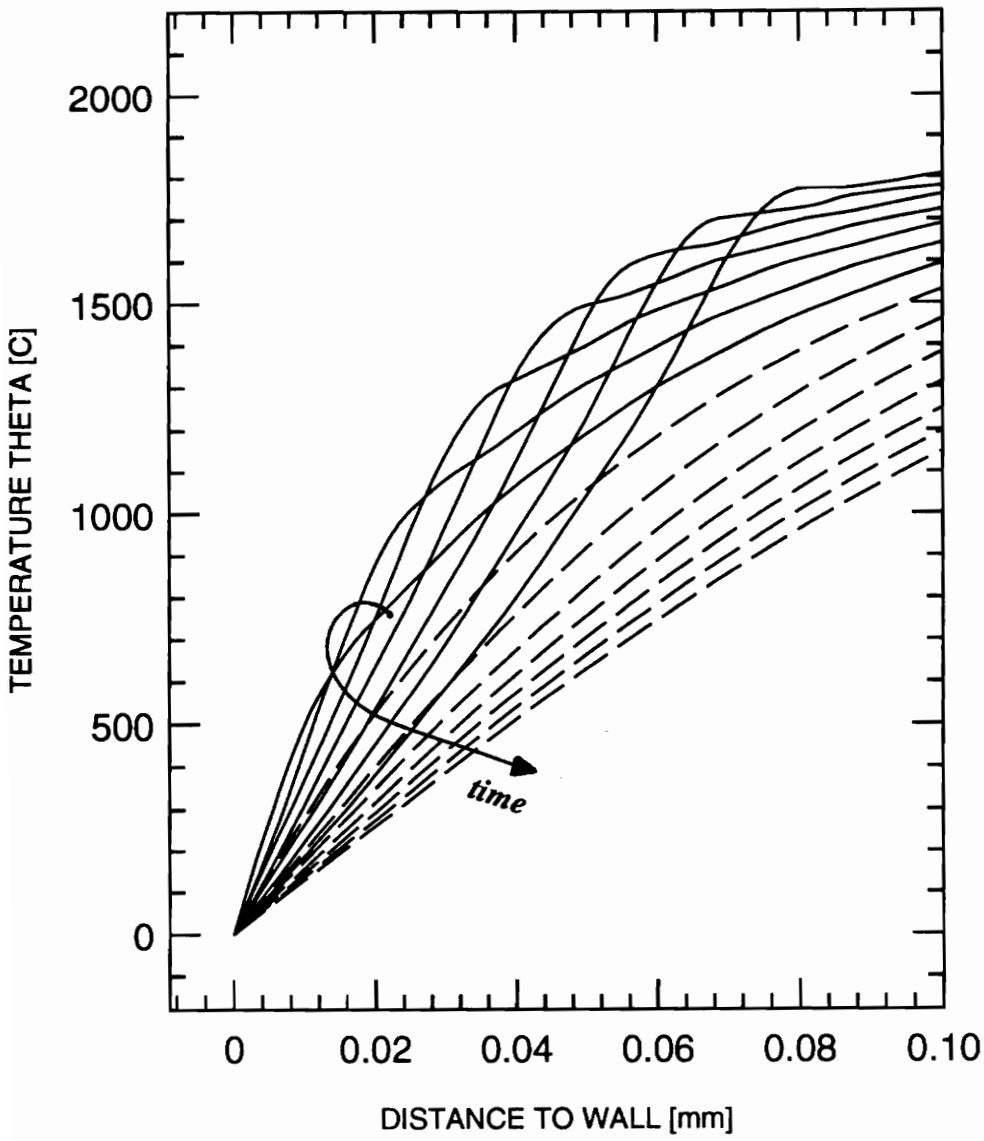

Figure 4.12: **Temperature profiles during heat source arrival at the cold wall for a stoichiometric mixture, Δt=0.037E-3 s apart from one another, solid lines for times $t \leq t_h$ and dashed lines for times $t > t_h$, T_u=293 K and P=1 atm.**

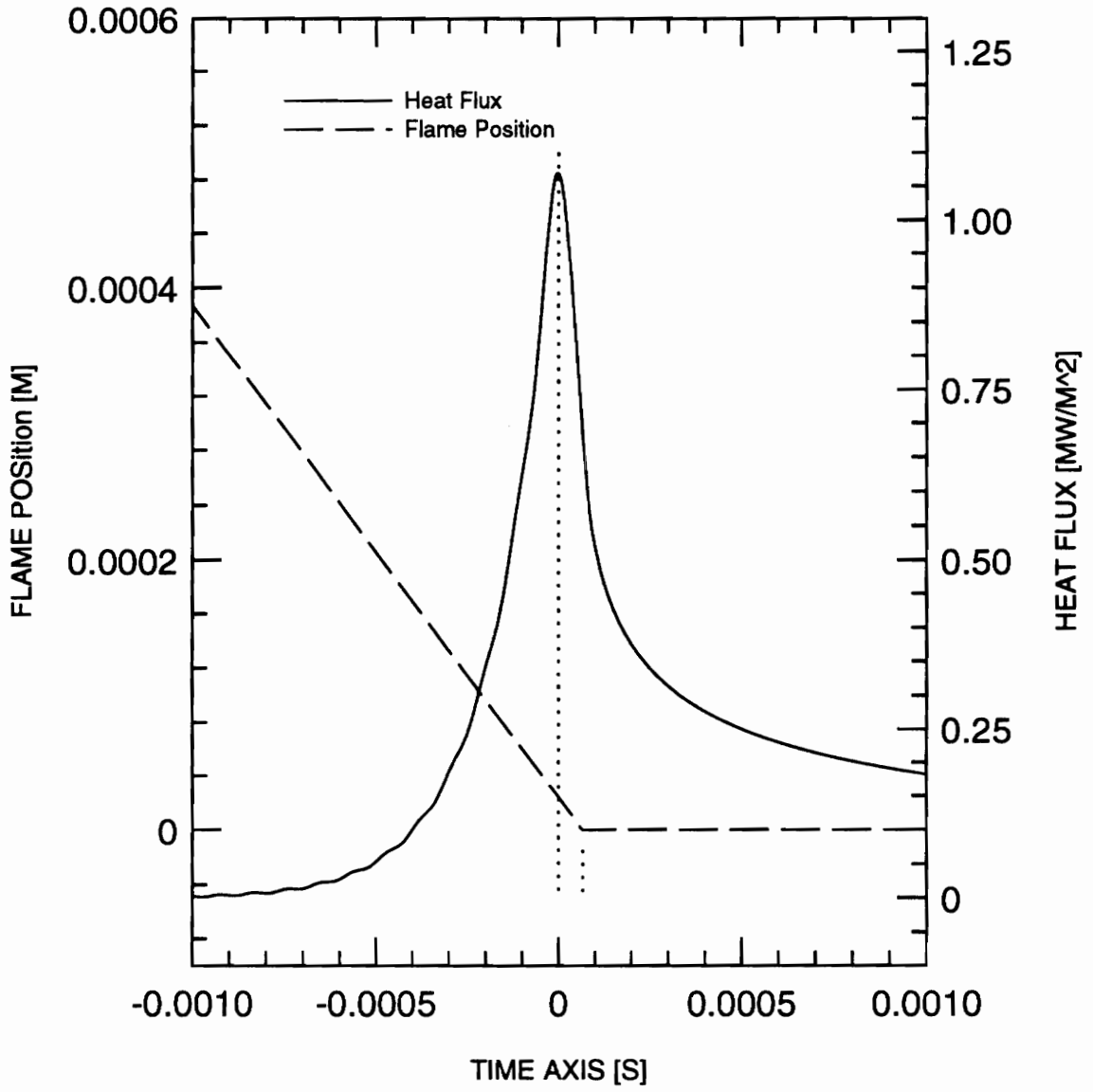

Figure 4.13: **Transient heat flux and flame position versus time for a stoichiometric mixture at T_u=293 K and P=1 atm. The dotted lines indicate the time lag between the arrival of the heat source and the occurrence of the maximum heat flux.**

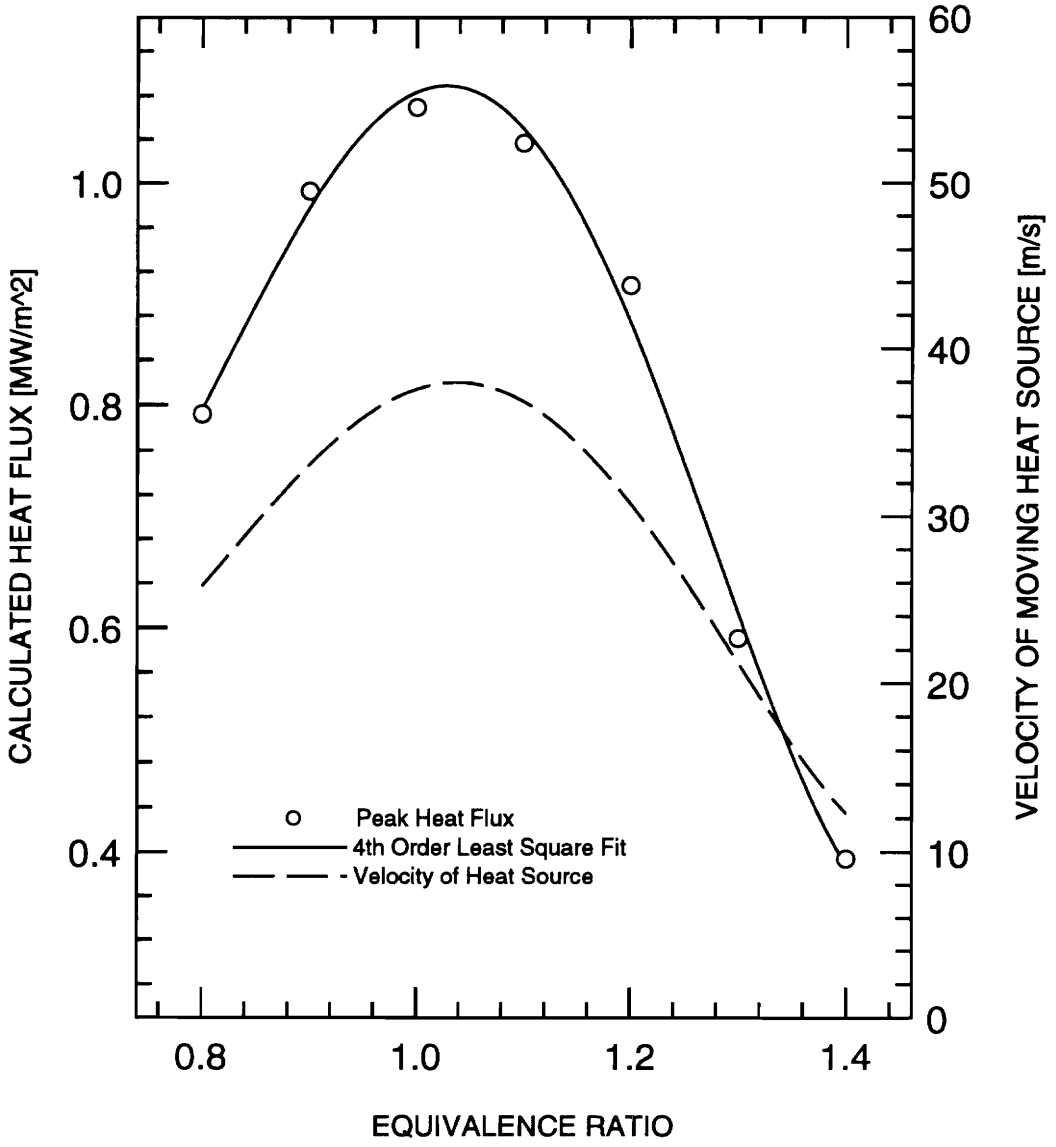

Figure 4.14: **Calculated peak heat transfer rates and velocity of heat source versus equivalence ratio variation at T_u=293 K. The coefficients of the fourth order least square fit are: a=24.4, b=-103.6, c=162.2, d=-107.4, e=25.5.**

Comparison of Predicted and Experimental Heat Flux

A comparison is made between the experimental and calculated heat fluxes for a stoichiometric mixture at T_u=293 K and P=1 atm in Figure 4.15. Both heat flux curves are arranged on common axis such that t<0 refer to times prior to the instance of maximum heat transfer, and the time t=0 corresponds to the instance of maximum heat transfer. The calculated heat flux begins to rise later and drops off earlier relative to the occurrence of the peak heat flux as compared to the experimental data. There is some disagreement between the predicted and experimental heat transfer.

Figure 4.15 also provides a comparison of the calculated heat flux to Vosen's [26] experimental data (constant volume combustion chamber flame quenching experiment, pressure at quench P=1.19 atm, T_u=293 K). The calculated heat flux curve follows Vosen's [26] heat flux curve well until shortly before the occurrence of the maximum heat flux amplitude. The predicted instantaneous heat flux curve then rises to about twice the value of Vosen's results. Immediately after the occurrence of the maximum amplitude, the predicted heat flux curve again closely follows Vosen's heat flux graph. It follows from visual inspection that the area under both heat flux graphs, and therefore the time integrated flame-wall heat transfer, are nearly identical.

Peak heat flux variation with equivalence ratio for experiment and simulation is shown in Figure 4.16. Calculated results match the trend of the experimental heat flux curve well although there is a quantitative difference up to 50% of the absolute amplitude of the heat flux.

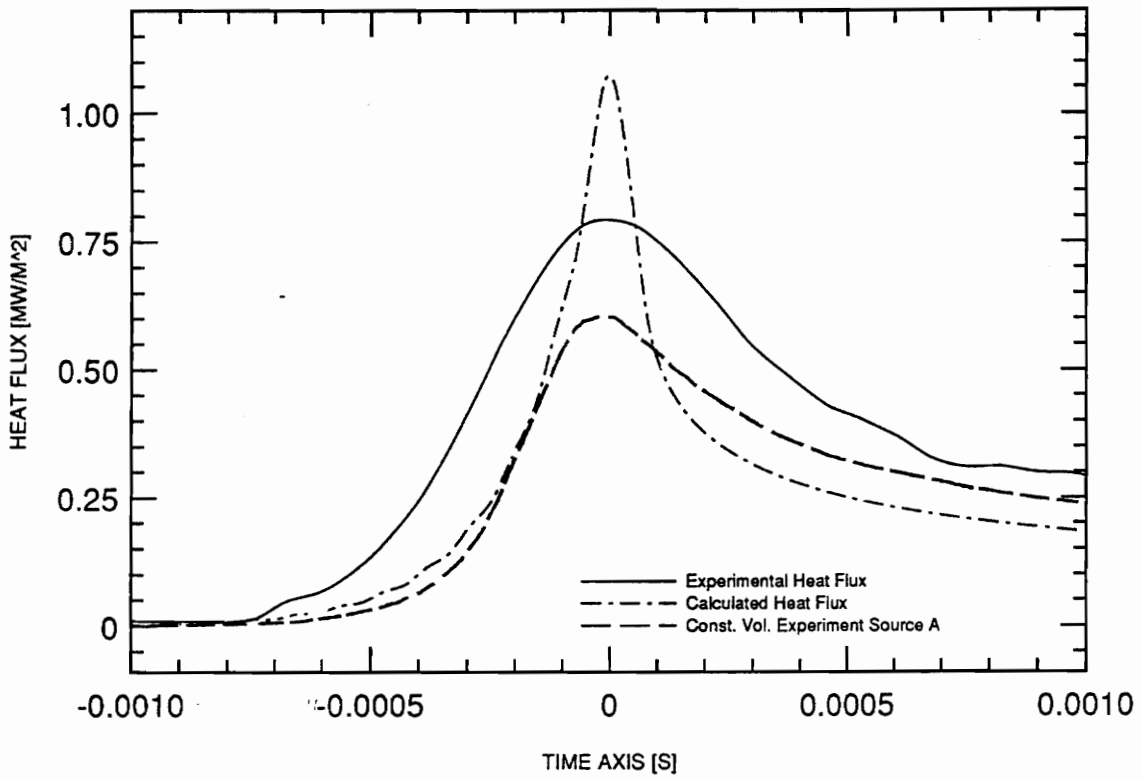

Figure 4.15: Comparison of the calculated and the experimental heat transfer data to the heat transfer measurement of Vosen [26] for a stoichiometric methane-air mixture at T_u=293 K and P≈1 atm, t<0 refer to times prior to, and t=0 corresponds to the maximum heat transfer rate.

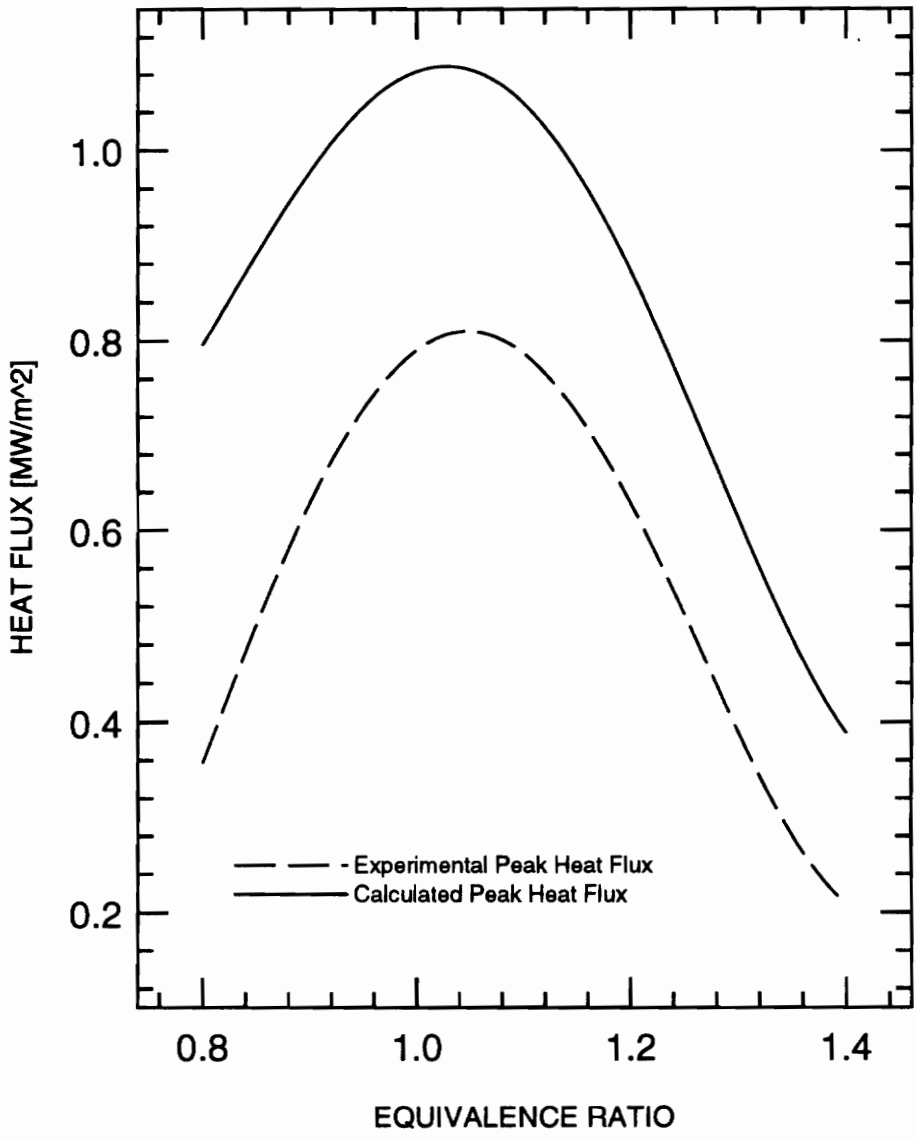

Figure 4.16: Calculated and experimental variations of peak heat transfer with equivalence ratio at T_u=293 K and P=1 atm.

Discussion

The rate at which heat is released by the heat source is $\dot{q}_s'' = h_{pr} S_u^c$ in energy per unit area per unit time where h_{pr} is the heat of reaction per unit volume and S_u^c is the velocity of the heat generation sheet (corrected flame speed). For near stoichiometric mixtures, the values of S_u^c and h_{pr} are high; therefore, energy is released very quickly in front of the quench wall, the temperature gradients at the wall rise and heat flux amplitudes are large. For rich or lean mixtures, heat sheet velocities and heat release per unit area are lower, the energy is transferred out of the system nearly as fast as it is generated without a large overshoot of the thermal gradients.

Figure 4.15 shows a considerable difference between calculated and experimental heat flux trends versus time. Heat source and flame propagation in the vicinity of the cold wall are fundamentally different. The experimental heat flux is a consequence of fuel consumption by a stationary flame at some distance from the wall, whereas the calculated heat flux is caused by a heat source that moves at uniform speed until it reaches the wall. However, one would expect the transient heat conduction model to well predict:

- instantaneous heat transfer before the onset of quenching, when both flame and heat source are outside the quenching layer
- instantaneous heat transfer after the flame is quenched, when the residual temperature profiles from the actual flame and the heat source sheet should be similar
- overall heat transfer, since the head-on wall is the only object heat is transferred to within the time period of interest (the experimental heat flux may be affected by heat loss to the tube walls after some time)

As shown in Figure 4.15, the predicted heat flux curve follows the trend of Vosen's results except for the short period of actual flame quenching. The overall heat transfer, which is the area under the heat flux graphs, is identical. A comparison between the calculated instantaneous heat flux and the experimental result of this study in Figure 4.15 casts doubt on the accuracy of the heat flux measurement.

4.3.2.2 Heat Flux at Elevated Wall Temperatures for Stoichiometric Mixtures and P=1 atm

Input Parameters

Adiabatic flame speeds as a function of the wall temperature are taken from Andrews and Bradley [36], $S_u^a - 10\frac{cm}{s} = 0.000371T_u^2 \frac{cm}{s\ K^2}$, and the temperature difference between unburned gases (and quench wall) and the freely traveling heat generation sheet always equals the temperature difference across an adiabatic flame (see Equation 4.13). Only the gas properties and flame speeds are changed in order to simulate flame quenching at elevated wall temperatures. The thermal properties of the gaseous mixture in the one-dimensional layer of gases are approximated by those of air. As a consequence of decreasing gas density with increasing unburned gas temperature, the available heat of reaction in the one-dimensional slab of gases is decreased.

Results

The effect of wall temperature changes on the instantaneous heat transfer rate is simulated by the transient heat conduction model. The predicted heat flux graphs versus time are qualitatively similar to those at ambient wall temperatures (see Figure 4.13). Figure 4.17 shows peak heat fluxes for wall temperature variations between 300 $K \leq T_u \leq 1100$ K The peak heat flux increases linearly with rising wall temperatures from 1.09 MW/m^2 to 3.22 MW/m^2.

Discussion

The heat release rate of the moving heat source is a function flame speed, $\dot{q}_s'' = h_{rp} S_u^{\ a}$ in energy per unit area per unit time. As indicated in Figure 4.17, the heat source velocity rises with the second power of the unburned gas temperature, whereas the thermal diffusivity (of air) only increases roughly linearly. Consequently, the temperature gradients at the wall as well as the instantaneous heat flux amplitude are increased with rising wall temperatures.

The heat transfer rate may be expressed as:

$$\dot{q}'' = h(T_s - T_\infty) \tag{4.18}$$

where h is the convective heat transfer coefficient, T_s the wall temperature and T_∞ the steady state flame temperature. The temperature difference between the wall and a freely traveling (steady-state) flame remains constant at all unburned gas temperatures, but the heat flux amplitudes are increased with rising unburned gas temperatures. Thus, a model

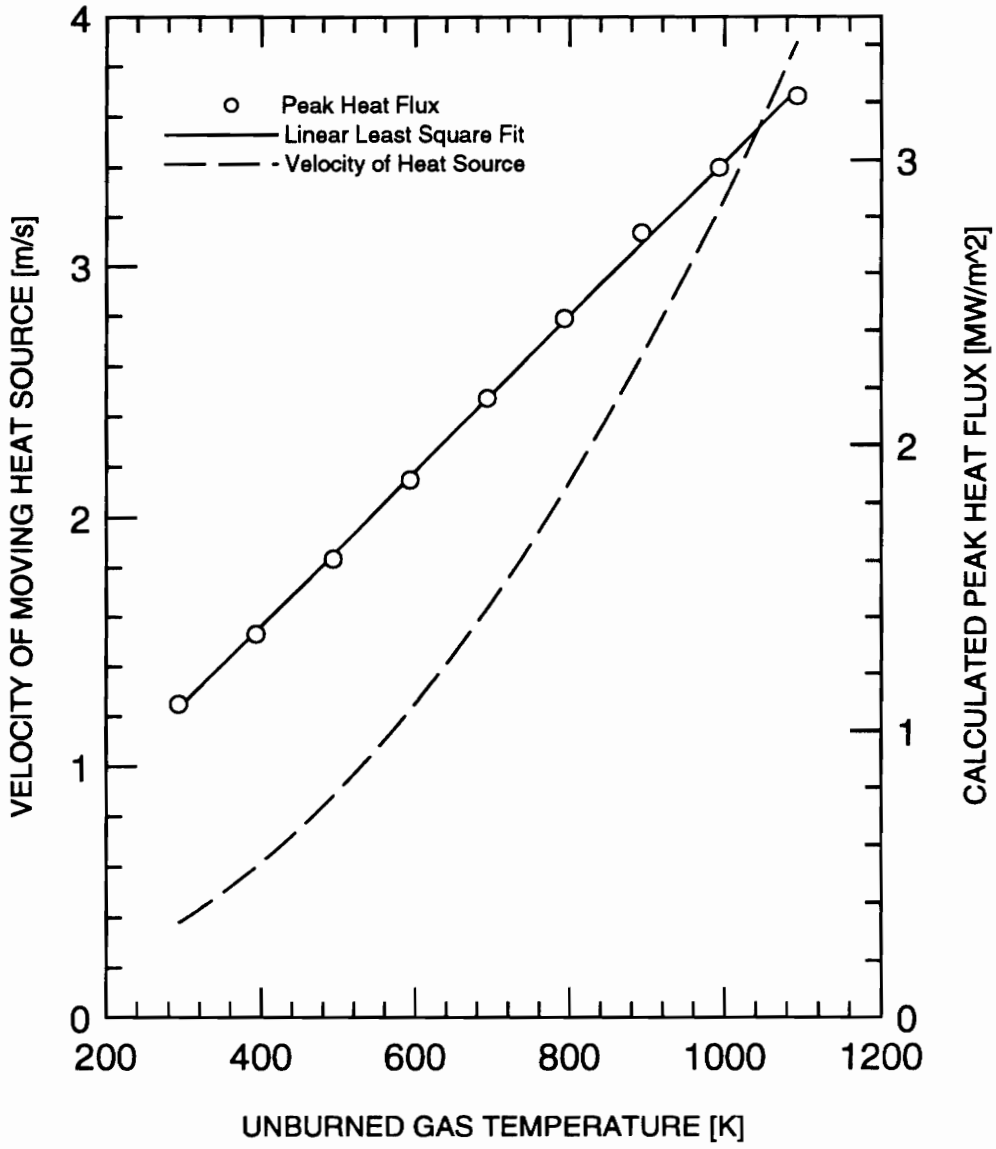

Figure 4.17: Peak heat flux and velocity of heat source at various unburned gas temperatures, flame speed from Andrews and Bradley [36], $S_u^a - 10\frac{cm}{s} = 0.000371T_u^2\frac{cm}{s\ K^2}$. **The coefficients of the linear least square fit of peak heat flux data are: a=0.285, b=0.00278.**

of flame-wall interaction that is based on transient heat conduction in a finite slab predicts that the heat transfer coefficient increases with rising wall temperature.

4.3.3 Evaluation of the Transient Heat Conduction Model and Summary

While the flame (heat generation source) is freely traveling without being affected by the presence of a cold wall, both first law energy balance model and transient heat conduction model predict identical temperature profiles in the preheat zone ahead of the flame front as shown in Figure 4.4 and Figure 4.11. This is not surprising, for the quasi steady-state first law balance model is capable of handling uniform flame movement. However, the quasi steady-state first law balance model has no memory of the temperature history, which is of importance to the transient quenching process. Previous heating and subsequent thermal diffusion across the insulating quenching layer to the cold wall is not accounted for in the quasi steady-state model, this being one of the reasons for failure of the simple quasi steady-state energy balance in predicting flame-wall heat transfer. In contrast, the transient heat conduction model is capable of representing transient temperature profiles the during the arrival of the heat source at the wall.

The transient heat conduction model is able to predict Vosen's [26] instantaneous flame-wall heat transfer well at the onset and after the occurrence of the actual flame quenching process. The model overpredicts the heat transfer rate during flame quenching because of the fundamental difference in heat source and flame propagation. During the quenching process, the flame remains at some distance to the wall where it continues to consume the quenching layer hydrocarbons. Flame movement in the transient heat conduction model is

represented by a heat source that moves with uniform speed all the way to the quench wall. However, since the head-on wall is the only object heat is transferred to, the total flame-wall heat transfer is predicted correctly.

It can be concluded that in order to predict heat transfer to the wall during the actual flame quenching process, one must know the heat release as a function of time and location $g_s = f(x,t)$; it is not satisfactory to assume that the heat is released by a infinitely thin reaction zone that travels at uniform speed until all reactants are consumed. The only way to obtain information about the temporal and spatially resolved heat release rate is to include a detailed chemical kinetic reaction mechanism and the conservation equations for a multi-component reacting system into the model formulation.

In summary, the results of calculations with the transient heat conduction model where a planar heat source approaches a cold wall are:

- Instantaneous heat transfer rates are predicted in agreement with Vosen's [26] results at the onset of flame quenching and after the flame is quenched. The heat transfer rates during the period of diffusion limited quenching layer fuel consumption are overpredicted due an improper modeling of the heat source (the location of the heat source and the timing of the heat release are simplified). The overall flame-wall heat transfer is in agreement with Vosen's [26] results.
- At ambient wall temperature and pressure, maximum heat transfer rates are obtained for methane-air mixtures close to stoichiometric. Heat transfer rates

level off as the mixture becomes richer or leaner. This trend is in good agreement with experimental data.

- Peak heat transfer rates are found to triple linearly as the wall temperature is raised from 300 K to 1100 K for stoichiometric mixtures at atmospheric pressures.

5. Summary and Conclusions

5.1 Summary

5.1.1 Experimental Study of Heat Transfer from Normally Impinging Flames

This thesis describes measurements of heat transfer from premixed, normally impinging laminar methane-air flames to a cold wall. Based on the concept of flame tubes, an apparatus was designed and optimized to support laminar, stable flame propagation at constant ambient pressure. Measurements of flame position and heat flux during head-on flame quenching on a metallic wall at the bottom end of the flame tube were made using a coaxial surface thermocouple and a CCD video camera. Experimental result showed that the freely propagating flame speed and flame-wall heat transfer are strong functions of the mixture equivalence ratio. Heat transfer rates and flame speed peak at mixtures slightly richer than stoichiometric ($\Phi = 1.05$). As the mixture shifts from stoichiometric to lean or rich, peak heat transfer rates and flame speeds level off. The time lag between idealized flame impingement on the cold wall and the occurrence of the maximum heat transfer rate increases weakly with the mixture equivalence ratio and is on the order of 0.015 seconds. Direct comparison between experimental data and Vosen's [26] heat transfer measurements in a constant volume combustion bomb shows a considerable difference in heat flux amplitude and time integrated heat transfer.

The heat flux data was non-dimensionalized on the basis of the heat release rate in a steady, laminar flame and a characteristic time for flame propagation in order to compensate for the effect of mixture equivalence ratio changes. After non-

dimensionalization, the heat flux data showed a slight dependency on the mixture equivalence ratio, which was interpreted to be the influence of the quenching distance on flame-wall heat transfer.

Run to run variations of flame speed and heat flux were found to be quite substantial. Although the propagating flame surfaces did not show visible defects, large-scale variations of the flame curvature were found to be responsible for varying test results at identical test conditions.

5.1.2 Models to Simulate Flame-Wall Interaction

This thesis also describes the development and the results of two models that predict the interaction between laminar flames and variable temperature walls. The purpose of the modeling work was to gain insight into the flame quenching process, to verify the experimental results and to predict flame-wall heat transfer for conditions that were not experimentally investigated.

The first model was based on a quasi steady-state first law balance in a control volume between a flame and a constant temperature wall. The mathematical formulation contains an Arrhenius type reaction equation that represents the temperature sensitivity of the chemical processes according to a single-step reaction mechanism. Simulations of the flame quenching process at various mixture equivalence ratios and unburned gas temperatures showed that the trend and the magnitude of single-wall quenching distances are predicted well as compared to the literature. However, the model significantly underpredicted flame-wall heat transfer when compared to the experimental results. The reason for this discrepancy is that the essential features of the flame quenching process,

namely the diffusion burning of quenching layer hydrocarbons by a temporarily stationary flame front at some distance from the wall and the dependency of heat transfer on the entire temperature history of the quenching process, are not represented by the quasi steady-state model.

The second model was based on transient heat conduction theory. A planar, moving heat generating sheet simulates the heat release of a propagating flame front in a one-dimensional slab of gases at rest, bounded by the wall at which quenching occurs. In order to account for the consumption of the quenching layer gases, the heat generating sheet propagates, under heat release, all the way to the quench wall. Since a set of non-linear boundary conditions are introduced by the moving heat source, the one-dimensional transient heat conduction problem was solved by the use of a Green's function. Instantaneous flame-wall heat transfer rates were simulated as a function of the mixture equivalence ratio and the unburned gas temperature. The flame-wall heat transfer was found to be strongly dependent on the flame speed. A simulation with varying mixture equivalence ratio showed that heat transfer rates peak with the flame speed near stoichiometric ($\Phi = 1.05$). The peak heat transfer rates tripled with a change in wall temperature from 300 K to 1100 K. The calculated heat transfer was found to overpredict the instantaneous flame-wall heat transfer during times when the actual flame is hovering at the quenching distance but the heat generating sheet is approaching the wall. It was concluded that in order to properly represent heat transfer at all times during the flame quenching process, a detailed chemical kinetic reaction mechanism and the conservation equations for a multi-component reacting system must be included in the model formulation.

5.2 Conclusions

5.2.1 Experimental Results

Measurements have been made of the heat transfer to a cold wall during the quenching of a premixed methane-air flame in a constant, ambient pressure combustor. The experiments were performed over a range of mixture equivalence ratios ranging from $\Phi = 0.8$ to $\Phi = 1.4$ The data and observations of the previous chapters support the following conclusions:

1. Visual inspection and a comparison of the experimentally measured flame speed to the literature showed that flame propagation was essentially laminar prior to quenching.
2. Instantaneous heat transfer from laminar, premixed methane-air flames to a cold wall at ambient pressure was found to be a strong function of the mixture equivalence ratio. The maximum heat transfer rates peak at slightly richer than stoichiometric (0.83 MW/m^2 at $\Phi = 1.05$) and level off as the mixture becomes lean (0.38 MW/m^2 at $\Phi = 0.8$) and rich (0.23 MW/m^2 at $\Phi = 1.4$). There is a quantitative difference of 25% in peak heat flux amplitudes between this study and the results of Vosen [26].
3. The time lag between the instant when the flame would impinge at the wall if it had continuously traveled at uniform speed and the occurrence of the peak heat flux is in the order of 0.015 s.
4. The experimental data is scattered due to large scale variations of the flame surface. Run to run variations of flame speed and peak heat flux were as high as 25% about the least square mean values.

5. Most of the effects of mixture equivalence ratio variation are compensated by non-dimensionalizing the heat transfer data on the basis of the heat release rate in a steady, laminar flame and a characteristic time for flame propagation.

5.2.2 Model Results

Two models were developed in order to predict flame-wall heat transfer and single-wall quenching distances as a function of the mixture equivalence ratio and the unburned gas (wall) temperature. A comparison of experimental results, numerical calculations and the literature yields the following:

1. The dependency of the quenching layer thickness on mixture composition and wall temperature was successfully represented by a quasi steady-state model that is based on one-step Arrhenius kinetics and a first law balance between the flame front and quenching wall.
2. Flame-wall heat transfer was substantially underpredicted by the quasi steady-state model because the time history of the quenching process and the essential transport phenomena and kinetics were not incorporated into the model formulation.
3. A transient heat conduction model, where the heat release of a flame was represented by a moving heat generating sheet, showed that the heat flux during quenching is strongly dependent on the reaction rate (flame speed) and the thermal diffusivity of the gas mixture.
4. The transient heat conduction model predicts Vosen's [26] instantaneous heat transfer at the onset of flame quenching and after the flame is quenched. The flame-wall heat transfer during the period of diffusion limited quenching layer fuel

consumption was overpredicted due an inadequate modeling of the heat source. In order to represent heat transfer at all times during quenching, a detailed chemical kinetic reaction mechanism and the conservation equations for a multi-component reacting system should be included in the model formulation.

5. Simulations with the transient heat conduction model showed a drastic increase in heat flux and convective heat transfer coefficient with rising wall temperature.

6. Recommendations for Future Work

The present work represents the first stage of a more comprehensive study. Long term objectives are to investigate the effects of varying wall temperature and pressure on heat transfer from head-on impinging laminar and turbulent flames. The next logical step is to develop and build an apparatus that supports laminar flame quenching at variable wall temperature and pressure conditions. This section provides ideas about the conceptual design (Section 6.1) and the instrumentation (Section 6.2) of such an apparatus.

6.1 Variable Temperature and Pressure Apparatus

Control parameters in the variable temperature apparatus are wall and unburned gas temperature, pressure and reactant composition. Previous experiments have shown that stable laminar flame propagation is absolutely necessary to obtain reproducible results and to reduce flame quenching to a one-dimensional phenomenon. The creation of an environment that supports laminar flame propagation under variable pressure and temperature conditions is expected to be difficult. According to Markstein [23], the effect of selective diffusion on flame propagation is more dominant, and the development of a cellular flame structure is more likely at elevated unburned gas temperatures. The experimental apparatus must feature devices and control mechanisms that ensure isotropic conditions prior to and throughout flame propagation. Uniform temperatures are of particular importance in order to avoid flame instabilities due to buoyancy currents. The apparatus must vent to a pressure vessel rather than the ambient air to allow quenching under variable pressure conditions.

Many traditional flame speed measurements were made in flame tubes with inner diameters on the order of 2 cm (the current apparatus is made from a tube of 5 cm inner

diameter). Small tubes are more inclined to support laminar flame propagation considering the principle of burner-stabilized flames. One would expect that the formation of polyhedral flame structures is more likely to be suppressed since the tube cross section is close to the individual cell size. The flame would probably develop its distinctive parabolic shape closer to the location of ignition in a small tube than in a large tube. Therefore it is recommended to test flame propagation in tubes with a cross section that corresponds to an inner diameter of 2 cm.

In order to ensure uniform temperatures throughout the entire gas mixture and surrounding walls, one could envision immersing the flame tube apparatus in a transparent vessel containing a highly heat conductive or a circulating fluid. Certain fluid properties such as optical transmittance and flammability (flashpoint) would have to be carefully examined. One heating element and one thermostat with control unit would be sufficient to keep the entire apparatus at the desired temperature. Several embedded heating elements and temperature sensors at different locations of the flame tube would be required if conventional insulation with low conductive materials is used. Spatial temperature variations would probably be unavoidable when multiple heating elements are used even when the flame tube system has reached the steady-state temperature. Ports for optical access would have to be left without insulation, giving rise to additional temperature variations.

The method of mixture control by partial pressures has proven to be accurate and reliable and should be utilized in the variable temperature and pressure apparatus. Since pressures on the order of P=10 atm and temperatures up to T=1000 K of interest, the materials must be selected with respect to their ability to endure such extreme conditions. The surge

valve, which connects the flame tube and pressure vessel, should be designed such that the opening mechanism does not introduce turbulence into the gases at rest. A ball valve could be used that is slowly turned open prior to ignition. The spark ignition system should be adjustable to provide the minimum required ignition energy for the pressure and temperature under investigation.

6.2 Diagnostic Techniques

Although it is desired to eventually measure gas temperature fields (e.g. CARS) and species concentration fields (e.g. degenerate four wave mixing) in order to obtain information about kinetic aspects and the pollutant formation of the flame quenching process, this section will discuss the diagnostic techniques required to determine the instantaneous heat transfer from flames at variable temperature walls as a function of the flame position only.

Previous experiments have shown that luminosity videography (a commercial video camera was used) lacks the spatial and temporal resolution necessary to capture the details of the flame quenching process. Vosen, Greif and Westbrook [13] have successfully used the Schlieren technique to locate the flame front during quenching and to display the flow field structure. The Schlieren technique (e.g. a standard Z configuration) should be used in conjunction with a camera and data acquisition system that allows framing rates of at least 300 frames/second. The test section at the bottom end of the flame tube must feature flat windows that support a collimated light beam. Schlieren will allow the magnification of the image of the test section.

The use of a coaxial surface thermocouple and the differentiation of the transient surface temperature signal has proven to be a practical method for the determination of flame-wall heat transfer. In order to verify heat transfer measurements, other methods (e.g. thin film resistance thermometer and/or multilayer thermocouple heat flux gages) could be used as well, and the results could be compared with each other. Since wall catalysis effects are expected to be of increasing importance with hot walls, all thermometers should have inert surfaces. Temperature and image acquisition may be triggered shortly before quench by the signal from a thin gas thermocouple or by a laser beam that is deflected due the presence of the flame front.

APPENDIX A
Mixture Control

The following appendix contains a description of the procedure used to achieve a desired mixture equivalence ratio. Dalton's model provides a relationship between the molar mixture stoichiometry and partial pressures. The theoretical basis of Dalton's model is that both mixture and individual components can be considered ideal gases. Under this conditions, the total pressure is the sum of partial pressures. The partial pressure of each individual mixture component is related to the mole fraction of the component as follows:

$$\frac{P_i}{P_{tot}} = \frac{n_i}{n_{tot}} = X_i \tag{A.1}$$

The mole fractions of the components are determined by the stoichiometry of the mixture.

$$\Phi\ CH_4 + 2(O_2 + 3.76N_2) \longrightarrow \text{Products} \tag{A.2}$$

Then

$$P_{CH_4} = \frac{P_{tot}\Phi}{\Phi + 9.52} \tag{A.3}$$

where P_{tot} is the ambient pressure, which must be determined by a barometer before each individual filling process.

Since ambient pressure is read, and the partial pressures are filled by columns of mercury, it is more convenient to use the following expression:

$$d = \frac{\rho_{HG} g h \Phi}{\Phi + 9.52} \qquad \text{(A.4)}$$

The variable h indicates the actual barometer height, while d represents the partial pressure of methane as read off the mercury manometer.

APPENDIX B

Determination of Heat Flux from Transient Surface Temperature and the Effect of Wall Material Non-Homogeneity on Heat Transfer Measurements

This appendix contains the necessary mathematical steps to use Carslaw and Jaeger's [19] heat conduction equation for a semi-infinite medium with specified surface temperature in conjunction with discretized surface temperature data and the effect of wall material non-homogeneity on heat transfer measurements:

B.1 Determination of Heat Flux from Transient Surface Temperature

B.2 The Effect of Wall Material Non-Homogeneity on Heat Transfer Measurements

B.1 Determination of Heat Flux from Transient Surface Temperature

Information about flame-wall heat flux during flame quench is obtained from the temperature history of the quench surface as measured by the surface thermocouple. The fundamental basis for calculating heat flux from transient surface temperature is considerations of the transient thermal conduction in a semi-infinite, homogenous medium. For a one-dimensional semi-infinite slab with constant properties and specified surface temperature, the heat flux is given by Carslaw and Jaeger [19]:

$$\dot{q}_w''(t) = \left[\frac{k_s \rho_s c p_s}{\pi}\right]^{(1/2)} \int_0^t \frac{dT_w(\lambda)}{d\lambda} \frac{d\lambda}{\sqrt{t-\lambda}} \tag{B.1}$$

The transient surface temperature is known from the experiment in discretized time steps, $\Delta\ t$ apart from each other. From Vosen [26] it follows that:

$$t = N\Delta\ \lambda$$

and

$$\lambda_j = j\Delta\ \lambda$$

Equation B.1 can be rewritten as:

$$\dot{q}_w''(t) = \left[\frac{k_s \rho_s c p_s}{\pi}\right]^{(1/2)} \sum_{j=0}^{N-1} \left\{ \int_0^{\lambda_{j+1}} \frac{dT_w(\lambda)}{d\lambda} \frac{d\lambda}{\sqrt{t-\lambda}} \right\} \tag{B.2}$$

In order to proceed further, some assumptions must be made as to the temperature variation between times λ_j and λ_{j+1}. It is assumed that the temperature varies linearly with time:

$$\frac{dT_w(\lambda)}{d\lambda} = \frac{T_w(\lambda_{j+1}) - T_w(\lambda_j)}{\lambda_{j+1} - \lambda_j} \qquad \lambda_j < \lambda < \lambda_{j+1}$$

Defining:

$$T_j \equiv T_w(\lambda_j) \quad ;$$

$$\Delta\ T_j \equiv T_{j+1} - T_j \quad ;$$

$$\Delta\ \lambda \equiv \lambda_{j+1} - \lambda_j \quad ;$$

the integral in equation B.2 therefore becomes:

$$\int_{\lambda_j}^{\lambda_{j+1}} \frac{dT_w(\lambda)}{d\lambda} \frac{d\lambda}{\sqrt{t-\lambda}} \approx \frac{\Delta\ T_j}{\Delta\ \lambda} \int_{\lambda_j}^{\lambda_{j+1}} \frac{d\lambda}{\sqrt{t-\lambda}} \tag{B.3}$$

Integrating equation (B.3):

$$\approx \frac{2\Delta T_j}{\Delta \lambda}\left\{\sqrt{t-\lambda_j}-\sqrt{t-\lambda_{j+1}}\right\}$$

or

$$\approx \frac{2\Delta T_j}{\Delta \lambda}\left\{\sqrt{N-j}-\sqrt{N-j-1}\right\}$$

Thus the heat flux is given by:

$$q_w''(t) = 2\left[\frac{k_s \rho_s c p_s}{\pi}\right]^{1/2} \sum_{j=0}^{N-1}\left\{\Delta T_j \Delta\sqrt{\tau_{n-j-1}}\right\} \tag{B.4}$$

where

$$\Delta T_j = T_w(\lambda_{j+1}) - T_w(\lambda_j)$$

and

$$\Delta\sqrt{\tau_{N-j-1}} = \sqrt{N-j}-\sqrt{N-j-1}$$

The indicated summations are performed by means of a FORTRAN program. The FORTRAN code is provided in Appendix H.

B.2 The Effect of Wall Material Non-Homogeneity on Heat Transfer Measurements

Information about flame-wall heat flux during flame quench is obtained from the temperature history of the quench surface as measured by the surface thermocouple. In order to treat the quenching wall as a homogeneous solid, the thermocouple and the surrounding wall are required to have similar properties. From Equation B.1, the criteria for similar wall materials is:

$$\frac{k_{th}}{\sqrt{\alpha_{th}}} = \frac{k_{sur}}{\sqrt{\alpha_{sur}}} \tag{B.5}$$

where index *th* refers to the outer thermocouple material (constantan) and *sur* to the wall material (AISI 4130). The properties of the thermocouple and surrounding wall at T=300 K from Incropera and Witt [41] are given in Table B.1.

material	$k\ \left[\frac{W}{m\ K}\right]$	$\rho\ \left[\frac{kg}{m^3}\right]$	$c_p\ \left[\frac{J}{kg\ K}\right]$	$\frac{k}{\sqrt{\alpha}} = \sqrt{k\rho c_p}$
constantan	23.0	8920.0	384.0	8876.0
AISI 4130	42.3	7858.0	442.0	12121.0

Table B.1: Thermocouple and wall properties.

Finite element models of various fast-response coaxial thermocouple designs were developed by Assanis and Badillo [25] to estimate the effect of small differences in thermal properties between thermocouple elements and wall material on transient heat flux measurements in IC engines. Coaxial thermocouple typeS J, E, K and S of 0.542 mm outer diameter were modeled as installed in the center of a cast iron diesel engine piston. Temperature distributions in the vicinity of the thermocouples and flame-wall heat flux as measured by the individual thermocouples were predicted and compared to the true temperature and heat flux of a homogeneous piston. Figure B.1 shows the radial profile of peak temperatures along the thermocouple surface for various thermocouple designs. The temperature profile of a type E thermocouple is a straight line in the center wire (in this model, constantan) and part of the outer tube (in this model, chromel) because the

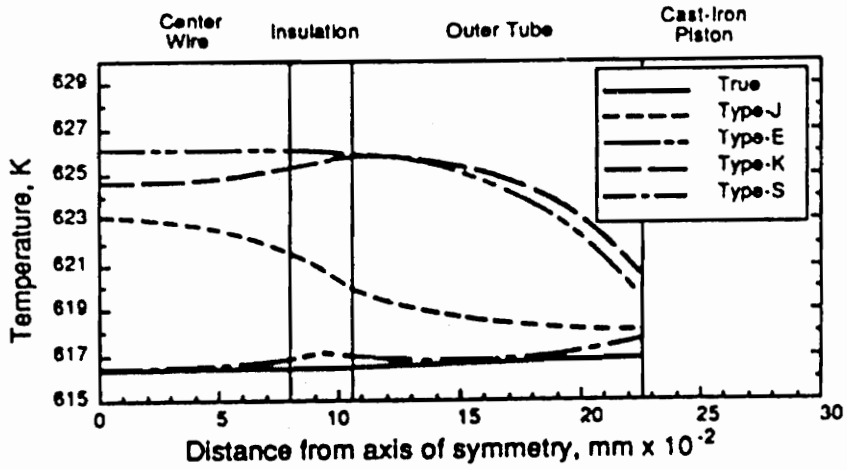

Figure B.1 **Radial profiles of peak temperatures along the thermocouple surface from the center-line of the center wire to the outer edge of a coaxial thermocouple installed in a cast-iron diesel engine piston from Assanis and Badillo [25].**

value $\frac{k}{\sqrt{\alpha}}$ of chromel and constantan are approximately identical. Only at the edge of the outer thermocouple is the temperature affected by the presence of the dissimilar material (steel). Because the value $\frac{k}{\sqrt{\alpha}}$ of steel is larger than that of chromel and constantan, the temperature rise in the steel material is smaller than the temperature rise in the thermocouple material. Thus, heat transfer from thermocouple to the heat sink (steel) occurs at the edge of the coaxial thermocouple. But flame-wall heat transfer occurs so rapidly that the heat sink surrounding the thermocouple cannot cool fast enough to control the transient temperature response of the thermocouple junction, which is located approximately above the layer of insulation (between chromel and constantan.

It can be concluded from Figure B.2 that the error introduced by dissimilar wall materials is very small if:

- a type E thermocouple is used in conjunction with a wall material that constitutes an equal or smaller heat sink than cast iron
- the dimensions of the thermocouple are equal or larger than those used in the model

As shown in Table B.2 the value $\frac{k}{\sqrt{\alpha}}$ of AISI 4130 is smaller than that of iron and the dimensions of the thermocouple used for the experiments greatly exceed those simulated in the model by Assanis and Badillo [25].

	Thermocouple outer diameter	wall material $\frac{k}{\sqrt{\alpha}}$
Assanis's [25] model	0.452 mm	14161.0
This study	1.65 mm	12121.0

Table B.2 Comparison of critical dimensions and properties

APPENDIX C

Timing Electronics

It is necessary to specify the amplitude and phase of heat transfer in order to describe the interaction of reacting boundary layers with walls. The flame position with respect to the quench surface and the transient heat flux signal must be synchronized in time. This is accomplished by an automated mechanism made from position switches, TTL circuitry and LED displays. Figure C.1 shows the sequence of events in terms of 0 volt (off) to 5 volt (on) step signals on the abscissa, starting from an arbitrary time zero on the left hand side of the plots.

The following section is numbered to break up the description into logical units.

1. A manual switch activates the DC motor that turns a spindle and thereby opens the flame tube's exhaust valve.

2. When the exhaust valve has reached a certain height, the first position switch is activated and a short pulse is released from a high voltage power supply to ignite the gas mixture.

3. Meanwhile, the exhaust valve has advanced further and closed the second position switch. This signal serves two purposes: it triggers the timing circuit and discontinues the motor's power supply.

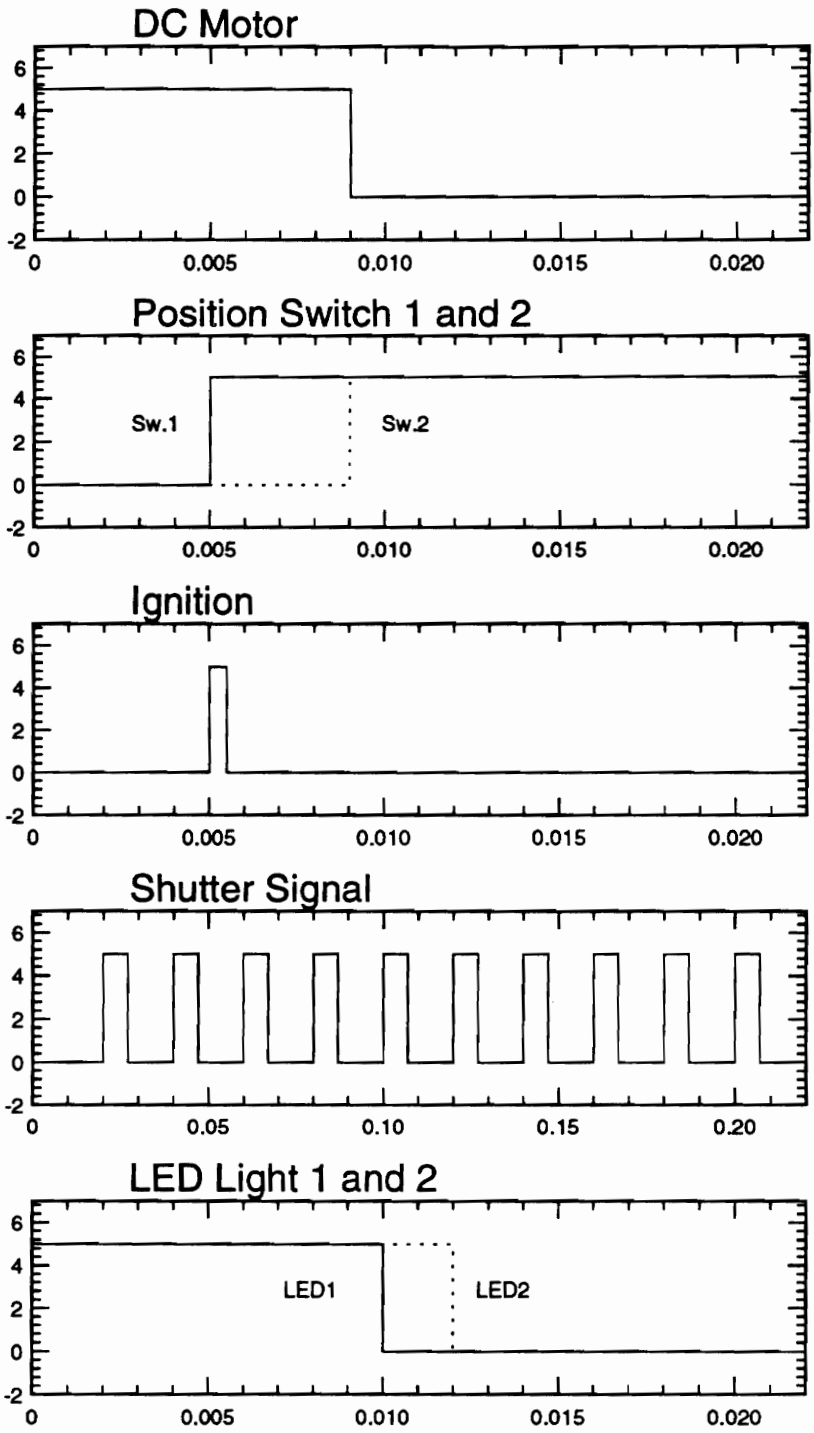

Figure C.1: Sequence of events in terms of 0 volt (off) to 5 volt (on) step signals

4. The timing circuit is made from dual flip flop, triple NAND gate and hex inverter TTL chips. It receives a low-to-high signal from the camera each time the electronic shutter is opened, and an image is about to be acquired. Only when the second position switch is closed during the last shutter cycle is a trigger signal sent out from this circuit on the next low-to-high shutter signal. Hereby it is assured that this trigger signal is released exactly at the time when the camera is just starting to take a new picture.

5. The output trigger signal is used to initiate the continuous sampling routine of the A/D board. Therefore this trigger indicates time zero. The Data Acquisition Board 2801A is operated in the DMA mode and digitizes the surface temperature signal as well as the camera shutter signal at a rate of 27,500 Hertz.

Obviously, field number one begins started to be acquired by the camera at time zero, and finishes 1/2000 of a second later. The next field is acquired following the next low-to-high shutter signal and so on. Since the camera shutter sequence is digitized and recorded to a data file, all fields can be labeled with numbers, number one being the field that was acquired starting from time equal zero.

6. Via an integrated transistor circuit, the trigger signal also switches LED 1 off. On the next low to high shutter signal 1/60 of a second later, LED 2 is switched off. The LED lights are positioned next to the combustor so they are visible to the camera.

7. The remaining problem now is to identify field number one out of the many fields that are continuously recorded to tape by a VCR. If it were possible to look at the images field by field, field number 1 would correspond to the first image on which LED 1 is dark. All consecutive frames could then be labeled with reference to this first frame.

However, since a commercial four-head VCR is used in this experiment, it is not possible to look at the images field by field. The frame advance feature always skips the even field and transports the tape to the next odd field. Only every alternate field can be viewed. Therefore, there can be a previous frame to the one that is viewed, on where the LED 1 is already dark.

However, by means of a second LED that is switched off one shutter cycle later than the first LED, the frame that is viewed can be exactly located in time. Since only every second frame can be viewed, and the LED's are switched off in consecutive order, two different combinations of LED conditions may exist:

- If there is a field where LED 1 is dark, but LED 2 is bright, then the frame was taken at t=0.
- If there is a field where LED 1 and LED 2 are dark with both LED's bright on the previous field, then the frame was taken 1/60 of a second after the trigger at t=0.

With the above procedure, it is possible to synchronize flame image and instantaneous heat flux acquisition.

APPENDIX D

Kornhauser's [29] Flame-Wall Heat Transfer Model and Derivation of Non-Dimensional Groups

Kornhauser [29] has developed a flame-wall heat transfer model that is based on an energy balance between the flame and wall. The flame speed is assumed to be constant regardless of the flame temperature, and the flame front travels until it arrives at the wall. The flame temperature is iterated from an energy balance in a control volume between flame front and wall. The energy balance reads:

$$\dot{q}_g'' = \dot{q}_c'' + \dot{q}_w'' \qquad \text{D.1}$$

where $\dot{q}_g''$ is the heat release per unit area:

$$\dot{q}_g'' = S_u \ \rho \ h_{rp} \qquad \text{D.2}$$

$\dot{q}_c''$ is the rate at which heat is consumed by preheating the reactants from the unburned gas temperature to the flame temperature:

$$\dot{q}_c'' = S_u \ \rho \ c_p \ (T_f - T_w) \qquad \text{D.3}$$

and $\dot{q}_w''$ is the heat transfer to the wall per unit area (linear gradient):

$$\dot{q}_w'' = \frac{k_g \ (T_f - T_w)}{x} \qquad \text{D.4}$$

The coordinate x represents the distance between flame and wall ($x=0$ is the location of the quench wall) and may be expressed in terms of the flame speed:

$$x = -S_u \ t \qquad \text{D.5}$$

With Equation D.5, the expression for wall heat transfer (Equation D.4) becomes:

$$\dot{q}_w'' = \frac{-k(T_f - T_w)}{S_u t} \qquad \text{D.6}$$

The Equation D.1 together with Equations D.2, D.3 and D.6 can be solved for the temperature difference between flame and wall:

$$T_f - T_w = \frac{\rho\ h_{pr}}{\rho\ c_p - \frac{k}{S_u^2 t}} \qquad \text{D.7}$$

and flame-wall heat transfer:

$$\dot{q}_w'' = - \frac{h_{rp} S_u \rho}{\frac{S_u^2 t}{\alpha} - 1} \qquad \text{D.8}$$

Non-dimensionalized, Equation D.8 reads:

$$\frac{\dot{q}_w''}{h_{rp} S_u \rho} = - \frac{1}{\frac{S_u^2 t}{\alpha} - 1} \qquad \text{D.9}$$

Thus, the non-dimensional variable for the wall heat flux is:

$$\hat{q} = \frac{\dot{q}_w''}{h_{rp} S_u \rho} \qquad \text{D.10}$$

and the non-dimensional variable for the time is:

$$\hat{t} = \frac{S_u^2 t}{\alpha} \qquad \text{D.11}$$

APPENDIX E

Solution of the Non-Homogeneous, Transient Heat Conduction Problem

This appendix provides a detailed discussion about the mathematical procedure that is used to solve the transient heat conduction problem from Equation 4.15 in Section 4.3.1. The mathematical formulation is given by:

$$\frac{\partial^2 T(x,t)}{\partial x^2} + \frac{1}{k} g(x,t) = \frac{1}{\alpha} \frac{\partial T(x,t)}{\partial t}$$

$$in \qquad 0 < x < L, \qquad t > o$$

with boundary conditions:

$$T = T_u \quad at \quad x = 0, \qquad t > 0$$

$$T = T_u \quad at \quad x = L, \qquad t > 0$$

initial condition:

$$T = T_u \quad for \quad t = 0, \quad in \quad 0 \le x \le L$$

and moving heat source in terms of the Dirac delta function:

$$g(x', \tau) = g_s \delta(x' - S_u \tau), \qquad 0 < t \le t_h$$

$$g(x', \tau) = 0 \qquad\qquad t > t_h \qquad\qquad \text{(E.1)}$$

It is convenient to solve the governing equations (E.1) in terms of a Green's function. Therefore, a problem with more general boundary conditions is considered:

$$\frac{\partial^2 T(x,t)}{\partial x^2} + \frac{1}{k} g(x,t) = \frac{1}{\alpha} \frac{\partial T(x,t)}{\partial t}$$

$$in \qquad 0 < x < L, \qquad t > o$$

with boundary conditions:

$$T = f_1(t) \quad at \quad x = 0, \qquad t > 0$$
$$T = f_2(t) \quad at \quad x = L, \qquad t > 0$$

and initial condition:

$$T = F(x) \quad for \quad t = 0, \quad in \quad 0 \le x \le L \tag{E.2}$$

An auxiliary problem with homogeneous boundary conditions is formulated in order to determine the appropriate Green's function:

$$\frac{\partial^2 \Psi(x,t)}{\partial x^2} = \frac{1}{\alpha} \frac{\partial \Psi(x,t)}{\partial t} \qquad in \qquad 0 < x < L, \qquad t > 0$$

with boundary condition:

$$\Psi = 0 \qquad at \quad x = 0 \quad and \quad x = L, \quad t = 0$$

and initial condition:

$$\Psi = F(x) \qquad for \quad t = 0, \quad in \quad 0 \le x \le L \tag{E.3}$$

The solution to the auxiliary problem (Equation E.3) is determined by separation of variables to:

$$\Psi(x,t) = \int_{x'=0}^{L} \left[\frac{2}{L} \sum_{m=1}^{\infty} exp(-\alpha \beta_m^2 t) \sin(\beta_m x) \sin(\beta_m x') \right] F(x') dx'$$

where

$$\beta_m = \frac{m\pi}{L}, \qquad m = 1, 2, 3, \ldots \tag{E.4}$$

According to Ozisik [40], the problem in terms of Green's function is:

$$\Psi(x,t) = \int_{x'=0}^{L} G(x,t/x',\tau)\ _{\tau=0} F(x')dx' \tag{E.5}$$

A comparison of equations E.4 and E.5 yields:

$$G(x,t/x',\tau)\ _{\tau=0} = \frac{2}{L}\sum_{m=1}^{\infty} exp(-\alpha\beta\ _m{}^2 t)sin(\beta_m x)sin(\beta_m x') \tag{E.6}$$

The desired Green's function is obtained by replacing t by $(\tau - t)$ in Equation E.6

$$G(x,t/x',\tau)\ _{\tau=0} = \frac{2}{L}\sum_{m=1}^{\infty} exp(-\alpha\beta\ _m{}^2 (t-\tau))sin(\beta_m x)sin(\beta_m x') \tag{E.7}$$

Then the solution of the non-homogeneous problem in Equation E.2 in terms of the above Green's function is:

$$\begin{aligned} T(x,t) = & \int_{x'=0}^{L} G(x,t/x',\tau)\ _{\tau=0} F(x')dx' \\ & + \frac{k}{L}\int_{\tau=0}^{t} d\tau \int_{x'=0}^{L} G(x,t/x',\tau)g(x',\tau)dx' \\ & + \alpha \int_{\tau=0}^{t} \frac{\partial\ G(x,t/x',\tau)}{\partial\ x'}\ _{x'=0} f_1(\tau)d\tau \\ & - \alpha \int_{\tau=0}^{t} \frac{\partial\ G(x,t/x',\tau)}{\partial\ x'}\ _{x'=L} f_2(\tau)d\tau \end{aligned} \tag{E.8}$$

Introducing the above expression for the Green's function to Equations E.7, the solution takes the form:

$$T(x,t)=\frac{2}{L}\sum_{m=1}^{\infty}exp(-\alpha\beta_m^2 t)sin(\beta_m x)\int_{x'=0}^{L}sin(\beta_m x')F(x')dx'$$

$$+\frac{\alpha}{k}\frac{2}{L}\sum_{m=1}^{\infty}exp(-\alpha\beta_m^2 t)sin(\beta_m x)\int_{\tau=0}^{t}exp(\alpha\beta_m^2\tau)d\tau$$

$$\int_{x'=0}^{L}sin(\beta_m x')g(x',\tau)dx'$$

$$+\alpha\frac{2}{L}\sum_{m=1}^{\infty}exp(-\alpha\beta_m^2 t)\beta_m sin(\beta_m x)\int_{\tau=0}^{t}exp(\alpha\beta_m^2\tau)f_1(\tau)d\tau$$

$$-\alpha\frac{2}{L}\sum_{m=1}^{\infty}(-1)^m exp(-\alpha\beta_m^2 t)sin(\beta_m x)\int_{\tau=0}^{t}exp(\alpha\beta_m^2\tau)f_2(\tau)d\tau$$

where $$\beta_m=\frac{m\Pi}{L},\qquad m=1,2,3,\ldots \tag{E.9}$$

Equation E.9 has four individual terms that serve different purposes: the first term accounts for the initial condition, the second term is the general representation of a heat source, and the third and fourth term bear the influence of boundaries at $x=0$ and $x=L$.

Since the slab of gases is initially at temperature T_u and the boundary at $x=0$ and $x=L$ remain at T_u for all times, the following transformation is carried out:

$$\theta=T-T_u \tag{E.10}$$

and Equation E.9 reduces to:

$$\theta(x,t)=\frac{\alpha}{k}\frac{2}{L}\sum_{m=1}^{\infty}exp(-\alpha\beta_m^2 t)sin(\beta_m x)\int_{\tau=0}^{t}exp(\alpha\beta_m^2\tau)d\tau$$

$$\int_{x'=0}^{L}sin(\beta_m x')g(x',\tau)dx' \qquad \text{(E.11)}$$

From Section 4.3.1, the moving heat generation sheet, that is turned off upon arrival at the boundary at $x=0$, is represented by a Dirac delta function:

$$g(x',\tau)=g_s\delta(x'-S_u\tau), \qquad 0<t\le t_h$$
$$g(x',\tau)=0 \qquad t>t_h \qquad \text{(E.12)}$$

It is now possible to perform the integrations in Equation E.11 and the solution takes the form:

$$\theta(x,t)=\frac{2\alpha\ g_s}{kL}\sum_{m=1}^{\infty}sin(\beta_m x)\left[\frac{1}{(\alpha\beta_m^2)^2+(\beta_m S_u)^2}\right]$$
$$\left[\alpha\beta_m^2 sin(\beta_m S_u t)-\beta_m S_u cos(\beta_m S_u t)+\beta_m S_u exp(-\alpha\beta_m^2 t)\right]$$
$$in \qquad 0\le x\le L \quad for \quad 0<t\le t_h$$

$$\theta(x,t)=\frac{2\alpha\ g_s}{kL}\sum_{m=1}^{\infty}sin(\beta_m x)\left[\frac{1}{(\alpha\beta_m^2)^2+(\beta_m S_u)^2}\right]$$
$$\left\{\left[exp(\alpha\beta_m^2(t_h-t))\left(\alpha\beta_m^2 sin(\beta_m S_u t_h)-\beta_m S_u cos(\beta_m S_u t_h)\right)\right]\right.$$
$$\left.+\beta_m S_u exp(-\alpha\beta_m^2 t)\right\} \qquad ,$$
$$in \qquad 0\le x\le L \quad for \quad t>t_h.$$

with β_m being the eigenvalues of the problem:

$$\beta_m=\frac{m\Pi}{L}, \qquad m=1,2,3,...$$

and $$\theta = T - T_u \tag{E.13}$$

Thus an analytic solution to problem in Equation E.1 is obtained and the transient temperature distribution in the one-dimensional slab of gases is known. The indicated summations are carried out by means of a FORTRAN code, which is provided in Appendix H.

APPENDIX F
Tables of Experimental and Model Data

Φ	$S_u^e \left(\frac{cm}{s}\right)$	$S_u^c \left(\frac{cm}{s}\right)$	$Q''_{max}\left(\frac{W}{m^2}\right)$	time lag $\Delta t\ (s)$	$\hat{Q}''_{max}$	time lag $\Delta \hat{t}$
.8	43.44	22.36	259128	0.0055	0.2805	48.30
.8	42.20	28.23	370547	0.0090	0.41299	74.57
.8	32.93	21.47	272425	0.0091	0.3891	45.81
.8	47.90	28.38	461746	0.0120	0.4533	128.06
.8	41.02	27.81	418898	0.0082	0.4803	64.11
.9	61.08	34.26	741688	0.0137	0.527	241.53
.9	55.13	34.01	589019	0.0095	0.464	143.00
.9	62.56	34.12	470469	0.0161	0.3265	292.76
.9	52.99	34.33	746385	0.0078	0.6116	101.76
1.	66.17	38.04	746385	0.0133	0.4658	270.30
1.	61.96	38.20	881851	0.0082	0.5877	146.12
1.	56.89	38.74	654272	0.0071	0.4749	106.66
1.	65.57	32.06	792076	0.0082	0.4988	163.65
1.1	66.75	34.40	821006	0.00925	0.5103	190.36
1.1	67.96	39.82	812153	0.0140	0.4958	300.28
1.1	70.34	34.53	752726	0.0179	0.4440	411.29
1.1	62.86	36.33	887261	0.0051	0.5857	93.58
1.2	61.06	37.91	789414	0.0159	0.557	275.00
1.2	47.30	31.97	574157	0.0147	0.5233	152.75
1.2	51.88	32.47	509302	0.0192	0.42322	293.72
1.2	53.59	30.22	543581	0.0157	0.4372	209.16
1.2	59.92	26.54	627664	0.0144	0.4515	239.83
1.3	44.61	20.13	512723	0.0164	0.5183	151.47
1.3	35.03	19.93	327259	0.0197	0.4213	112.20
1.3	32.93	17.81	336607	0.0193	0.4609	97.13
1.3	42.80	23.79	484891	0.0141	0.5108	120.05
1.3	35.93	20.26	320896	0.0259	0.4027	155.18
1.4	20.66	15.76	272198	0.0200	0.6188	39.54
1.4	23.07	13.54	273127	0.0157	0.556	38.71
1.4	14.97	10.93	164278	0.0247	0.5154	25.64
1.4	23.95	9.75	122073	0.0249	0.2394	66.16

Table F.1: Experimental results

Φ	0.8	0.9	1.0	1.1	1.2	1.3	1.4
$\rho\left(\frac{Kg}{m^3}\right)$	1.139	1.134	1.130	1.125	1.121	1.116	1.112
$c_p\left(\frac{J}{KgK}\right)$	1098.94	1105.47	1111.69	1119.45	1125.32	1132.73	1138.21
$k\left(\frac{W}{mK}\right)$	2.692E-2	2.699E-2	2.706E-2	2.713E-2	2.719E-2	2.726E-2	2.732E-2
$S_u{}^c\left(\frac{cm}{s}\right)$	26.94	34.65	39.60	39.52	34.24	25.72	18.03
$S_u{}^a\left(\frac{cm}{s}\right)$ [34]	30.0	37.0	42.5	46.0	41.0	33.0	26.0
$T_f{}^a$ (K)	1995	2134	2226	2210	2136	2051	1979
$T_f{}^c$ (K)	1922	2084	2127	2067	1993	1818	1695
d_{ql} [] harri(mm)	0.721	0.527	0.410	0.408	0.568	0.9399	1.568
d_{ql} [31] (mm)	0.32	0.245	0.22	0.21	0.22	0.23	0.265

Table F.2: Model input data and literature data

APPENDIX G

Manufacturing Drawings

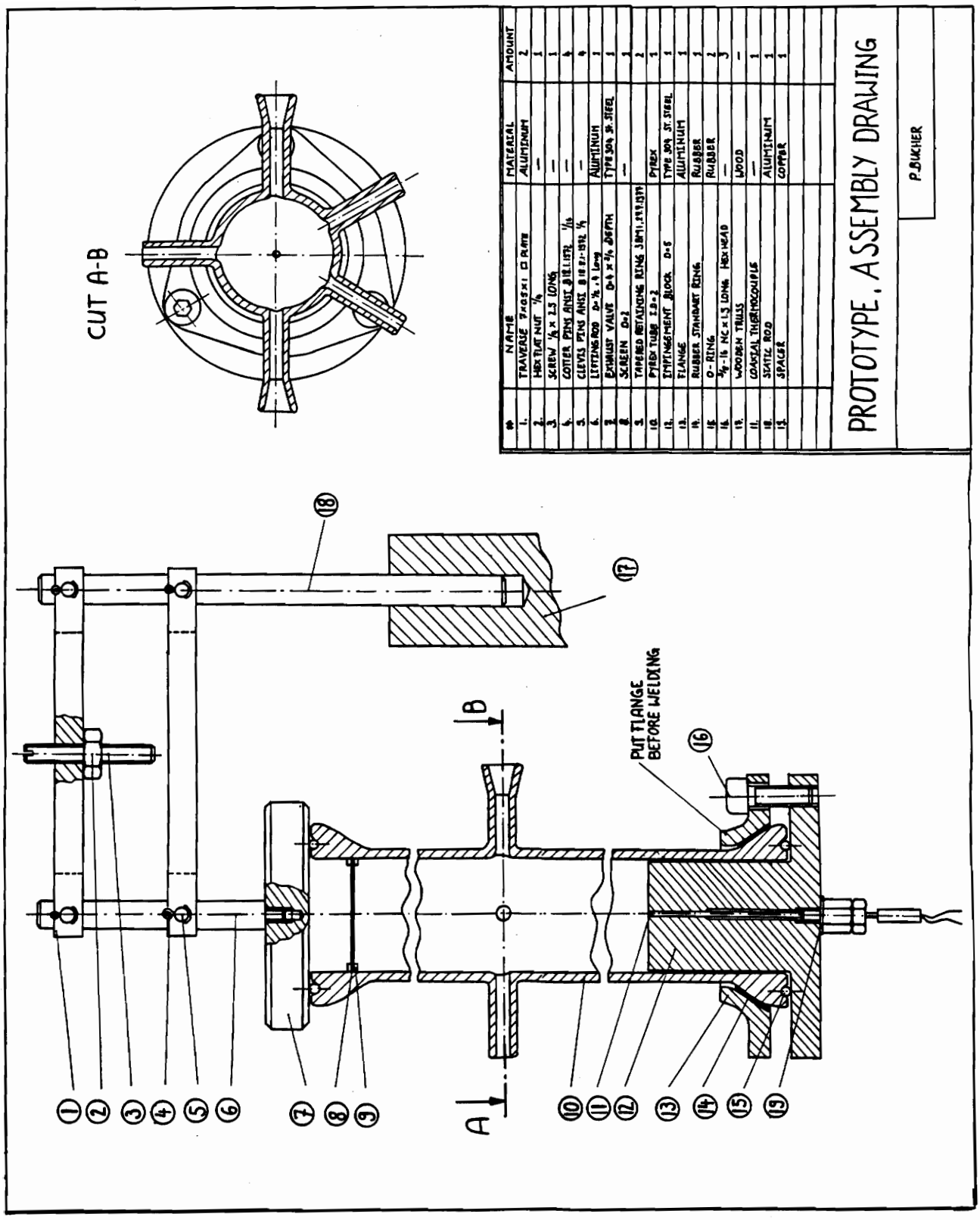

Figure G.1: Flame tube assembly drawing

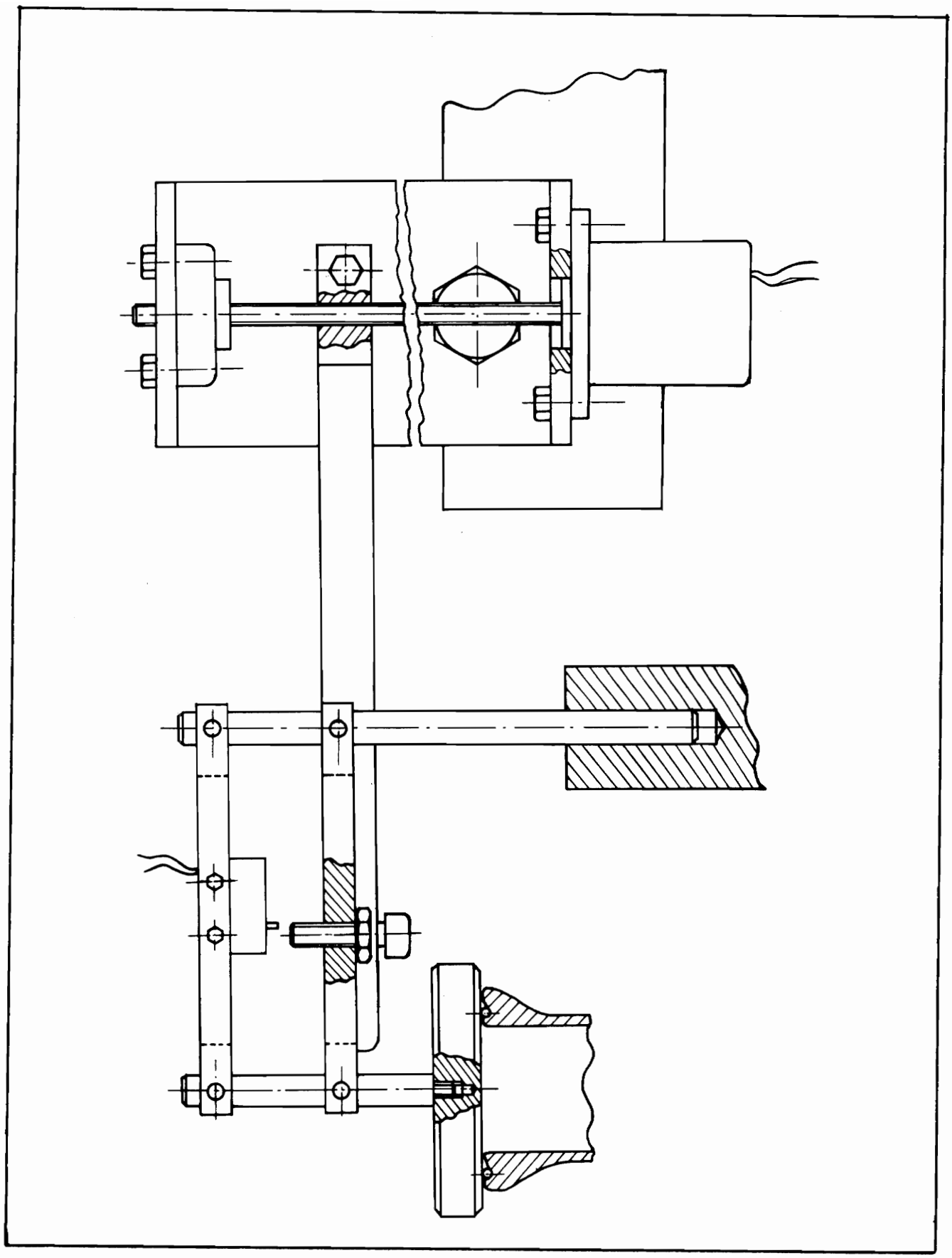

Figure G.2: Exhaust valve lifting mechanism

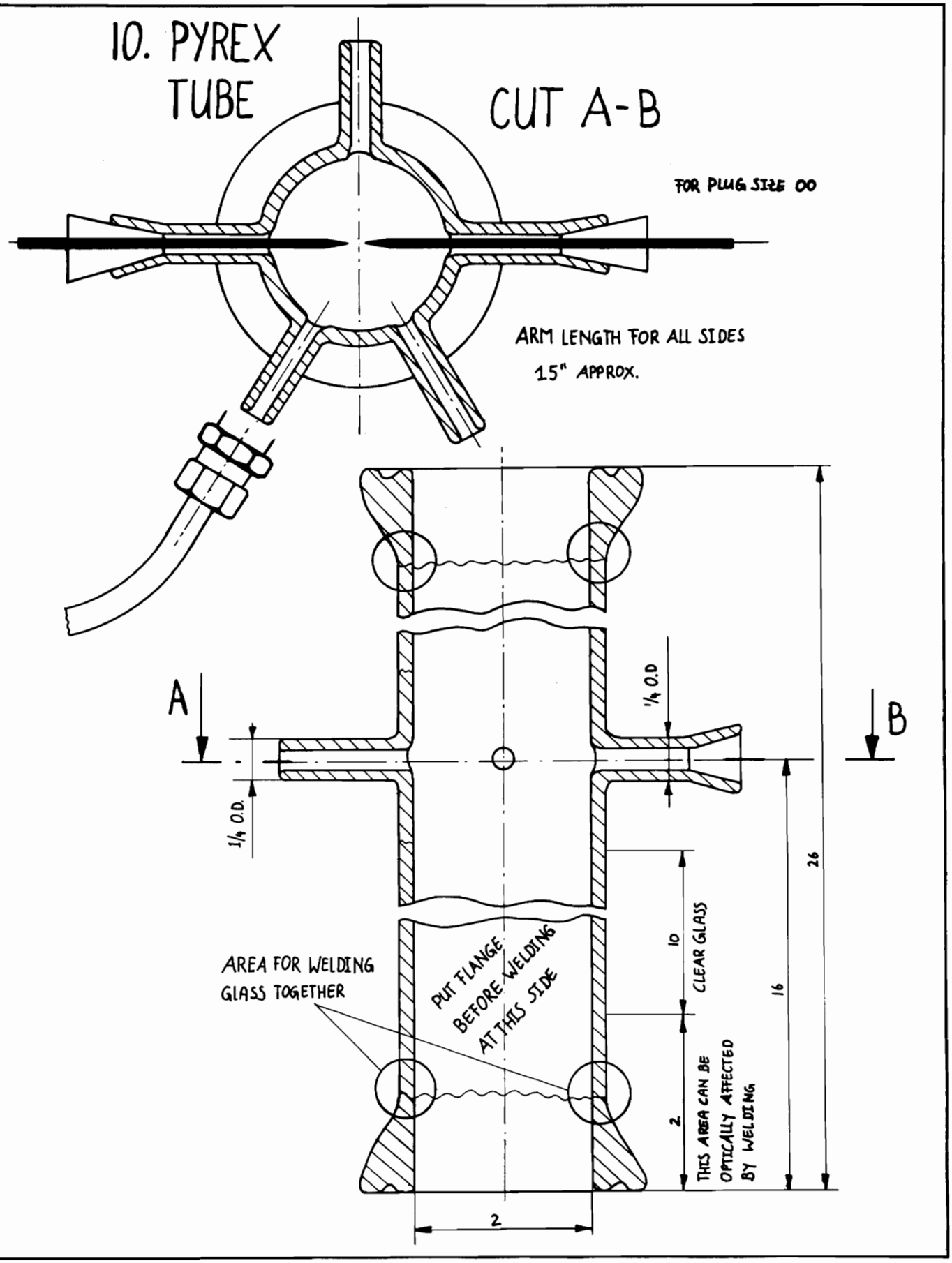

Figure G.3: Pyrex glass tube

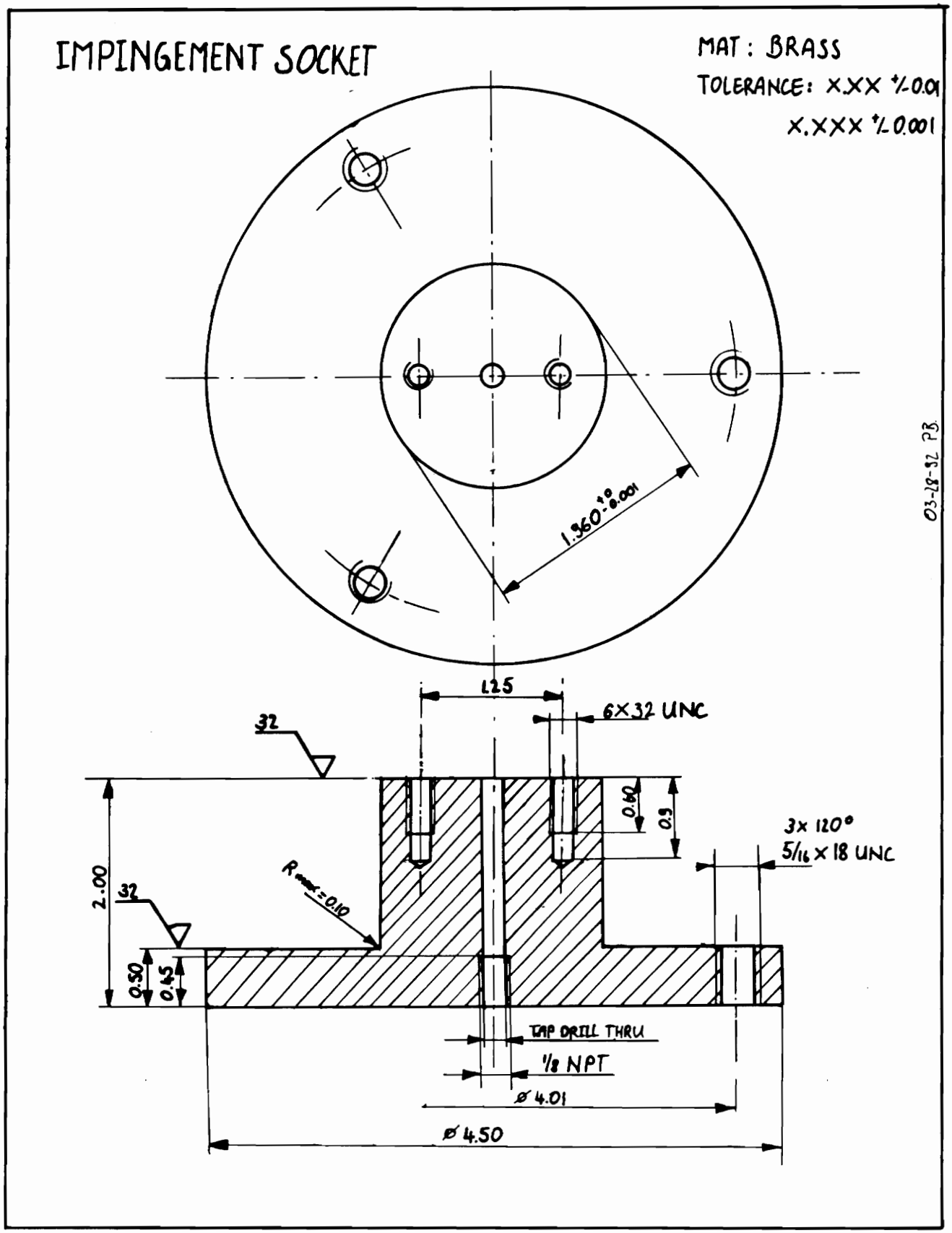

Figure G.4: Impingement Socket

Figure G.6: Flame impingement block

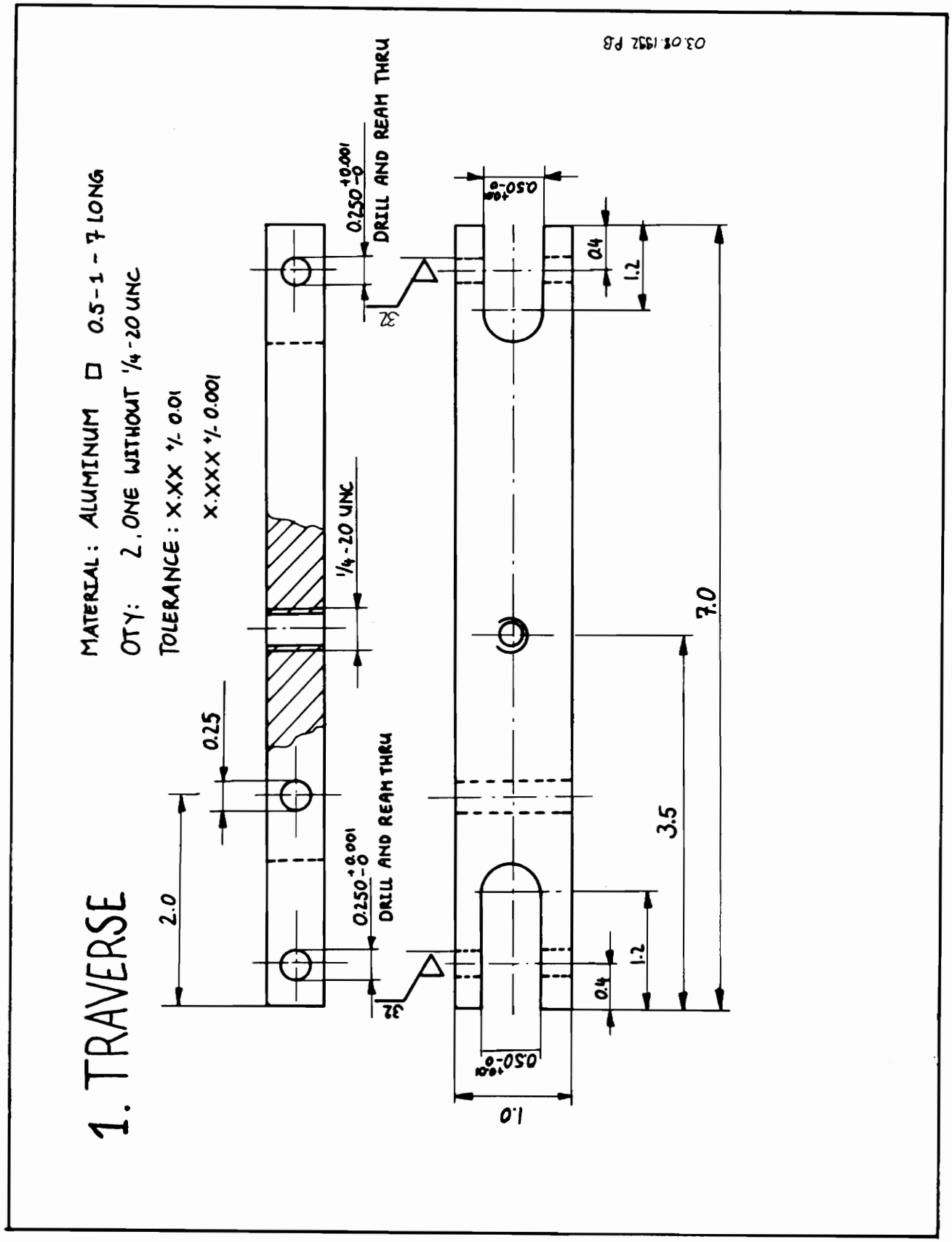

Figure G.7: Exhaust valve lifting traverse

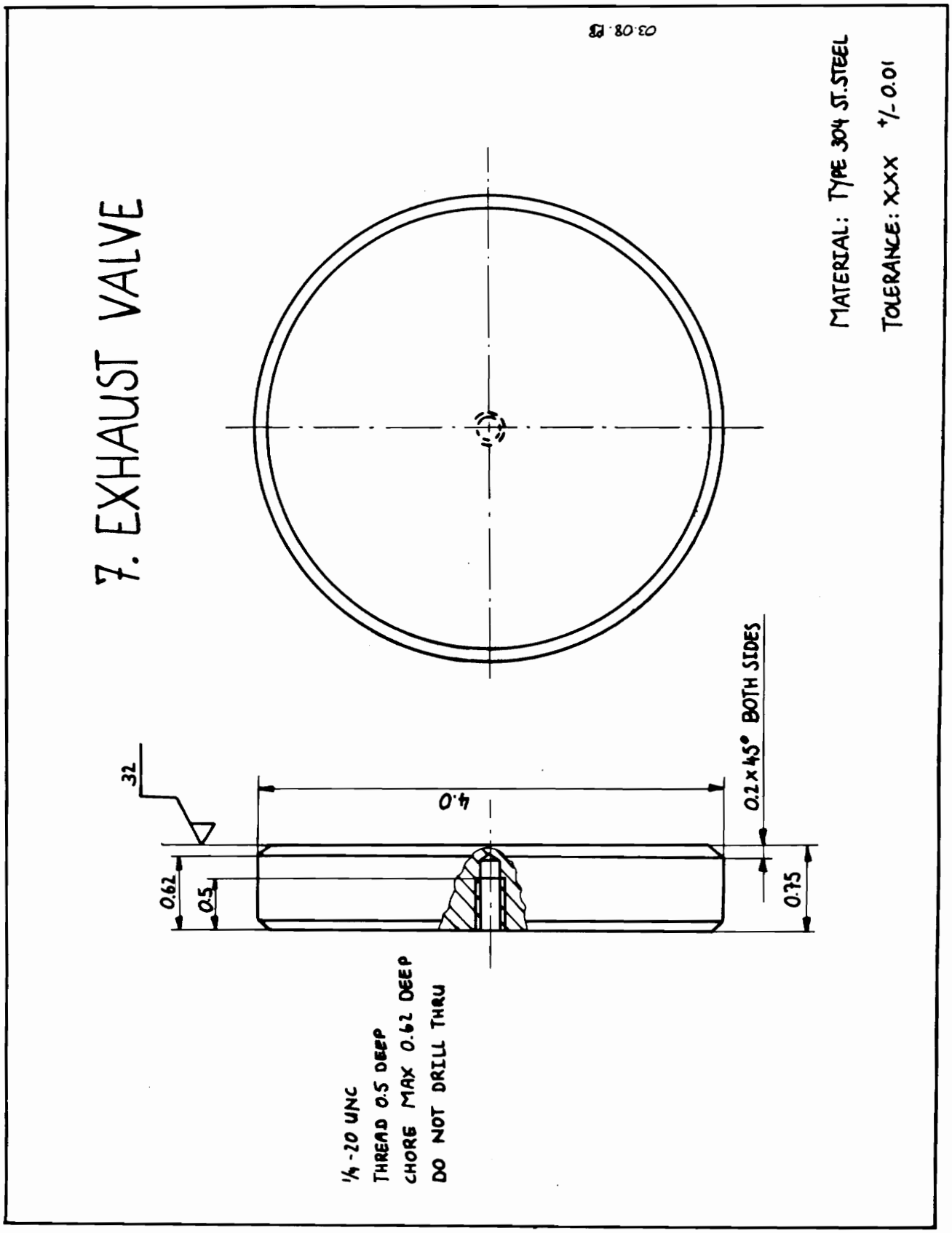

Figure G.8: Stainless steel exhaust valve

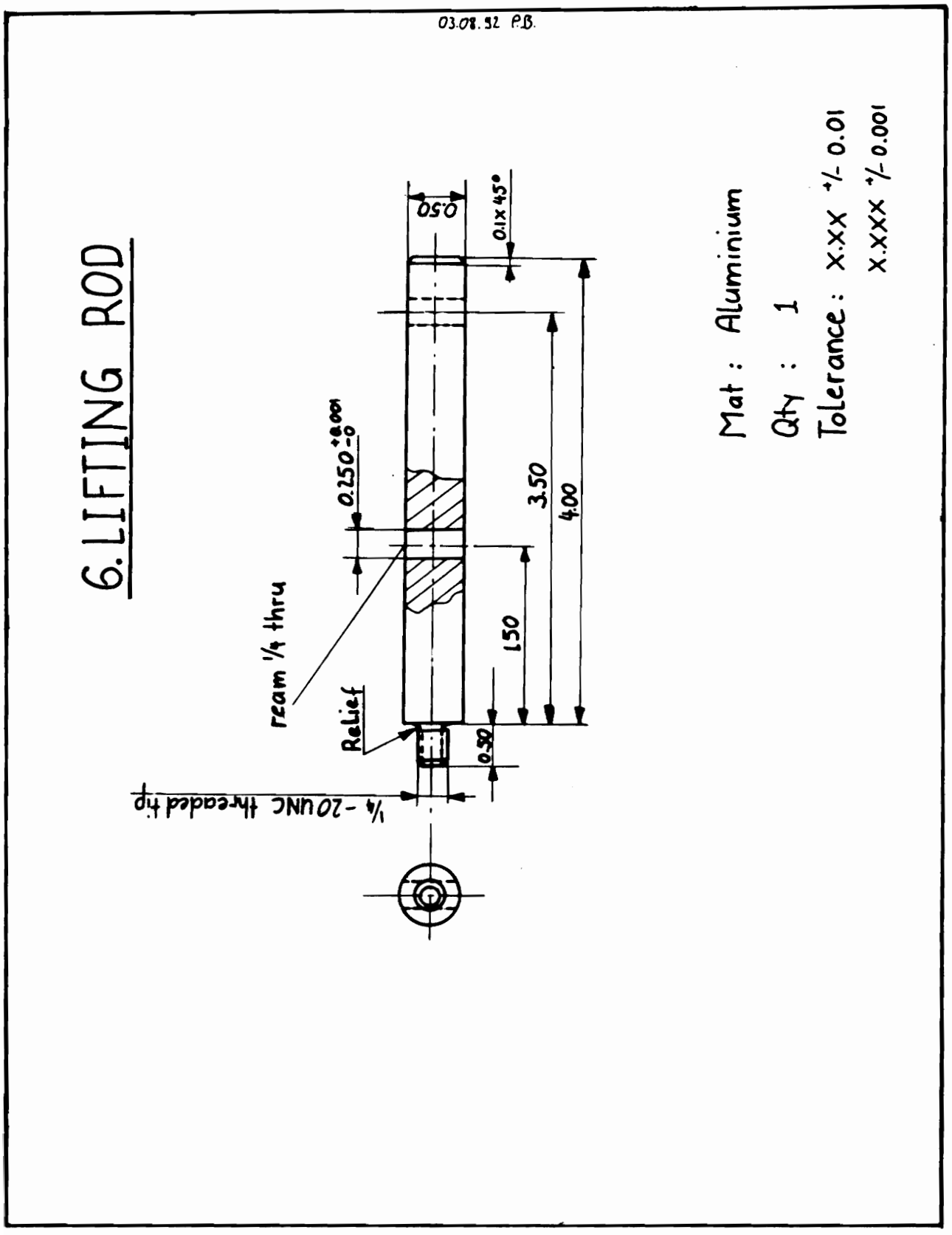

Figure G.10: Exhaust valve lifting rod

APPENDIX H

FORTRAN Programs

FORTRAN CODE: HEAT FLUX FROM WALL TEMPERATURE

```
C       Q=HEAT FLUX
C       V=TIME IN DISCRETIZED STEPS, COLUMN 1 IN SMOO.DAT
C       DTEMP=TEMPERATURE DIFFERENCE BETWEEN TIME I AND
C       TIME I+1, COL.4 IN SMOO.DAT
C       RT=INTEGRATION VARIABLE
C       TEMPERATURE AND HEAT FLUX IN S.I. UNITS
C       TIME=0 CORRESPONDS TO J=0, ASSUME THAT T(0)=T(1), GIVING
C       Q(0)=Q(1)=0
C       INPUT FILE SMOO.DAT
C
        INTEGER N,J
        REAL Q(3000)
        REAL DTEMP(3000),V(3000)
        REAL RT(3000)

C       READ SMOO.DAT
        OPEN(UNIT=1,STATUS='OLD',FILE='SMOO.DAT')
        OPEN(UNIT=2,STATUS='NEW',FILE='FLUX.DAT')
        DO 10 I=1,2999
        READ(1,*,END=10)V(I),DUM1,DUM2,DTEMP(I)
  10    CONTINUE
C
C       PROPERTIES OF OUTER THERMOCOUPLE MATERIAL CONSTANTAN
        DENS=8920
        COND=23.
        SPHT=384.
        PI=3.1416
C       DT IS THE TIME INTERVAL BETWEEN DATAPOINTS
        DT=0.000075
C
C       COMPUTE INTERMEDIATE VALUES
        CONST=2.0*((COND*DENS*SPHT/(PI*DT))**0.5)
        DO 30 J=1,2990
        RT(J)=SQRT(FLOAT(J))-SQRT(FLOAT(J-1))
  30    CONTINUE
C
C       USING DUHAMEL'S INTEGRAL
        Q(1)=0.0
        DO 200 N=2,2988
        S=0.0
        DO 100 J=1,N-1
```

```
            S=S+DTEMP(J)*RT(N-J)
  100       CONTINUE
            Q(N) = CONST*S
C           WRITE TIME AND HEAT FLUX TO OUTPUT FILE FLUX.DAT
            WRITE(2,*)V(N),Q(N)
  200       CONTINUE
C
            STOP
            END
```

FORTRAN CODE: DATA SAMPLING AND A/D CONVERSION VIA PCLAB

```
C       THIS PROGRAM SAMPLES THE THERMOCOUPLE SIGNAL (CHANNEL 1)
C       AND THE CAMERA SHUTTER SIGNAL (CHANNEL 0) AT THE EXTERNAL
C       TRIGGER (EXT.TRIG) IN PCLAB DMA CONTINUOUS SAMPLE MODE
C       THE SAMPELING RATE IS 27,500 DATAPOINTS/SECOND
C       TI=TIME IN SECONDS
C       XR=OUTPUT VOLTAGE IN VOLTS
        REAL TI,XR
C
C       PCLAB SUBROUTINE DEFINITION
C
        INTEGER*2 STATUS,STARTC,ENDCHA,GAIN,TIMING,SAMPLE,COUNT
        INTEGER*2 XINIT,XTERM,XSB,XST,XSCD,DATPTS,ANALOG(99000)
        INTEGER*2 XDLY,XSTB,XWD,XSC,XGC,XCEV,XREV,XGF,CHANLS,C2
        INTEGER*2 XAV,XAOT,XSA,XAS,XBAD,XCAD,XTAD,XWAD,XSAD,V2
        INTEGER*2 XDV,XDOT,XSD,XDS,XBDD,XCDD,XTDD,XWDD,XSDD,C0
        INTEGER*2 XEFO,XEFI,XODV,XODOT,XIDV,XIDOT,XIXR,XIXW,V0
        INTEGER*2 XSECW,XGDE,XRD,XFDL,XESC,XDSC,PLOTS,PLTPNT,C1
        INTEGER*4 CLOCKD
        INTEGER NN,N2,N3,N4
        EXTERNAL XINIT,XTERM,XSAD,XSDD,XWD,XSC,XCEV,XESC,XDSC
C
C       END OF PCLAB SUBROUTINE DEFINITION
C
C       OPEN OUTPUT FILE DATA.DAT
        OPEN(UNIT=1,STATUS='new',FILE='DATA.DAT')
C
C       SET PCLAB PARAMETER AND PREPARE FOR DMA-SAMPLING
        STATUS=0
        NN=32000
        CLOCKD=30
        TIMING=2
C       SET INTERNAL CLOCK ON MAXIMUM SPEED
C       EACH CLOCK TICK = .00000125 SEC., MINIMUM CLOCK TICKS = 30
C
C       SET CAMERA SIGNAL ON CHANNEL 0 AND THERMOCOUPLE SIGNAL ON
C       CHANNEL 1
        STARTC=0
        ENDCHA=1
        GAIN=1
        SAMPLE=NN
        STATUS=XDSC
        STATUS=XRD
        STATUS=XINIT
C
C       FIND START ADDRESS (RAM) THAT ALLOWS 64KBYTE STORAGE (32000 INTEGER
C       DATAPOINTS)
        N3=0
```

```
      DO 3 I=1,20
      STATUS=XFDL(ANALOG(N3),N2)
      WRITE(*,*)N2
      N3=N3+N2+1
      N4=N3+NN
      IF (N2.GT.NN) GOTO 9
 3    CONTINUE
 9    CONTINUE
C
C     SET START AND END ADDRESS FOR DMA CONTINUOUS SAMPLING
C     WAIT ON TRIGGER
      STATUS=XSCD(30)
      STATUS=XSA(TIMING, STARTC, ENDCHA, GAIN)
      STATUS=XDSC
      STATUS=XBAD(NN,ANALOG(N3))
      STATUS=XTAD(COUNT)
      STATUS=XWAD(ANALOG(N4))
      STATUS=XESC
      STATUS=XTERM
C
C     SAMPLE ON TRIGGER AND WRITE DATA TO OUTPUT FILE DATA.DAT
C     CONVERT INTEGER DATA TO VOLTAGE
      DO 10 I=N3,N4
      XR=(FLOAT(ANALOG(I))*10./4098.0)
      TI=FLOAT(I-N3)*30.*1.25E-6
      WRITE(1,*)TI,XR
 40   FORMAT (1X,F12.5,F12.5)
 10   CONTINUE
      CLOSE(UNIT=1)
C
      STOP
      END
```

FORTRAN CODE: CONVERSION OF THERMOCOUPLE VOLTAGE TO TEMPERATURE

```
C       CONVERSION OF VOLTAGE TO TEMPERATURE FOR
C       THERMOCOUPLE TYPE E, LINEAR INTERPOLATION
C       V=THERMOCOUPLE VOLTAGE IN MILIVOLTS
C       N=TIME IN SECONDS
C       TABLE=VOLTAGE THAT CORRESPONDS TO A TEMPERATURE ACCORDING TO
C       THERMOCOUPLE REFERENCE TABLES
C       I,J,K=COUNTERS
        IMPLICIT REAL(A-Z)
        DIMENSION V(33000),T(33000),TABLE(150),N(33000)
        INTEGER I,J,K
C
C       OPEN SEVERAL DATA FILES
C       DATA.DAT CONTAINS TIMES (COL.1) AND CORRESPONDING THERMOCOUPLE
C       VOLTAGE (COL.2)
C       ETHERM.DAT CONTAINS THE THERMOCOUPLE REFERENCE TABLE
C
        OPEN(UNIT=1,STATUS='OLD',FILE='DATA.DAT')
        OPEN(UNIT=2,STATUS='OLD',FILE='ETHRM.DAT')
        OPEN(UNIT=4,STATUS='NEW',FILE='TOUT.DAT')
        OPEN(UNIT=5,STATUS='NEW',FILE='SOUT.DAT')
        OPEN(UNIT=6,STATUS='NEW',FILE='QOUT.DAT')
C       READ THERMOCOUPLE VOLTAGE FILE
              DO 10 I=1,31999
              READ(1,*,END=10)N(I),V(I)
  10    CONTINUE
C
C       READ THERMOCOUPLE REFERENCE TABLE
              DO 20 I=1,101,2
              READ(2,*,END=20)TABLE(I),TABLE(I+1)
  20    CONTINUE
C
C       CONVERSION VOLTS TO TEMPERATURE
        DO 300 I=2,31998,2
            V(I)=V(I)*2.
                  DO 200 J=1,101
                  IF (V(I).LT.TABLE(J)) GOTO 250
 200    CONTINUE
 250    T(I)=J-2.+(V(I)-TABLE(J-1))/(TABLE(J)-TABLE(J-1))
 300    CONTINUE
C
C       PRINTOUT EVERY 18. TEMPERATURE DATA POINT
        DO 400 I=2,26666,36
        WRITE(4,*)N(I),T(I)
 400    CONTINUE
C
C       SELECT WINDOW FOR FLUX DIFFERENTIATION, NUMBER OF DATA I=4000
```

```
C       SET MAXIMUM TEMPERATURE AT I=2000
        DO 450  I=500,26666,2
        IF(((T(I)-T(20)).GT.1.0).AND.((T(I+2)-T(20)).GT.1.0)) GOTO 460
 450    CONTINUE
 460    CONTINUE
        DO 470 J=(I-3000),(I+3000),2
        WRITE(6,*)N(J),T(J)
 470    CONTINUE
C
C       PRINTOUT CAMERA SHUTTER SIGNAL IN SEPARATE DATA FILE (SOUT.DAT)
C       A SPACER IS SET FOR EVERY LOW TO HIGH TRIGGER SIGNAL (IN 1/60 SECOND
C       INTERVALS) TO IDENTIFY THE BEGINNING OF A CAMERA FIELD
        SPACER=10.1
        DO 500 I=3,26666,2
        IF((V(I).LT.3.).AND.(V(I-2).GT.3.))THEN
        WRITE(5,*)N(I),SPACER
        ENDIF
 500    CONTINUE
C
              STOP
              END
```

FORTRAN CODE: LEAST SQUARE DIGITAL SMOOTHING OF THE SURFACE TEMPERATURE DATA

```
C       THIS PROGRAM LEAST SQUARE FITS A LINE THROUGH M (AN ODD NUMBER)
C       TEMPERATURE DATA POINTS AND ASSIGNES A FITTED TEMPERATURE TO THE
C       DATA POINT AT (M-1)/2+1
C       T=TIME IN SECONDS
C       V=TEMPERATURE IN CELSIUS
C       VN=LEAST SQUARE TEMPERATURE IN CELSIUS
C       SX,SXS,SY,SYS,D,A,B=COUNTERS
        REAL*8 V(18000),VN(18000),T(18000),SX,SXS,SY,SYS,D,A,B
        INTEGER I,J,N,M
C       QOUT.DAT CONTAINS THE RAW TEMPERATURE DATA
C       SMOO.DAT IS THE OUTPUT FILE THAT CONTAINS THE SMOOTHENED DATA
        OPEN (UNIT=1,STATUS='OLD',FILE='QOUT.DAT')
        OPEN (UNIT=2,STATUS='NEW',FILE='SMOO.DAT')
C       READ TEMPERATURE FILE QOUT.DAT
        DO 10 I=1,3000
        READ(1,*,END=10)T(I),V(I)
 10     CONTINUE
C
C       SET NUMBER OF DATA POINTS FOR THE STRAIGHT LINE FIT
        M=8
        N=M/2-1
C
C       FIT DATA
        DO 200 I=10,2999
        DO 100 J=(I-N),(I+N+1)
        SX=SX+T(J)
        SY=SY+V(J)
        SXS=SXS+(T(J))**2.
        SXY=SXY+T(J)*V(J)
 100    CONTINUE
        D=FLOAT(M)*SXS-SX**2.
        A=1./D*(FLOAT(M)*SXY-SX*SY)
        B=1./D*(SXS*SY-SX*SXY)
        VN(I)=A*T(I)+B
        VN(I+1)=A*T(I+1)+B
        DTN=VN(I+1)-VN(I)
C       WRITE SMOOTHENED DATA TO OUTPUT FILE
        WRITE(2,500)T(I),V(I),VN(I),DTN
        DTN=0.
        SX=0.
        SY=0.
        SXS=0.
        SXY=0.
 200    CONTINUE
 500    FORMAT(1X,E13.8,2X,E13.8,2X,E13.8,2X,E14.8)
        STOP
        END
```

FORTRAN CODE: FIRST LAW BALANCE MODEL

```
C       THIS PROGRAM CALCULATES THE SINGLE-WALL QUENCHING LAYER
C       THICKNESS BY MEANS OF A FIRST LAW BALANCE BETWEEN MOVING FLAME
C       FRONT AND QUENCH WALL
        IMPLICIT REAL (A-Z)
        INTEGER I,J,Y
C
C       OPEN OUTPUT FILES TO SAVE SEVERAL INSTANTANEOUS TEMPERATURE
C       PROFILES BETWEEN FLAME AND WALL
        OPEN(UNIT=20,STATUS='new',FILE='MODE.DAT')
        OPEN(UNIT=1,STATUS='NEW',FILE='1.DAT')
        OPEN(UNIT=2,STATUS='NEW',FILE='2.DAT')
        OPEN(UNIT=3,STATUS='NEW',FILE='3.DAT')
        OPEN(UNIT=4,STATUS='NEW',FILE='4.DAT')
        OPEN(UNIT=5,STATUS='NEW',FILE='5.DAT')
        OPEN(UNIT=6,STATUS='NEW',FILE='6.DAT')
        OPEN(UNIT=7,STATUS='NEW',FILE='7.DAT')
        OPEN(UNIT=8,STATUS='NEW',FILE='8.DAT')
        OPEN(UNIT=9,STATUS='NEW',FILE='9.DAT')
        OPEN(UNIT=10,STATUS='NEW',FILE='10.DAT')
        OPEN(UNIT=11,STATUS='NEW',FILE='11.DAT')
        OPEN(UNIT=12,STATUS='NEW',FILE='12.DAT')
        OPEN(UNIT=13,STATUS='NEW',FILE='13.DAT')
        OPEN(UNIT=14,STATUS='NEW',FILE='14.DAT')

C       EA=ACTIVATION ENERGY IN JULES/KG
C       R=SPECIFIC GAS CONSTANT IN JULES/KG/K
C       KO=CONDUCTIVITY OF THE UNBURNED MIXTURE IN W/M/K
C       TFA=ADIABATIC FLAME TEMPERATURE IN K
C       TW=WALL TEMPERRATURE IN K
C       SUA=ADIABATIC FLAME SPEED IN M/S
C       HPR=HEAT OF REACTION IN JULES/KG
C       ALP=THERRMAL DIFFUSIVITY IN M^2/S
C       RO=DENSITY OF GAS MIXTURE IN KG/M^3
C       CP=SPECIFIC HEAT IN JULES/KG/K
C       Z=DISTANCE TO QUENCH WALL IN M
C       TF=ACTUAL FLAME TEMPERATURE IN K
C       SU=ACTUAL FLAME SPEED IN M/S

        EA=4545.
        R=300.88
        KO=2.706E-2
        TFA=2225.72
        TW=293
        SUA=0.425
        HPR=2605980.
        RO=0.87114
        CP=1111.69
```

```
C
C       ITERATE INSTANTANEOUS FLAME TEMPERATURE IN FINITE TIME STEPS
C       Z IS THE DISTANCE FROM THE WALL AT TIME=T(J)
        DO 2000 J=1,1400
        Z=0.001-FLOAT(J-1)*0.000003333
        ALP=KO/RO/CP
        DO 100 I=3125,400,-1
C
C       ASSUME TEMPERATURE AND ITERATE
        TF=1.*(FLOAT(I))/1.
        SU=EXP(-EA/(2.*R)*(1/TF-1/TFA))*SUA
        QG=RO*HPR*SU
        QC=RO*CP*(TF-TW)*SU
        QW=KO*SU/ALP*(TF-TW)/(EXP(SU/ALP*(Z))-1.)
        ERR=QG-QC-QW
        IF (ERR.GT.0.) GOTO 200
        IF (TF.LT.420)GOTO 1100
        100 CONTINUE
C
C       WRITE ACTUAL DISTANCE, FLAME TEMPERATURE, FLAME SPEED AND WALL
C       HEAT FLUX TO OUTPUT FILE
 200    WRITE(20,*)Z,TF,SU,QW
C
C       CALCULATE TEMPERATURE PROFILES AND WRITE TO OUTPUT FILES
        DO 2200 Y=1,101
        X=Z/100.*FLOAT(Y-1)
        T=TW+(TF-TW)/(EXP(SU/ALP*(Z))-1.)*(EXP(SU/ALP*X)-1.)
        WRITE(J,*)X,T
 2200   CONTINUE
C
 2000   CONTINUE
C
C       RESET HEAT FLUX AND FLAME SPEED
        QW=0.
        SU=0.
        STOP
        END
```

FORTRAN CODE: TRANSIENT HEAT CONDUCTION MODEL

```
C       THIS CODE CALCULATES THE INSTANTANEOUS HEAT TRANSFER RATES FROM A
C       MOVING HEAT GENERRATION SHEET TO A WALL
C
        IMPLICIT REAL*8(A-Z)
        INTEGER I,J,K,P
C
C       INITIALIZE OUTPUT FILES TO SAVE SEVERAL INSTANTANEOUS TEMPERATURE
C       PROFILES
        OPEN(UNIT=1,STATUS='NEW',FILE='1.DAT')
        OPEN(UNIT=2,STATUS='NEW',FILE='2.DAT')
        OPEN(UNIT=3,STATUS='NEW',FILE='3.DAT')
        OPEN(UNIT=4,STATUS='NEW',FILE='4.DAT')
        OPEN(UNIT=5,STATUS='NEW',FILE='5.DAT')
        OPEN(UNIT=6,STATUS='NEW',FILE='6.DAT')
        OPEN(UNIT=7,STATUS='NEW',FILE='7.DAT')
        OPEN(UNIT=8,STATUS='NEW',FILE='8.DAT')
        OPEN(UNIT=9,STATUS='NEW',FILE='9.DAT')
        OPEN(UNIT=10,STATUS='NEW',FILE='10.DAT')
        OPEN(UNIT=11,STATUS='NEW',FILE='11.DAT')
        OPEN(UNIT=12,STATUS='NEW',FILE='12.DAT')
        OPEN(UNIT=13,STATUS='NEW',FILE='13.DAT')
        OPEN(UNIT=14,STATUS='NEW',FILE='14.DAT')
        OPEN(UNIT=15,STATUS='NEW',FILE='FLUX.DAT')

C       SU=FLAME SPEED IN M/S
C       L=TOTAL LENGTH OF SLAB IN M
C       DEL=QUENCHING LAYER THICKNESS IN M
C       TOFF=INSTANT WHEN HEAT SOURCE IS TURNED OFF IN S
C       DTI=TIME STEP IN S
C       ALP=THERMAL DIFFUSIVITTY IN M^2/S
C       KO=CONDUCTIVITY IN W/M/K
C       GS=HEAT SOURCE STRENGTH IN W/M^2
C
        SU=.35
        L=0.002
        DEL=.0000
        LL=L-DEL
        TOFF=LL/SU
        DTI=.00000166666
        TDT=TOFF-40.*DTI
        ALP=2.255E-5
        KO=2.7E-2
        GS=851934.
C
C       SET COUNTER TO P=0, HEAT SOURCE IS MOVING
        P=0
C
```

```
C       GO FORWARD IN TIME
        DO 300 K=1,80
        TI=(FLOAT(K-1))*DTI+TDT
C       CHECK FOR STATUS OF HEAT SOURCE
        IF(TI.GT.TOFF)      P=1
        TTT=TOFF-TI
        IF(TI.LE.TOFF) XXX=SU*TTT
        IF(TI.GT.TOFF) XXX=0.
C       CALCULATE TEMPERRATURE PROFILE BETWEEN HEAT GENERATION SHEET
C       AND WALL
        DO 200 J=1,81
        X=FLOAT(J-1)*0.00000625+0.0015
        TIN=0.
        T=0.
        TB=0.
        TG=0.
C       DO 100 I=1,200
C       CALCULATE CONSTANTS
        B=FLOAT(I)*3.1416/L
        EXX=EXP(-ALP*B**2.*TI)
        EXO=EXP(ALP*B**2.*(TOFF-TI))
C
C       INITIAL PROFILE
        A=2./L*EXX*SIN(B*X)
        F=TF/B*(COS(B*L)-COS(B*DEL))
        TIN=TIN+A*(-F)
C
C       INFLUENCE OF BOUNDARY @ X=0
        TB=TB+ALP*2./L*B*SIN(B*X)*
     +  TF/(ALP*B**2.)*(1-EXX)
C        INFLUENCE OF HEAT GENERATION SHEET
        IF(P.EQ.0) THEN
C
C       HEAT GENERATION FRONT IS MOVING
        DO 100 I=1,180
        H=2.*GS*ALP/(L*KO)*SIN(B*X)
        M=1./((ALP*B**2.)**2.+(SU*B)**2.)
        N=(ALP*B**2.*SIN(B*SU*TI)-B*SU*COS(B*SU*TI))
        O=EXP(-ALP*TI)/((B**2.)**(1./B**2.)*
    +   (ALP**2.*B**2.+SU**2.)**(1./B**2.))*(SU*B)
        TG=TG+H*(M*N+O)
        IF(J.EQ.80)  Q2=TG
        IF(J.EQ.81)  Q1=TG
 100    CONTINUE
C       ELSE
C
C       NO HEAT GENERATION, RELAXING TEMP.PROFILES
        DO 101 I=1,50
        B=FLOAT(I)*3.1416/L
        EXX=EXP(-ALP*B**2.*TI)
        EXO=EXP(ALP*B**2.*(TOFF-TI))
```

```
      H=2.*GS*ALP/(L*KO)*SIN(B*X)
      M=1./((ALP*B**2.)**2.+(SU*B)**2.)
      N=EXO*(ALP*B**2.*SIN(B*SU*TOFF)-B*SU*COS(B*SU*TOFF))
      O=EXX*(SU*B)
      TG=TG+H*M*(N+O)
      IF(J.EQ.80) Q2=TG
      IF(J.EQ.81) Q1=TG
101   CONTINUE
      ENDIF
C
C     SUPERPOSITION OF HEAT SOURCE, BOUNDARY CONDITION AND INITIAL
C     CONDITION
      T=TIN+TB+TG
200   CONTINUE
C     CALCULATE INSTANTANEOUS HEAT TRANSFER RATE
      QQ=KOC*(Q2-Q1)/(0.002/80.)
C
C     WRITE TO HEAT TRANSFER OUTPUT FILE FLUX.DAT
      WRITE(15,*)T,X,QQ
300   CONTINUE
      STOP
      END
```

References

1. Havstad, P.H., Gerwin, I.J. and Wade, W.R., "A Ceramic Insert Uncooled Diesel Engine," SAE Technical Paper Series, no. 860447 (1986).

2. Morel, T., Wahiduzzaman, S. and Fort, E.F., "Heat Transfer Experiments in Insulated Diesel Engines," SAE Technical Paper Series, no. 880186 (1988).

3. Woschni, G., Spindler, W. and Kolesa, K., "Heat Insulation of Combustion Chamber Walls - A Measure to Decrease the Fuel Consumption of I.C. Engines?," SAE Technical Paper Series, no. 870339 (1987).

4. Cheng, W.K., Wong, V.W. and Gao, F., "Heat Transfer Measurement Comparisons in Insulated and Non-Insulated Diesel Engines," SAE Technical Paper Series, no. 890570 (1989).

5. Frideman, R. and Johnston, W.C., "The Wall Quenching of Laminar Propane Flames as a Function of Air-Fuel Ratio," *J. Applied Physics* vol. 21, pp. 791, 1950.

6. Daniel, W.A., "Flame Quenching at the Walls of an Internal Combustion Engine," *Sixth Symposium (International) on Combustion*, Academic Press, pp. 886-894, 1956.

7. Goolsby, A.D. and Haskel, W.W., "Flame-Quench Distance Measurement in CFR Engine," *Combustion and Flame*, no. 26, pp. 105-114, 1976.

8. Girand, A. and Leyer, J.C., "Direct Measurement of the Head-On Flame Quenching Distance in Closed Chambers," *Sixth Symposium (International) on Combustion*, Academic Press, pp. 443-452, 1956.

9. Fairchild, P.W., Fleeter, R.D. and Fendell, F.E., "Raman Spectroscopy Measurements of Flame Quenching in a Duct Type Crevice," *Twentieth Symposium (International) on Combustion*, Academic Press, pp. 85-90, 1984.

10. Lavoie, G.A. "Correlations of Combustion Data for IC Engine," SAE Technical Paper Series no. 780229, (1978).

11. Monnot, G., *Principles of Fired Heat*, Gulf Publishing Co., pp. 75-92, 1985.

12. Germerdonk, R. and Nguyen, N.N., "Increase of Local Heat Transfer Coefficient by 'Convective Vive' Phenomenon," *German Chemical Engineering*, Vol 8, pp 81-86, 1985.

13. Vosen, S.R., Greif, R. and Westbrook, C.K., "Unsteady Heat Transfer During Laminar Flame Quenching," *Twentieth Symposium (International) on Combustion*, Academic Press, pp. 75-83, 1984.

14. Westbrook, C.A., Adamczyk, A.A. and Lavoie, G.A., "A Numerical Study of Laminar Flame Quenching", *Combustion and Flame,* Vol 40, pp.81-90, 1981.

15. Ishikawa, N. and Branch, M.C.,"A Simple Model of Transient Thermal Flame Quenching," SAE Technical Paper Series, no. 770648, (1977).

16. Isshiki, N. and Nishiwaki, N., "Basic Study on Inside Convective Heat Transfer of Internal Combustion Engines," *5th International Heat Transfer Conference*, FC9.2, 1974.

17. Coward, H.F. and Hartwell, F.J., "Mechanism of Flame Movement," *J. chem. Soc.*, pp. 1996 and 2676, 1932.

18. Fuller, L.E., Parks, D.J. and Fletcher, E.A., "Flat Flames in Tubes-Easy Fundamental Flame Speed Measurements," *Combustion and Flame*, Vol. 13, pp. 455-460, 1969.

19. Carlslaw, H.S. and Jaeger, J.C., "*Conduction of Heat in Solids*," Oxford University Press, London, 1948.

20. Bubnoff, N., "Ueber den Innenkegel gespaltener Kohlenwasserstofflammen," *Z. Physik. Chem.* no. 88, pp. 641, 1914.

21. Coward, H.F. and Brinsley, F., "The Dilution Limits of of Inflammability of Gaseous Mixtures," *J. Chem. Soc.*, No. 105, pp. 1859, 1914.

22. Goldmann, F., "Diffusionsvorrgaenge an der unteren Explosionsgrenze von Wasserstoff-Sauerstoff Gemischen," *Z. Physik. Chem.* B5, 305, 1929.

23. Markstein, G.H., "*Nonsteady Flame Propagation*", Pergamon Press, pp 75-103, 1964.

24. Guenoche, H., Manson, N. et Monnot, G., "L'influence des conditions aux limites longitudinales sur la propagation des deflagrations dans les tubes cylindrriques lisses," Comptes Rendus Academie des Sciences, Paris, vol 226, 1948.

25. Assanis, D.N. and Badillo, E. "Evaluation of Alternative Thermocouple Designs for Transient Heat Transfer Measurements in Metal and Ceramic Engines," SAE Technical Paper Series, no. 890571, (1989).

26. Vosen, S.R., "*Unsteady Heat Transfer during the Interaction of a Laminar Flame with a Cold Wall*", Dissertation, University of California, Birkley, UMI Dissertation Services, 1983.

27. Brassin, A., Lisbet, R., Combourieu, J., and Lafiette, P., *Bull. de la Societe Chimique de France*, vol. 7, pp.2521, 1967.

28. Egerton, A.C., and Lefebvre, A. H., *Proc. Roy. Soc. (London)* vol. 222A, pp. 206, 1954.

29. Kornhauser, A.A. Flame-Wall Heat Transfer Model, Private Communications, Blacksburg, Virginia, 1993.

30. Cary, N.C., "SAS Introductory Guide" SAS Institute, 1983.

31 Harris, M.E., Grumer, J. von Elbe, G. and Lewis, B., "Burning Velocities, Quenching, and Stability Data on Nonturbulent Flames of Methane and Propane with Oxygen and Nitrogen," *Third Symposium on Combustion, Flame and Explosion Phenomena*, Academic Press, pp. 80-89, 1947.

32. Hocks, W., Peters, N. and Adomeit, G., "Flame Quenching in Front of a Cold Wall under Two-Step Kinetics," *Combustion and Flame*, Vol. 41, pp. 157-170, 1981.

33. Adamczyk, A.A. and Lavoie, G.A., "Laminar Head-On Quenching - A Theoretical Study," SAE Technical Paper Series, no. 780969, (1969).

34. Kurkov, A.P. and Mirsky, W., "An Analysis of Flame Extinction by a Cold Wall," *Twelfth Symposium (International) on Combustion*, Academic Press, pp. 615-625, 1968.

35. Westbrook, C.K. and Dryer, F.L., "Simplified Reaction Mechanisms for the Oxidation of Hydrocarbon Fuels in Flames," *Combustion, Science and Technology*, Vol. 27, pp. 31-43, 1981.

36. Andrews, G.E. and Bradley, D., "The Burning Velocity of Methane-Air Mixtures," *Combustion and Flame*, Vol. 13, pp 275-288, 1972.

37. Chemical Equilibrium Solver Program, STANJAN, version 3.89, Reynolds, W.C., Stanford, California, 1987.

38. Mason, E.A. and Saxena, S.C., Phys. of Fluids, Vol.1. pp. 361, 1958.

39. Heywood, J.B. "*Internal Combustion Engine Fundamentals,*" McGraw Hill Publishing Co. pp.465, New York, 1988.

40. Ozisik, M.N., "*Heat Conduction,*" Jhon Wiley & Sons, pp.217, 1980.

41. Incropera, F.P. and Witt, D.P., "*Fundamentals of Heat and Mass Transfer,*" John Wiley and Sons, pp.A4, New York, 1990.

VITA

The author was born on November 8, 1966 in Radolfzell am Bodensee, Germany, the son of Roswitha and Georg Bucher. He received his basic education at the Rudolf Steiner School, Wahlwies, Germany from where he graduated in 1986 with the Fachabitur. From December 1986 to July 1988 he served (mandatory service) in a home for handicapped juveniles in Mainz, Germany. In August 1998 he entered the Fachhochschule Wiesbaden, Department of Mechanical Engineering, Ruesselsheim, Germany, receiving the Diplom Ingenieur (FH) in July 1991. Between 1985 and 1990 the author was a part-time machine shop employee at FERAG AG, Weinfelden, Switzerland. He awarded a Fulbright Scholarship and began graduate studies at Virginia Tech in the Department of Mechanical Engineering in August 1991 as a Graduate Research Assistant. His plans for the immediate future are to work as a Research Assistant at Princeton University. The Author is a member of the Verein Deutscher Ingenieure (VDI), Association of German Engineers.